Universidad del País Vasco Euskal Herriko Unibertsitatea
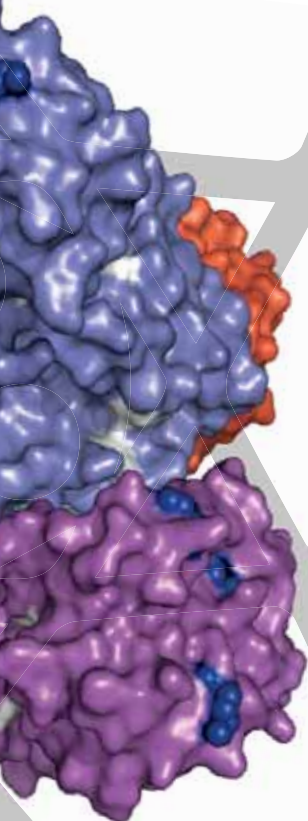
Application of enzymes in Nitrogen-13 radiochemistry: biocatalytic synthesis of PET radionuclides with biomedical interest

San Sebastián 2017

Eunice S Da Silva

Application of enzymes in Nitrogen-13 radiochemistry; biocatalytic synthesis of PET radionuclides with biomedical interest

Eunice da Silva

2017

Cover calligraphy Laura Saa

Cover design Eunice S. Da Silva

Application of enzymes in Nitrogen-13 radiochemistry; biocatalytic synthesis of PET radionuclides with biomedical interest

PhD Thesis

to obtain the degree of PhD in

Synthetic and Industrial Chemistry

at the University of Basque Country

by

Eunice da Silva

2017

Universidad del País Vasco   Euskal Herriko Unibertsitatea

Thesis Supervisors:

Jordi Llop, PhD (Radiochemistry & Nuclear Imaging Lab, CIC biomaGUNE)

Fernando Lopez-Gallego, PhD (Heterogeneous Biocatalysis Lab, CIC biomaGUNE)

University tutor:

Esther Lete, PhD, Professor (Department of Organic Chemistry Faculty of Science and Technology University of the Basque Country)

Contents

Summary

With the widespread installation of biomedical cyclotrons and positron emission tomography (PET) scanners around the world, scientists are increasingly recognizing PET as an accessible and valuable tool for the investigation of physiological or biological challenges in the pre-clinical and clinical setups. The continuous progress of nuclear imaging techniques demands for the development and implementation of efficient, clean and sustainable synthetic routes to manufacture novel radiotracers. This task is especially challenging for the synthesis of radiotracers labeled with short-lived β^+ emitters, which are extremely valuable since they substantially reduce the radiation burden on the subject under investigation. Hence, extremely rapid and selective synthetic schemes must be designed to access radiotracers radiolabeled with short half-lived positron emitters.

Biocatalysis, although surprisingly underused in radiochemistry, constitutes an attractive alternative to conventional chemistry. Enzymes present an exquisite chemical selectivity and high turnover numbers; they also evolved to work under physiological conditions, where the concentration of the metabolites is tightly regulated and are rarely in excess. Furthermore, enzymes are also the most sophisticated chiral catalysts yielding enantiopure products in most of the cases. Hence, the use of enzymes can now be seen as an innovative approach to radiolabel biologically active molecules with short half-lived positron emitters, for their use in positron emission tomography. Although years 70´s and 80´s are considered the golden era of biocatalysis in radiochemistry, advances

in enzyme engineering during the last decade have significantly enhanced the toolbox of enzymes available for chemical reactions, which may find application in the context of radiochemistry. The biocatalytic approaches for the synthesis of PET radiotracers using Nitrogen-13, Carbon-11 and Fluorine-18 that have been reported during the last four decades are reviewed in **Chapter 2**.

The main target of this PhD thesis was the development of new bio-strategies in the context of nitrogen-13 radiochemistry, and mainly the preparation of ^{13}N-labeled precursors and their incorporation in biological molecules with interest in preclinical application.

In **Chapter 4**, the reduction of $[^{13}N]NO_3^-$ to $[^{13}N]NO_2^-$ using a heterogeneous biocatalyst is described. For the design and fabrication of a suitable heterogeneous biocatalyst, a eukaryotic nitrate reductase from *Aspergillus niger* was immobilized on different carriers. Optimal immobilization and recovered activities were obtained when this enzyme was immobilized on porous agarose beads activated with a positively charged tertiary amino group. This immobilized preparation was 12-fold more thermostable than the soluble enzyme and could be re-used in up to 7 reaction cycles, preserving its initial activity. A pure preparation of $[^{13}N]NO_2^-$ was obtained after 4 min reaction at room temperature and it was successfully applied in a two-step chemo-enzymatic radiosynthesis of *S*-$[^{13}N]$nitrosoglutathione.

A one-pot, enzymatic and non-carrier-added synthesis of a variety of ^{13}N-labeled amino acids (*L*-$[^{13}N]$alanine, $[^{13}N]$glycine, and *L*-$[^{13}N]$serine) is described in **Chapter 5**. To that aim, an *L*-alanine dehydrogenase from *Bacillus subtilis* was used, together with nicotinamide adenine dinucleotide (NADH) as the redox cofactor, and labeled ammonia as the

amine source. Moreover, the addition of formate dehydrogenase from *Candida boidinii* in the same reaction vessel allowed the *in situ* regeneration of NADH during the radiochemical synthesis of the amino acids. The enzymatically labeled amino acids have been used to analyze their *in vivo* biodistribution in healthy mice. Likewise, the capacity to selectively accumulate in the tumor has been assessed in a prostate cancer mouse model, by using dynamic PET-CT imaging.

Lastly, **Chapter 6** describes the immobilization of *L*-Alanine dehydrogenase from *Bacillus subtillis* on agarose microbeads, activated with glyoxyl groups (aliphatic aldehydes) and two other carriers. These immobilized enzyme preparations were extensively characterized towards temperature, pH and kinetic parameters. Finally, the optimal heterogeneous biocatalyst was applied in the synthesis of *L*-[^{13}N]alanine using pyruvate and labeled ammonia as the substrates.

Resumen

La instalación generalizada de ciclotrones biomédicos a nivel mundial ha suscitado un gran interés entre la comunidad científica, que ve la tomografía por emisión de positrones (PET, del inglés *Positron Emission Tomography*) como una herramienta accesible para abordar de manera no invasiva, longitudinal y traslacional determinados problemas biológicos, fisiológicos y/o médicos inabordables mediante otras técnicas. Sin embargo, la utilización de la PET exige el desarrollo e implementación de rutas sintéticas que permitan la preparación eficiente y robusta de radiotrazadores marcados con isótopos emisores de positrones. Esto resulta especialmente complicado en el caso de la síntesis de radiotrazadores marcados con emisores de positrones de vida media corta. Dichos emisores de positrones resultan extremadamente valiosos ya que permiten reducir de manera significativa la dosis de radiación efectiva recibida por el sujeto investigado.

La biocatálisis, aunque ha sido sorprendentemente infrautilizada en el contexto de la radioquímica, constituye una alternativa atractiva a la química convencional. Las enzimas presentan una excelente selectividad química y una gran capacidad catalítica. Además, han evolucionado de manera natural para trabajar en condiciones fisiológicas, donde la concentración de los metabolitos está fuertemente regulada y raramente en exceso. Las enzimas son también los catalizadores quirales más sofisticados que se conocen ya que son capaces de producir productos

enantioméricamente puros incluso en esquemas de reacción muy complejos.

En este contexto, la biocatálisis ha emergido como una estrategia altamente innovadora para marcar moléculas biológicamente activas con emisores de positrones de vida media corta, con el fin último de utilizar dichas moléculas marcadas (radiotrazadores) en estudios de imagen mediante PET.

La edad de oro de la aplicación de la biocatálisis en radioquímica fueron las décadas de los 70 y 80. Sin embargo, los avances en ingeniería enzimática llevados a cabo durante la última década han mejorado significativamente la cantidad, calidad y versatilidad de las enzimas disponibles. Este hecho ha abierto nuevas perspectivas en la utilización de la catálisis enzimática en el contexto de la radioquímica.

El primer objetivo de la presente tesis doctoral ha sido efectuar una revisión exhaustiva de los diferentes enfoques biocatalíticos utilizados para la preparación de radiotrazadores marcados con isótopos emisores de positrones. Todos los trabajos reportados en las últimas cuatro décadas en lo que se refiere a la síntesis de radiotrazadores PET utilizando Nitrógeno-13, Carbono-11 y Flúor-18, así como las perspectivas de futuro que ofrece esta tecnología se describen y discuten en el **Capítulo 2** del presente documento.

Una vez superada la fase de documentación, se definió el principal objetivo de esta tesis doctoral, que consistía en el desarrollo de nuevas estrategias basadas en biocatálisis en el contexto de la radioquímica del nitrógeno-13, con el objetivo último de preparar precursores marcados con ^{13}N y su incorporación en moléculas biológicas con interés en la aplicación

preclínica, esto es, en la realización de estudios de imagen en animales de experimentación.

El primer objetivo experimental concreto de la tesis doctoral fue abordar el desarrollo de un proceso enzimático para la reducción de $[^{13}N]NO_3^-$ a $[^{13}N]NO_2^-$. Cabe destacar que la irradiación directa de agua ultrapura con protones acelerados permite la formación eficiente de nitrógeno-13 mediante la reacción nuclear $^{16}O(p,\alpha)^{13}N$, siendo la especie química formada mayoritariamente el anión $[^{13}N]NO_3^-$. Dicha especie no tiene gran aplicación como sintón radiactivo; sin embargo, su reducción a $[^{13}N]NO_2^-$ permite abordar la preparación de una gran variedad de moléculas marcadas, incluyendo nitrosaminas, nitrosotioles y azoderivados, entre otros. Hasta la fecha, la reducción mencionada arriba se llevaba a cabo de manera eficiente en una columna de cadmio. Sin embargo, la utilización de este metal podría conllevar problemas asociados a su toxicidad en el caso de pretenderse la aplicación en el entorno clínico, y se estimó muy oportuno desarrollar un proceso enzimático que permitiera evitar la utilización de cadmio. La consecución de este objetivo se planteó mediante la utilización de un biocatalizador heterogéneo. Para el diseño del biocatalizador heterogéneo se inmovilizó una nitrato reductasa eucariota de *Aspergillus niger* en diferentes soportes porosos. El rendimiento óptimo de inmovilización y actividades enzimáticas recuperadas se obtuvieron cuando esta enzima se inmovilizó en unidades porosas de agarosa, activadas con un grupo amino terciario cargado positivamente. Este soporte presentó los grupos funcionales óptimos en términos de densidad y reactividad para lograr una mayor actividad enzimática después del proceso de inmovilización. Con el estudio de los parámetros cinéticos aparentes de la nitrato reductasa inmovilizada en este tipo de soportes, pudimos observar que la inmovilización daba lugar a un aumento de la K_m

aparente para el NADPH, este aumento parece ser debido a una serie de problemas difusionales que presenta el cofactor a la hora de alcanzar los centros activos de las enzimas inmovilizadas en el microambiente poroso. Además, esta preparación inmovilizada fue 12 veces más termoestable que la enzima soluble y pudo reutilizarse hasta 7 ciclos de reacción, preservando su actividad inicial. En condiciones óptimas (4 minutos, temperatura ambiente; estas condiciones son comparables a las utilizadas anteriormente en el proceso de reducción en presencia de cadmio), pudo obtenerse $[^{13}N]NO_2^-$ puro que posteriormente pudo utilizarse para abordar la síntesis de S-$[^{13}N]$nitrosoglutationa (**Figura R.1**). De la realización de este trabajo resultó la primera de las publicaciones asociadas a la presente tesis doctoral (da Silva, E. S. *et al.,* Catalysis Science & Technology, 2015, 5, 2705-2713).
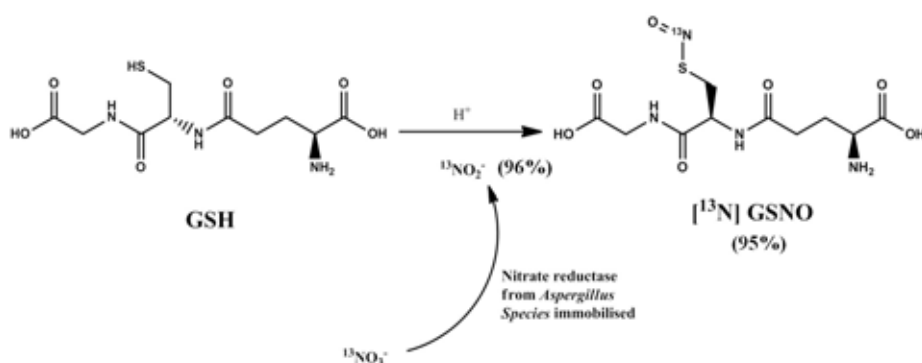
**Figura R.1.** Síntesis de S-$[^{13}N]$nitrosoglutathiona ($[^{13}N]$GSNO) a partir de $[^{13}N]NO_3^-$ producido en el ciclotrón.

Una vez desarrollado el método de reducción descrito en el capítulo 4, se planteó la posibilidad de emplear métodos biocatalíticos para la

preparación de compuestos biológicamente activos, concretamente aminoácidos. Para la selección de los aminoácidos a marcar se contó con la colaboración del profesor Arkaitz Carracedo, de CIC bioGUNE, que dispone de un modelo animal de cáncer de próstata y dedica parte de su investigación al estudio de aberraciones metabólicas en estos tumores. En este contexto, en el **Capítulo 5** de la presente tesis doctoral se presenta la síntesis enzimática, en un solo paso y sin *carrier* añadido de diferentes aminoácidos marcados con nitrógeno-13, concretamente *L*-[^{13}N]alanina, [^{13}N]glicina y *L*-[^{13}N]serina (**Figura R.2a**). Para ello, se usó una *L*-alanina deshidrogenase de *Bacillus subtilis* NADH–dependiente. Esta enzima es capaz de llevar a cabo la aminación reductiva de α-cetoácidos mediante el uso de [^{13}N]amoníaco como fuente de grupos amino. Sin embargo, esta enzima no fue capaz de sintetizar *L*-aminoácidos muy voluminosos como la *L*-fenilalanina y al *L*-norvalina, debido a que presenta unos valores de K_m para el amonio demasiado altos en la síntesis de los aminoácidos voluminosos anteriormente descritos. Tras optimización de las condiciones experimentales (cantidad de catalizador, pH, etc) pudo conseguirse la preparación de los tres aminoácidos con rendimiento radioquímico suficiente para abordar estudios en los modelos animales proporcionados por el Prof. Carracedo. Además, el acoplamiento de este enzima con una formiato deshidrogenasa de *Candida boidinii* en el mismo medio de reacción permitió la regeneración *in situ* de NADH durante la radiosíntesis de los aminoácidos (**Figura R.2b**), de modo que pudo disminuirse hasta 50 veces la concentración del cofactor sin comprometer los rendimientos radioquímicos de la reacción.
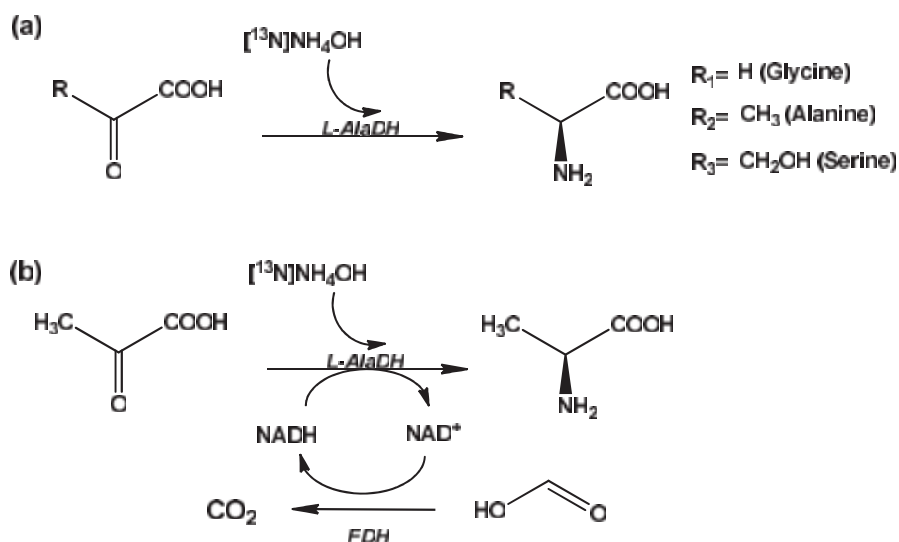
Figura R.2. (**a**) preparación enzimática de L-[^{13}N]alanina, [^{13}N]glycina, y L-[^{13}N]serina utilizando L-alanina dehidrogenasa (L-AlaDH) obtenida de *Bacillus subtilis*; (**b**) Preparación de L-[^{13}N]alanina con regeneración del cofactor NADH.

Los aminoácidos marcados enzimáticamente se utilizaron en primer lugar para estudiar su biodistribución *in vivo* en ratones sanos (**Figura R.3**). Todos los aminoácidos mostraron acumulación en la zona abdominal, hecho que ya había sido observado para otros aminoácidos en estudios anteriores reportados en la literatura. Dos de los aminoácidos (L-[^{13}N]alanina y [^{13}N]glycina) mostraron poca eliminación por orina, convirtiéndose en potenciales trazadores para la visualización *in vivo* de los tumores de próstata.
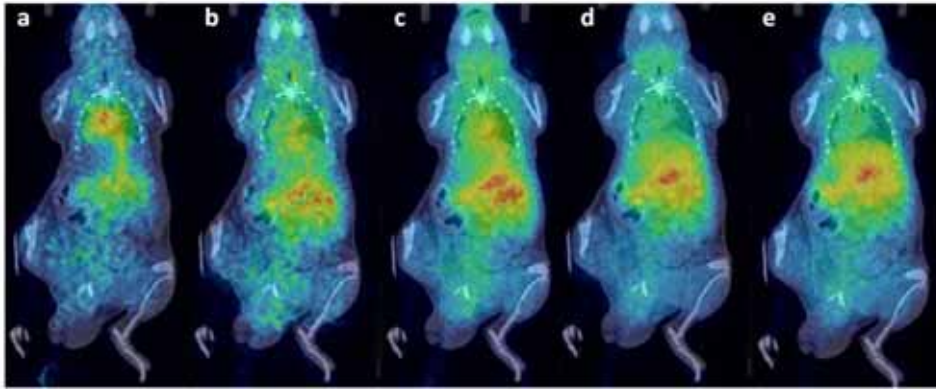
Figura R.3. Imágenes PET-CT representativas obtenidas a diferentes tiempos tras administración intravenosa de *L*-[^{13}N]alanina en ratón. Se muestran proyecciones coronales corregistradas con cortes representativos de imágenes CT; 0-30 s (**a**); 31-70 s (**b**); 71-230 s (**c**); 231-740 s (**d**); 741-3020 s (**e**).

Los estudios efectuados en animales con tumor mostraron que los aminoácidos se acumulaban selectivamente en la próstata, y que dicha acumulación aumentaba en presencia de tumor (**Figura R4**). Sin embargo, es necesario efectuar estudios más exhaustivos y a diferentes tiempos tras aparición de los tumores para obtener resultados más concluyentes. Los resultados derivados del capítulo 5 se recogen en la segunda publicación asociada a esta tesis doctoral (da Silva, E. S. *et al*., Chemistry – A European Journal, 2016, 22, 13619-13626).
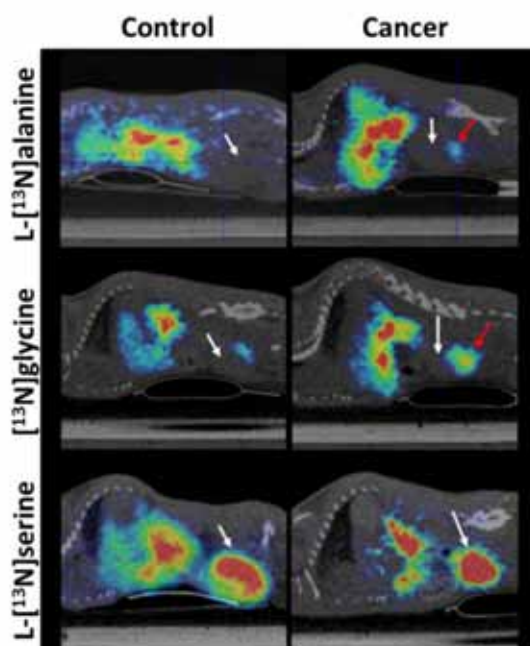
Figure R.4. Imágenes PET-CT (proyecciones sagitales) de animales control y animales con tumor, obtenidas tras administración de los aminoácidos marcados con nitrógeno-13. La posición de la vejiga y de la próstata se indican con una fleche blanca y roja, respectivamente. Como puede observarse, tan solo el aminoácido L-[^{13}N]serina muestra eliminación significativa por orina.

El trabajo desarrollado en el capítulo 5 implicaba la utilización de enzimas en disolución. Sin embargo, con el fin de evitar la presencia de enzima en la disolución final, así como para posibilitar la realización de reacciones en flujo, se consideró conveniente explorar la posibilidad de inmovilizar las enzimas. Así pues, en el **Capítulo 6** se describe la inmovilización de la enzima L-alanina deshidrogenase de *Bacillus subtillis* en microesferas de agarosa porosa, activadas con grupos de glioxal (aldehídos alifáticos), además de otros dos soportes. Estas preparaciones enzimáticas inmovilizadas se caracterizaron en términos de temperatura, pH y

parámetros cinéticos. En base a estudios físico-químicos de la superficie de esta enzima, se propouso una orientación óptima a través de la cuál la enzima era inmovilizada en soportes activados con grupos aldehídos, dando lugar a enzimas inmovilizadas con una gran estabilidad y una actividad suficiente para su aplicación en procesos biotecnológicos. Finalmente, se aplicó el biocatalizador heterogéneo óptimo para abordar la síntesis de L-[^{13}N]alanina, usando piruvato y amoniaco marcado como sustratos. Los resultados demostraron que con las enzimas inmovilizadas podían obtenerse buenos rendimientos radioquímicos, equivalentes a los obtenidos utilizando las enzimas en disolución. Sin embargo, pudo reciclarse el catalizador hasta en 5 ciclos consecutivos, sin que esto afectara de manera significativa al rendimiento obtenido (**Figura R5**). De este trabajo, que abre pues las puertas al desarrollo de reacciones en flujo, resultó la tercera de las publicaciones relacionadas con la presente tesis docotral (da Silva, E. S. *et al*., Process Biochemistry, *in press*).
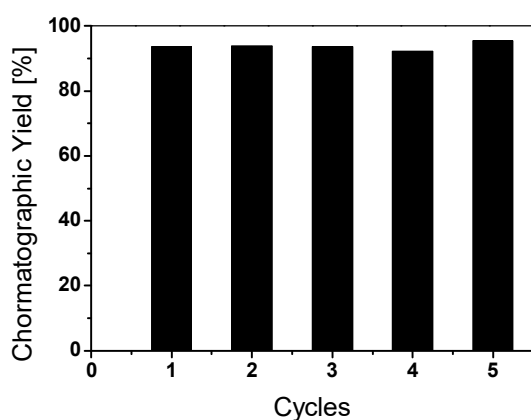
Figura R.5. Rendimiento cromatográfico obtenido al efectuar síntesis consecutivas de L-[^{13}N]-alanina utilizando la enzima inmovilizada. La reacción se llevó a cabo con 45 μg x mL^{-1} de enzima inmovilizada a 25 ºC, pH 8 y t= 20 minutos.

En resumen, en esta tesis doctoral, hemos demostrado que la aplicación de métodos biosínteticos permite la radiosíntesis selectiva y eficiente de compuesto marcadas que serían muy díficiles de obtener mediante métodos químicos. Los excelentes resultados que hemos obtenido aquí han sido gracias a capacidad que tienen los enzimas para catalizar un amplia diversidad de reacciones químicas con una gran quimio- regio- y enantoselectividad. En esta tesis, hemos mostrado que las enzimas se pueden aplicacar en radioquímica tanto en su forma solúble como en su forma inmovilzada. Y por eso en este contexto, hemos sido capaces de desarrollar diferentes procesos sínteticos para la generación de radiotrazadores basados en Nitrogeno 13.

Chapter 1

General introduction

BIOCATALYSIS

One of the principal functions of enzymes as natural biocatalysts is to enhance the rate of virtually all chemical reactions within a cell. They increase the rates of chemical reactions without being permanently altered or consumed. They also increase the reaction rates without changing the equilibrium between the reactants and the products.

These unique catalytic properties shown by enzymes make them desirable in many chemical processes. Enzymes work under mild reaction conditions (physiological pH and temperature), and constitute biodegradable and environment-friendly catalysts with high activity and chemo-, regio- and stereoselectivity.[1] Additionally, the use of enzymes does not require the time-consuming protection/deprotection/activation steps frequently used in synthetic chemistry. These advantages enable shorter synthetic routes with less generation of waste products, thus being both environmentally and economically more attractive than traditional organic syntheses. Furthermore, enzymes can catalyze a wide spectrum of chemical and biochemical reactions that can be readily assembled in sophisticated pathways to synthesize complex molecules. These complex pathways formed by multi-enzyme systems have naturally evolved to work within the cellular milieu; however, in the last decades chemists have isolated enzymes and make them work *ex-vivo* under non-natural conditions. Moreover, advances in protein engineering have allowed the application of enzymes to chemical processes different from the natural ones. Therefore, intrinsic features of enzymes together with the recent technologies have paved the way for the implementation of biocatalysis in industrial processes[1,2] as well as in the medical and pharmaceutical fields, where enzymes have been successfully exploited for the chemical

synthesis of drugs and building blocks[3-5] and for the treatment of a variety of diseases.[1]

Enzymes also present some inherent drawbacks associated with their natural origin: (i) they are poorly stable either in the presence of non-polar solvents, under high temperatures or under extreme pH values; (ii) they show limited reactivity towards artificial substrates (non-natural reactions); and (iii) they are highly soluble in water, limiting thus their reusability in batch reactions or their applicability in continuous-flow processes.[6] Fortunately, the significant advances in genomics and computational biology have resulted in novel experimental and computational protein engineering tools, which have significantly enhanced the toolbox of available enzymes.[7] On the other hand, enzyme immobilization has addressed the solubility issue by heterogenization of the biocatalysts, which enables both reutilization in batch reactions and integration into flow reactors. In addition, immobilized enzymes show often increased stability, facilitate the product separation and avoid time-consuming purification steps.[8] All these facts open new avenues for the application of enzymatic chemistry to the preparation of radiolabeled compounds in multiple biomedical applications.[1,9-12]

ENZYME IMMOBILIZATION: THE WORKHORSE OF HETEROGENEOUS BIOCATALYSIS

Enzyme immobilization involves the fixation of an enzyme to an insoluble matrix (carrier); however, optimizing the immobilization of enzymes is challenging. In spite of the difficulties, this methodology has been accepted as one of the most successful methods to overcome the

limitations of free enzymes.[13,14] There are several reasons to immobilize enzymes (**Table 1.1**): first, immobilized enzymes act as heterogeneous biocatalysts that can be easily manipulated and separated from the products once the reaction is completed, preventing the contamination of the product and facilitating the downstream processing; second, by using an optimal immobilization methodology, the immobilization may enhance both operational and storage stability, while denaturation by exposure to heat or organic solvents can be prevented; third, when the immobilized enzymes are highly stable, the resulting heterogeneous biocatalyst can be recycled for several operational cycles and directly integrated into continuous chemical processes.[14]

The immobilization of enzymes has been intensively exploited since the 70's. However, no universal immobilization protocols to improve both activity and stability of the immobilized enzymes have been described. For this reason, enzyme immobilization is still an empirical approach where trial-and-error approximations are more common than rational approaches. However, the results obtained during more than 40 years of research in enzyme immobilization have demonstrated that the physic-chemical properties of the support material and the immobilization chemistry (the type of bonds between the enzyme and the solid surface) are essential to achieve active and stable heterogeneous biocatalysts. In theoretical terms, structural information about the enzyme can guide the selection of the best immobilization protocol; however, examples of rational enzyme immobilization are scarce because of the chemical and geometrical complexity of protein structures and the heterogeneity of the solid material surfaces. Mass transfer limitations need often to be addressed by selecting the proper microstructure of the solid carrier to favor the access of the substrates from the reaction media to the immobilized catalytic centers.[15]

The immobilization chemistry and the nature of the solid carrier are fundamental to control the protein orientation and the substrate/product diffusion, and both factors will be crucial to ensure high activity and stability of the final heterogeneous biocatalysts.[16]

Table 1.1. Properties of immobilized enzymes: advantages and drawbacks. Adapted from the reference.[17]

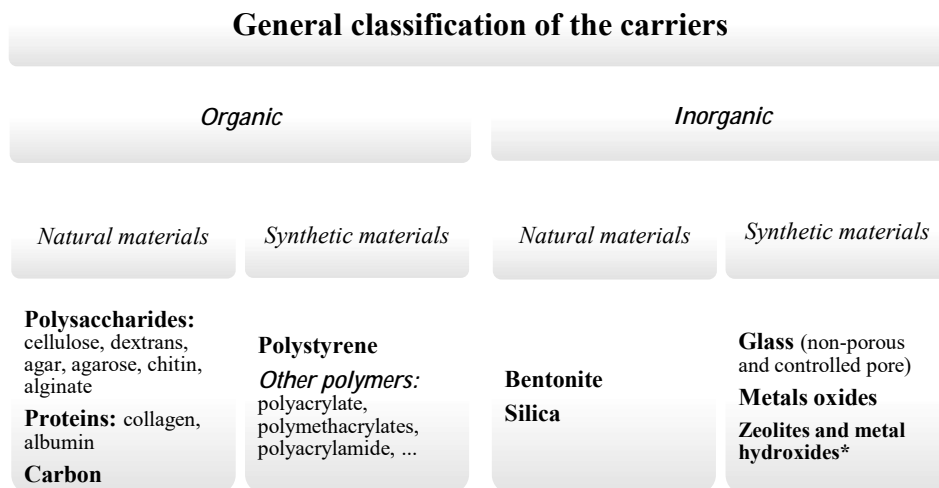| Advantages	Drawbacks
Reuse of the biocatalyst	Loss in enzyme activity
Easier reactor operation	Mass transfer limitation
Easier product separation	Additional cost
Stability of the enzyme	

Selection of a Suitable Carrier Material

The properties of the selected carrier are essential for the performance of the heterogeneous biocatalyst. Ideal carrier properties include physical strength, hydrophilicity, inertness, ease of derivatization, biocompatibility, resistance to microbial attack, and availability at low cost.[18] However, even though immobilization on solid carriers is an established technology, there are still no general rules for selecting the best carrier for a given application. Both the immobilization chemistry and the selection of the optimal carrier are usually based on trial-and-error.

In general, the carriers can be classified as inorganic and organic, according to their chemical composition. In turn, the organic carriers can be subdivided into natural and synthetic polymers (**Figure 1.1**). Natural polymers such as chitin, chitosan and cellulose have many advantages over

many synthetic polymers in terms of biodegradability, non-toxicity, physiological inertness, hydrophilicity and remarkable affinity to proteins. The green properties of those materials make them attractive, especially in specific applications including food, pharmaceutical, medical and agricultural processing.[14,16] However, membranes prepared from synthetic polymers have been largely preferred as enzyme carriers because of their low cost, easy surface modification, resistance to biodegradation and thermal and chemical stabilities.

Inorganic materials can also be classified into natural and synthetic materials. Naturally occurring silica-based materials are the most suitable and versatile matrices for enzyme immobilization and have been widely used in industrial manufacturing of enzyme-processed products,[19,20] as well as for research[21] and medical purposes.[22,23] Silica can be easily fabricated to provide desirable morphology, pore structures, and micro-channels.[24,25] Additionally, the surface of silica gel can be easily modified by chemical methods to provide different types of functional groups at the surface.[19,26,27] Furthermore, silica is cheap, mechanically stable, chemically inert, and environmentally friendly. In the last decade, other synthetic inorganic materials such as metal oxides, metal phosphates, zeolites and metal organic framework (MOFs) are gaining relevance in the protein immobilization field.[28]

General classification of the carriers

Organic		Inorganic	
Natural materials	*Synthetic materials*	*Natural materials*	*Synthetic materials*
Polysaccharides: cellulose, dextrans, agar, agarose, chitin, alginate **Proteins:** collagen, albumin **Carbon**	**Polystyrene** *Other polymers:* polyacrylate, polymethacrylates, polyacrylamide, ...	**Bentonite** **Silica**	**Glass** (non-porous and controlled pore) **Metals oxides** **Zeolites and metal hydroxides***

*Metal-organic-frameworks (MOFs) because they are kind of hybrid materials.

Figure 1.1. General classification of the carriers used for enzyme immobilization. Adapted from the reference[16].

In addition to the nature of the carrier, physical characteristics such as particle diameter, swelling behavior, mechanical strength and compression behavior also affect the performance of the immobilized systems. Pore and particle size of the carrier determine the total surface area and critically affect the maximum amount of enzyme that can be bound. Here, we can also categorize the solid carriers as non-porous and porous. Non-porous carriers show less diffusional limitations, but microscopic particles (suitable for re-utilization) have low loading capacities. Nanoparticles have a much larger surface area per mass unit but they are laboriously manipulated in batch reactors and cause filter clogging during their reutilization. Hence, porous, micrometric particles are generally preferred because their high surface area enables higher enzyme loads, their manipulation during the operational cycles is much easier and finally the

vast majority of the immobilized enzymes are physically protected by the porous microenvironment. In the context of this PhD thesis. As example, cross-linked agarose porous beads (agarose BCL) have been used. The material is hydrophilic and biocompatible, it can be manufactured in the micrometric size within a range of porosity and is commercially available at large scale.[29,30] Its main limitation, the high cost, can be overcome by employing reversible methods that allow regeneration and re-use of the carrier once the immobilized enzymes become inactive.

Selection of the optimal immobilization chemistry. The pathway to the enzyme stabilization

In the last decades, a plethora of immobilization protocols has been reported in the literature.[2,13,14,16,31] Depending on the enzyme and immobilization strategy, the final stability and activity of the enzyme may be significantly affected.

The chemistries to immobilize enzymes onto solid carriers can be divided into two main groups based on the nature of the enzyme-carrier bonds: (i) reversible chemistries, where the enzyme-carrier interaction can be easily reverted by changing the media conditions, thus enabling the enzyme elution or lixiviation; and (ii) irreversible chemistries, where the enzymes are irreversibly attached to the carrier (**Figure 1.2**).[6,14] Reversible immobilization can be achieved by physical adsorption of the enzyme based on ionic, van der Waals or hydrophobic interactions, on affinity interactions and on reversible covalent bonds. Irreversible immobilization mainly involves irreversible covalent bonds between the protein and the surface.
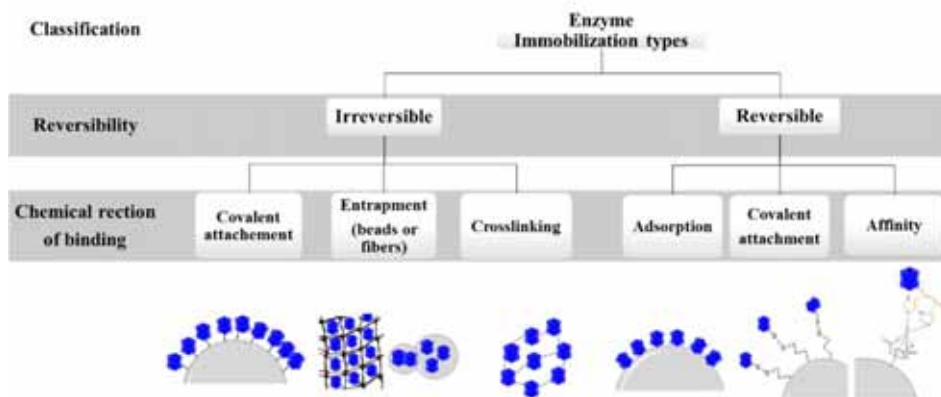
Figure 1.2. Schematic representation of the main different methods of enzyme immobilization. Adapted from the reference[16].

Methods of Reversible Immobilization

Reversibly immobilized enzymes can be detached from the carrier under gentle conditions. The use of these enzymatic systems is highly attractive because when the enzymatic activity decays, the carrier can be regenerated and reloaded with the fresh enzyme. This methodology is particularly interesting when the cost of the carrier is high. Indeed, the cost of the carrier is often a primary factor in the overall cost of immobilized biocatalysts. In addition, the reversibility between the enzyme and the carrier surface has proven useful for processes where the enzymes must work at the boundary of insoluble substrates and then need to be recovered for subsequent operational cycles.[32]

In 1916, one of the first immobilized enzymes prepared by adsorption was reported by Nelson and Griffin, who showed that invertase physically adsorbed on charcoal (solid powder) kept its catalytic activity.[33] One hundred years later, physical adsorption still remains the oldest, simplest,

and most widely used method for protein immobilization.[34] The phenomenon of physical adsorption can be driven by weak and non-specific forces such as hydrogen bonding, by Van der Waals forces (alone or combined), by hydrophobic interactions or by stronger salt bridges (combination of hydrogen bonding and charge-charge interactions).[16,35]

Immobilization by ionic adsorption (commonly named as ionic exchange) is vastly exploited in reversible protein immobilization because protein surfaces are rich in positively (basic residues) and negatively charged amino acids that can easily interact with negative and positive groups on the carrier surface, respectively.[34] Protein-carrier interactions are strong enough to retain the protein attached to the solid phase during the operation but they can be mainly disrupted by ionic strength and high or low pH. This immobilization chemistry has revealed highly useful to stabilize the quaternary structure of multimeric proteins.

Another classical method to reversibly immobilize protein is the affinity immobilization. Affinity binding is also included which relies on the creation of different (bio)affinity bonds between a functionalized (activated) carrier and a specific group present on the protein surface.[14] In most cases, proteins are engineered with affinity tails that selectively react with affinity groups on the carrier surface.[6,16,36] The most well-known genetically encoded affinity tag is the polyhistidine tag (Hist-tag) that is selectively bound to carriers activated with metal-chelates (Cu(II), Co(II), Zn(II), or Ni(II)); the metal determines the selectivity and the strength of the interaction.[37-41] This immobilization is easily and selectively reverted by adding imidazole groups that compete with the histidines for the chelates. This chemistry provides a remarkable selectivity and an extraordinary control of protein orientation, and minimizes the

conformational changes suffered by the proteins, yielding highly active but poorly stabilized proteins upon the immobilization protocol.[36]

Finally, the reversible immobilization based on disulfide bridges is the most representative method of reversible covalent immobilization. A thiol from the protein surface (from the cysteine) selectivity reacts with a disulfide group on the carrier surface. This immobilization is easily reverted by reducing agents such as dithiothreitol.[16,42,43] The major advantage of this immobilization chemistry is the high selectivity for cysteine as unique natural amino acid able to participate in such thiol-disulfide exchange. Since cysteine residues are rarely found in the protein surfaces, engineering proteins with unique cysteines is a powerful strategy to immobilize proteins on disulfide activated materials through any desired orientation.[44,45]

Methods of Irreversible Immobilization

The concept of irreversible immobilization means that once the enzyme is attached to the carrier, the enzyme cannot be physically separated from the solid material. Unlike reversible immobilization, when the enzymes are irreversibly bound to the carriers, the solid material cannot be regenerated once the enzyme becomes inactive. This is an important issue when using expensive materials. However, irreversible attachment avoids the enzyme lixiviation during the operational process and frequently improves the enzyme stability, resulting in increased operational life of the heterogeneous biocatalysts. Stabilization of proteins through immobilization mainly relies on multivalent attachments that rigidify protein structures. In other words, the greater the number of covalent linkages between the enzyme and the carrier, the more rigid the enzyme

structure becomes. This multivalent covalent attachment has been demonstrated as one of the main reasons to explain the higher stability of the immobilized proteins.[18] Paradoxically, the rigidification of the protein structure may noticeably decrease the protein activity. This fact is particularly important for enzymes, where rigidification might reduce some fundamental flexibility required for the catalysis. For this reason, it is essential to reach a compromise between the stability (rigidification) and activity.

Figure 1.2 shows the three main methodologies for irreversible immobilization: irreversible attachment to a pre-existing carrier, irreversible entrapment/microencapsulation of the enzyme into synthetic materials, and irreversible cross-linking of enzyme aggregates. Irreversible immobilization on the pre-existing carrier will be the only technique described in detail in this chapter because it was fundamental to the experimental work of this thesis.

The vast majority of the irreversible immobilization chemistries are based on a nucleophilic attack of protein surface residues (Lys, Cys, His and even Tyr) to a battery of reactive groups (cyanogen bromide, vinyl groups, aldehyde and epoxide groups) present on the surface of the carrier. Glutaraldehyde has been exploited to activate aminated carriers to immobilize primary amine groups, *i.e.*, the *N*-terminus and the ε-amino group of the lysines.[16,46,47] This immobilization is highly efficient but its action mechanism is not fully understood.

CNBr-activated carriers are highly versatile. A plethora of materials have been activated with this groups (membranes, surfaces, nanoparticles, etc.), and some of these materials are commercially available.[48] Dozens of proteins have been immobilized through this immobilization chemistry

that requires very mild conditions and where the primary amines (mainly from the *N*-terminus) of proteins react with the cyanogen bromides to form cyanate esters or imidocarbonates.[49-52] The major disadvantage of this immobilization chemistry is the low stability of cyanogen bromide groups under aqueous conditions that often limit the multivalency of the attachment and the protein load of the final immobilized preparation.

Epoxide and glyoxyl groups are alternative groups for irreversible immobilization that present a much higher stability than the cyanogen bromides and whose immobilization mechanism is better understood and reliable that for the glutaraldehyde groups. Glyoxyl groups are small aliphatic aldehydes that form reversible imino bonds with the primary amino groups (ε-NH$_2$ from Lys and *N*-terminus) in the enzyme forming reversible Schiff's bases. Finally, those imine bonds must be reduced to achieve irreversible secondary amine bonds between the protein and the carrier.[53,54] Under alkaline conditions, glyoxyl groups establish a multivalent covalent attachment with those protein regions that display the highest amount of most reactive lysine residues, rigidifying such protein regions.[55] The main drawbacks of this chemistry are the mandatory alkaline pH (around 10) needed to achieved the multivalent immobilization and the reduction step required to irreversibly immobilize the protein.[56] In spite of such disadvantages, carriers activated with glyoxyl groups promote an intense multivalent protein immobilization that has stabilized a plethora of proteins by a factor of 100-1000.[53,57]

Epoxide groups, unlike glyoxyl groups, can be attacked by a larger battery of protein nucleophiles such as Cys, His, Asp, Glu, Tyr and of course Lys. This nucleophilic attack yields irreversible secondary amine bonds without requiring any reduction step. Nevertheless, after the immobilization, the

remaining epoxy groups must be blocked by aminated or thiolated compounds to deactivate the surface in order to avoid undesired post-immobilization interactions. Remarkably, the vast majority of economically viable carriers based on polymetacrylate are activated with epoxide groups which have allowed industrial exploitation of this chemistry.[55,58] The biggest limitation of this immobilization chemistry is the low reactivity of the epoxy groups. Consequently, this chemistry promotes lower stabilization factors than the glyoxyl under comparable conditions (carrier activation degree and nature, enzyme orientation, etc.).

Table 1.2. Characteristics, advantages and drawbacks of most common enzyme immobilization methods.

Method	Bonding type	Advantages	Drawbacks
Adsorption/ Ionic bonding	Hydrophobic, *Van der Waals* or ionic interactions	Simple and economical Soft conformational change of the enzyme Can be recycled, regenerated and reused	Desorption Non-specific adsorption
Covalent binding	Chemical binding between functional groups of the enzyme and carrier	No enzyme release Potential for enzyme stabilization	Matrix and enzyme are not regenerable Major loss of activity
Entrapment	Occlusion of an enzyme within a polymeric network	No chemical modification Wide applicability for multimeric enzymes Easy handling and reusage	Mass transfer limitations Enzyme release
Cross-linking	Covalent bonds between enzymes by a functional reactant	Strong linkage – low enzyme release Biocatalyst stabilization	Mass transfer limitations Loss of activity

MOLECULAR IMAGING

Molecular imaging can be defined as a set of non-invasive techniques that allow the visualization of cell function and the monitoring of molecular processes in living organisms. Since the 90's, molecular imaging has opened a wide range of possibilities for the investigation of biological, physiological and medical processes which cannot be studied using other techniques.[59-61] Positron emission tomography (PET), single photon emission computerized tomography (SPECT) and optical/fluoresce imaging are considered molecular imaging techniques.

The anatomical information provided by molecular imaging techniques is usually scarce. Thus, both in the clinical and in the preclinical settings, such techniques are combined with other modalities able to provide accurate anatomical information. The combination of the resulting images (multimodality) offers information at the anatomical and molecular levels. Anatomical modalities include magnetic resonance imaging (MRI) and computed tomography (CT). Under the administration of a contrast agent, these modalities can be also considered molecular imaging modalities.

It is worth mentioning that each imaging modality has strengths and limitations. Thus, while nuclear imaging techniques (PET and SPECT) offer unparalleled sensitivity, they rarely reach a resolution below 1 mm in the preclinical setting and a few mm in the clinical systems. On the contrary, MRI can offer high resolution (up to a few micrometers) while its sensitivity is low (**Table 1.3**). Consequently, the application of one modality or another will depend on the problem under investigation and often the combination of two or more modalities will provide the most accurate data.

Table 1.3. Properties of most common clinical and pre-clinical imaging modalities.[59,60,62-66]

Technique	Energy used	Common contrast agents	Imaging agent mass	Spatial resolution	Temporal resolution	Sensitivity of detection	Penetration depth	Quantification efficiency
CT	X rays	I or Ba agents	mg range	0.03-1 mm	Minutes	0.1 mol.l^{-1}	>300 mm	---
SPECT	γ rays	γ emitters	<1 ng	0.5-15 mm	Minutes	10^{-11} mol.l^{-1}	>300 mm	High
PET	Annihilation photons	β$^+$ emitters	<1 ng	1-10 mm	Seconds-minutes	10^{-12} mol.l^{-1}	>300 mm	High
MRI	Radio frequency waves	Gd^{3+} agents or Fe$_3$O$_4$ nanoparticles	0.01-100mg	0.03-1mm	Minutes-hours	10^{-5} mol.l^{-1}	>300 mm	Medium
Optical	Visible to infrared light	Fluorophores or lanthanides	<1 ng-10mg	2-10 mm	Seconds-minutes	10^{-11} mol.l^{-1}	1-20 mm	Medium

Nuclear Imaging techniques

Nuclear imaging techniques rely on the administration of a radiotracer, i.e., a molecule labeled with a radioactive isotope to enable external and non-invasive detection. Gamma ray-emitters are appropriate radioisotopes because high-energy gamma rays can travel through biological tissues without suffering significant scatter or attenuation. These gamma rays can be detected using specific instrumentation, and the original concentration of radiotracer can be accurately quantified using tomographic reconstruction algorithms. As a result, a series of tomographic images conveying information on absolute radioisotope concentration can be obtained over time, *in vivo* and in a non- invasive way. Positron emission tomography (PET), single photon emission computed tomography (SPECT) and scintigraphy are nuclear imaging techniques. Nowadays, these techniques are available in combination with anatomical imaging such as CT or MRI (**Figure 1.3**).

Positron emission tomography will be the only technique described in detail in this chapter because it was the only modality used in the context of this PhD thesis.
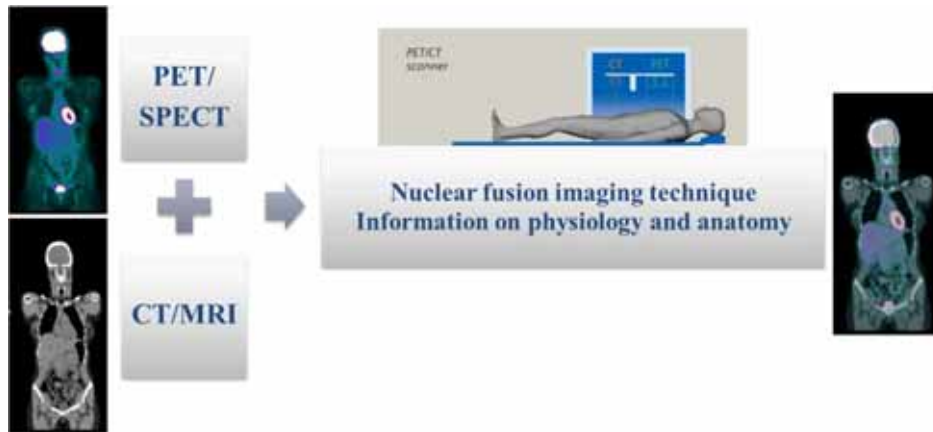

Figure 1.3. Fusion modalities of medicine nuclear techniques.

Positron emission tomography (PET)

Positron emission tomography relies on positrons (β^+) emitted from radioisotopes. The positron, after travelling short distances (few millimeters) within the body annihilates with an electron in the surrounding matter. The combined mass of the positron and the electron is converted into two collinear ɣ photons with 511 keV each travelling in opposite directions (annihilation). These gamma rays can be detected by especial detectors displayed in a ring surrounding the object of study. By simultaneous detection of both 511 keV γ rays, lines of response (LORs) are identified and used to locate the position in which the annihilation

event occurred. The detection of hundreds of thousands of photons enables the generation of an image (**Figure 1.4**).
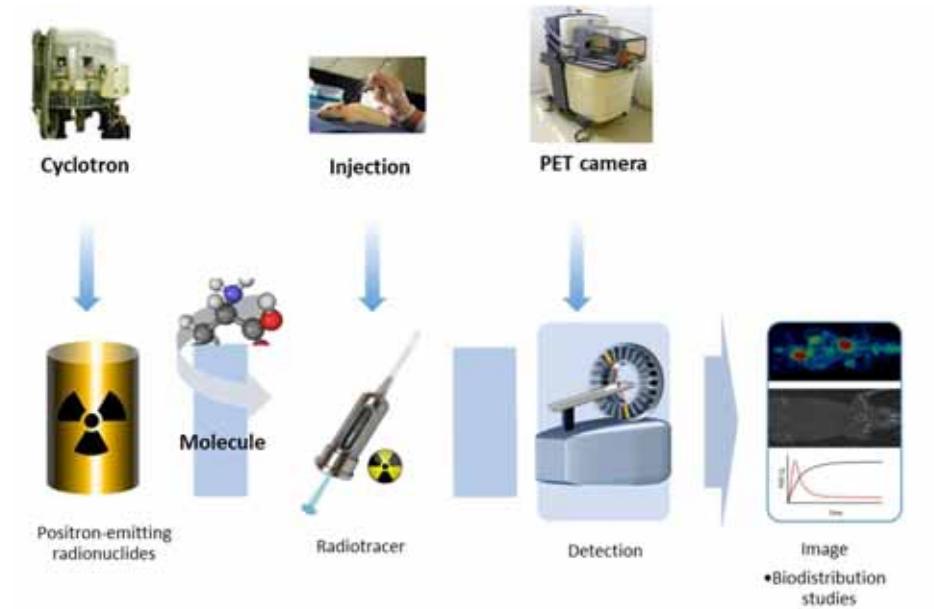
Figure 1.4. Key steps involved in the development of a molecular imaging study.

PET allows whole body 3D scanning and is commonly associated with CT, or more recently with MRI. This improves the limitations of its poor anatomic correlation and allows the generation of an attenuation map for attenuation correction during image reconstruction. In the clinical field, PET is widely used to image cancer and inflammation states through a fluorinated analogue of glucose, 2-[^{18}F]fluoro-2-deoxy-glucose ([^{18}F]FDG), that can identify changes in cellular glucose metabolism during inflammatory processes or related with the hyperactivity of cancer cells. PET can also be used to investigate more specific physiological and

molecular mechanisms of human disease through the use of appropriate radiolabeled imaging probes and to study the biodistribution of new drugs and the effectiveness of new therapies.[60]
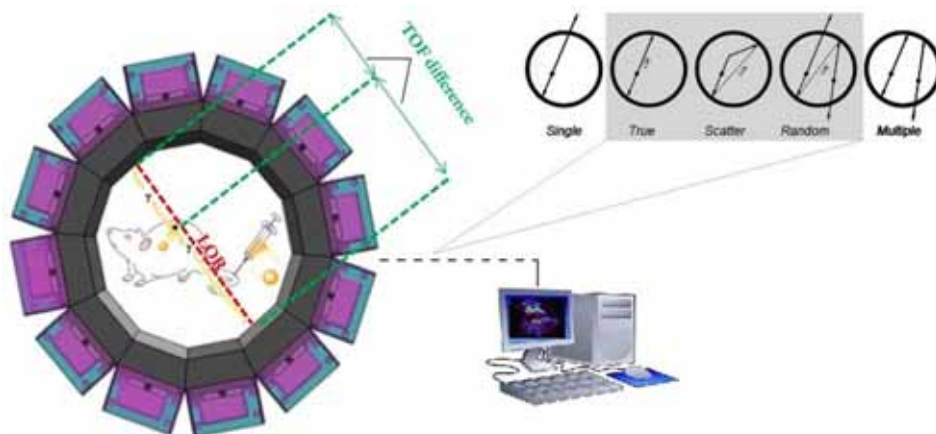
Figure 1.5. A simplified diagram illustrating the principles of PET scan.

Fluorine-18 (^{18}F) and carbon-11 (^{11}C) are frequently used radionuclides in PET. Nitrogen-13 (^{13}N) and oxygen-15 (^{15}O) are also used to a lesser extent (see **Table 1.4**). This is, in part, due to the fact that they can be produced efficiently in biomedical cyclotrons and have a radioactive decay almost exclusively by β^+ emission, but especially because they are isotopes of elements with low atomic mass that are highly prevalent in all organic molecules. Hence, any molecule of interest can *a priori* be radiolabeled with one of these positron emitters without modifying its biological activity. In the context of this PhD thesis, ^{13}N was the PET isotope exploited.

Table 1.4. Features of most common radionuclides used in PET. Adapted from references [67] and [68].

Radionuclide	$T_{1/2}$	Nuclear reaction	Target	Primary precursors	Decay product
^{15}O	2.04 min	$^{14}N(d,n)^{15}O$	$N_2(+O_2)$	$[^{15}O]O_2$	^{15}N
^{13}N	9,97 min	$^{16}O(p,\alpha)^{13}N$	H_2O $H_2O+EtOH$	$[^{13}N]NO_{2/3}$ $[^{13}N]NH_3$	^{13}C
^{11}C	20.4 min	$^{14}N(p,\alpha)^{11}C$	$N_2(+O_2)$ $N_2(+H_2)$	$[^{11}C]CO_2$ $[^{11}C]CH_4$	^{11}B
^{18}F	109.8 min	$^{20}Ne(d,\alpha)^{18}F$ $^{18}O(p,n)^{18}F$	$Ne(+F_2)$ $[^{18}O]H_2O$	$[^{18}F]F_2$ $[^{18}F]F^-$	^{18}O

Nitrogen-13

Nitrogen-13 is the longest-lived radioisotope of nitrogen and has been used mostly under the chemical form $[^{13}N]NH_3$ or $[^{13}N]$amino acids. Nitrogen-13 with high specific activity can be generated by proton irradiation of pure water *via* the $^{16}O(p,\alpha)^{13}N$ nuclear reaction. It decays by positron emission to its stable isotope carbon-13. The nitrogen-13 generated by irradiation of pure water is a mixture of radiolabeled nitrate ($[^{13}N]NO_3^-$), nitrite ($[^{13}N]NO_2^-$) and ammonia ($[^{13}N]NH_3$), being $[^{13}N]NO_3^-$ the major species (approx. 85% of total radioactivity).[69] The $[^{13}N]NO_3^-$ can be reduced to $[^{13}N]NO_2^-$, which can be used as labeling agent for the synthesis of a wide variety of labeled species, including nitrosothiols, nitrosamines, azo derivatives and triazoles.[70-75]

Cyclotron produced $[^{13}N]NO_3^-$ can be also reduced to $[^{13}N]NH_3$ by classical or in-target reduction methods.[76] Classical reduction methods include the treatment with titanium hydroxide,[77] Raney-nickel catalyst,[78] or Devarda's alloy.[79] More commonly, $[^{13}N]NH_3$ can be generated directly in the irradiated target by the addition of ethanol,[80,81] hydrogen gas[80] or methane[82] to the pure water, which act as scavengers and prevent radiolytic oxidation of the ammonia. Ammonia can be also produced in-target using

cryogenic targets.[83] Besides direct application as flow and perfusion marker,[84-86] [^{13}N]NH$_3$ is the main precursor for the synthesis of natural amino acids.[57,87-96]

REFERENCES

(1) Illanes, A.: *Enzyme Biocatalysis: Principles and Applications*; Springer Netherlands, 2008.

(2) DiCosimo, R.; McAuliffe, J.; Poulose, A. J.; Bohlmann, G. Industrial use of immobilized enzymes. *Chemical Society Reviews* **2013**, *42*, 6437-6474.

(3) Tao, J.; Lin, G. Q.; Liese, A.: *Biocatalysis for the Pharmaceutical Industry: Discovery, Development, and Manufacturing*; Wiley, 2009.

(4) Pollard, D. J.; Woodley, J. M. Biocatalysis for pharmaceutical intermediates: the future is now. *Trends in biotechnology* **2007**, *25*, 66-73.

(5) Patel, R. N.: *Biocatalysis in the Pharmaceutical and Biotechnology Industries*; CRC Press, 2006.

(6) Homaei, A. A.; Sariri, R.; Vianello, F.; Stevanato, R. Enzyme immobilization: an update. *Journal of Chemical Biology* **2013**, *6*, 185-205.

(7) Bommarius, A. S. Biocatalysis: A Status Report. *Annual review of chemical and biomolecular engineering* **2015**, *6*, 319-345.

(8) da Silva, E. S.; Gomez-Vallejo, V.; Llop, J.; Lopez-Gallego, F. Efficient nitrogen-13 radiochemistry catalyzed by a highly stable immobilized biocatalyst. *Catalysis Science & Technology* **2015**.

(9) Bezborodov, A. M.; Zagustina, N. A. Enzymatic biocatalysis in chemical synthesis of pharmaceuticals (Review). *Applied Biochemistry and Microbiology* **2016**, *52*, 237-249.

(10) Bolivar, J. M.; Eisl, I.; Nidetzky, B. Advanced characterization of immobilized enzymes as heterogeneous biocatalysts. *Catalysis Today* **2016**, *259, Part 1*, 66-80.

(11) Sheldon, R. A.; van Pelt, S. Enzyme immobilisation in biocatalysis: why, what and how. *Chem Soc Rev* **2013**, *42*, 6223-6235.

(12) Reetz, M. T. What are the Limitations of Enzymes in Synthetic Organic Chemistry? *Chemical record (New York, N.Y.)* **2016**, *16*, 2449-2459.

(13) Bickerstaff, G.: *Immobilization of Enzymes and Cells*; Humana Press, 1996.

(14) Datta, S.; Christena, L. R.; Rajaram, Y. R. S. Enzyme immobilization: an overview on techniques and support materials. *3 Biotech* **2013**, *3*, 1-9.

(15) Fessner, W. D.: *Biocatalysis: From Discovery to Application*; Springer Berlin Heidelberg, 2000.

(16) Guisan, J. M.: *Immobilization of Enzymes and Cells*; Humana Press, 2006.

(17) Katchalski-Katzir, E. Immobilized enzymes--learning from past successes and failures. *Trends in biotechnology* **1993**, *11*, 471-478.

(18) Mohamad, N. R.; Marzuki, N. H. C.; Buang, N. A.; Huyop, F.; Wahab, R. A. An overview of technologies for immobilization of enzymes and surface analysis techniques for immobilized enzymes. *Biotechnology, Biotechnological Equipment* **2015**, *29*, 205-220.

(19) Blanco, R. M.; Terreros, P.; Fernández-Pérez, M.; Otero, C.; Díaz-González, G. Functionalization of mesoporous silica for lipase immobilization: Characterization of the support and the catalysts. *Journal of Molecular Catalysis B: Enzymatic* **2004**, *30*, 83-93.

(20) Carlsson, N.; Gustafsson, H.; Thörn, C.; Olsson, L.; Holmberg, K.; Åkerman, B. Enzymes immobilized in mesoporous silica: A physical–chemical perspective. *Advances in Colloid and Interface Science* **2014**, *205*, 339-360.

(21) Qhobosheane, M.; Santra, S.; Zhang, P.; Tan, W. Biochemically functionalized silica nanoparticles. *Analyst* **2001**, *126*, 1274-1278.

(22) Bharti, C.; Nagaich, U.; Pal, A. K.; Gulati, N. Mesoporous silica nanoparticles in target drug delivery system: A review. *International Journal of Pharmaceutical Investigation* **2015**, *5*, 124-133.

(23) Liberman, A.; Mendez, N.; Trogler, W. C.; Kummel, A. C. Synthesis and surface functionalization of silica nanoparticles for nanomedicine. *Surface science reports* **2014**, *69*, 132-158.

(24) Wang, Y.; Caruso, F. Mesoporous Silica Spheres as Supports for Enzyme Immobilization and Encapsulation. *Chemistry of Materials* **2005**, *17*, 953-961.

(25) Takahashi, H.; Li, B.; Sasaki, T.; Miyazaki, C.; Kajino, T.; Inagaki, S. Immobilized enzymes in ordered mesoporous silica materials and improvement of their stability and catalytic activity in an organic solvent. *Microporous and Mesoporous Materials* **2001**, *44–45*, 755-762.

(26) Luechinger, M.; Prins, R.; Pirngruber, G. D. Functionalization of silica surfaces with mixtures of 3-aminopropyl and methyl groups. *Microporous and Mesoporous Materials* **2005**, *85*, 111-118.

(27) Maria Chong, A. S.; Zhao, X. S.; Kustedjo, A. T.; Qiao, S. Z. Functionalization of large-pore mesoporous silicas with organosilanes by direct synthesis. *Microporous and Mesoporous Materials* **2004**, *72*, 33-42.

(28) Lian, X.; Fang, Y.; Joseph, E.; Wang, Q.; Li, J.; Banerjee, S.; Lollar, C.; Wang, X.; Zhou, H. C. Enzyme-MOF (metal-organic framework) composites. *Chem Soc Rev* **2017**.

(29) Zucca, P.; Fernandez-Lafuente, R.; Sanjust, E. Agarose and Its Derivatives as Supports for Enzyme Immobilization. *Molecules (Basel, Switzerland)* **2016**, *21*.

(30) Porath, J.; Axén, R. Immobilization of enzymes to agar, agarose, and sephadex support. *Methods in Enzymology* **1976**, *44*, 19-45.

(31) da Silva, E. S.; Gómez-Vallejo, V.; Llop, J.; López-Gallego, F. Structural, kinetic and operational characterization of an immobilized l-aminoacid dehydrogenase. *Process Biochemistry*.

(32) Kudina, O.; Zakharchenko, A.; Trotsenko, O.; Tokarev, A.; Ionov, L.; Stoychev, G.; Puretskiy, N.; Pryor, S. W.; Voronov, A.; Minko, S. Highly efficient phase boundary biocatalysis with enzymogel nanoparticles. *Angewandte Chemie (International ed. in English)* **2014**, *53*, 483-487.

(33) Nelson, J. M.; Griffin, E. G. Adsorption of invertase. *Journal of the American Chemical Society* **1916**, *38*, 1109-1115.

(34) Jesionowski, T.; Zdarta, J.; Krajewska, B. Enzyme immobilization by adsorption: a review. *Adsorption* **2014**, *20*, 801-821.

(35) Cao, L.; Schmid, R. D.: *Carrier-bound Immobilized Enzymes: Principles, Application and Design*; Wiley, 2006.

(36) Kimple, M. E.; Brill, A. L.; Pasker, R. L. Overview of Affinity Tags for Protein Purification. *Current protocols in protein science / editorial board, John E. Coligan ... [et al.]* **2013**, *73*, Unit-9.9.

(37) Agarwal, G.; Naik, R. R.; Stone, M. O. Immobilization of histidine-tagged proteins on nickel by electrochemical dip pen nanolithography. *J Am Chem Soc* **2003**, *125*, 7408-7412.

(38) Fischer, N. O.; Blanchette, C. D.; Chromy, B. A.; Kuhn, E. A.; Segelke, B. W.; Corzett, M.; Bench, G.; Mason, P. W.; Hoeprich, P. D. Immobilization of His-tagged proteins on nickel-chelating nanolipoprotein particles. *Bioconjugate chemistry* **2009**, *20*, 460-465.

(39) Hefti, M. H.; Milder, F. J.; Boeren, S.; Vervoort, J.; van Berkel, W. J. A His-tag based immobilization method for the preparation and reconstitution of apoflavoproteins. *Biochimica et biophysica acta* **2003**, *1619*, 139-143.

(40) Miyazaki, M.; Kaneno, J.; Yamaori, S.; Honda, T.; Briones, M. P.; Uehara, M.; Arima, K.; Kanno, K.; Yamashita, K.; Yamaguchi, Y.; Nakamura, H.; Yonezawa, H.; Fujii, M.; Maeda, H. Efficient immobilization of enzymes on microchannel surface through His-tag and application for microreactor. *Protein and peptide letters* **2005**, *12*, 207-210.

(41) Gupta, M. N.; Jain, S.; Roy, I. Immobilized metal affinity chromatography without chelating ligands: purification of soybean trypsin inhibitor on zinc alginate beads. *Biotechnology progress* **2002**, *18*, 78-81.

(42) Ovsejevi, K.; Manta, C.; Batista-Viera, F. Reversible covalent immobilization of enzymes via disulfide bonds. *Methods in molecular biology (Clifton, N.J.)* **2013**, *1051*, 89-116.

(43) Carlsson, J.; Axen, R.; Unge, T. Reversible, covalent immobilization of enzymes by thiol-disulphide interchange. *European journal of biochemistry* **1975**, *59*, 567-572.

(44) Gulla, K. C.; Gouda, M. D.; Thakur, M. S.; Karanth, N. G. Enhancement of stability of immobilized glucose oxidase by modification of free thiols generated by reducing disulfide bonds and using additives. *Biosensors and Bioelectronics* **2004**, *19*, 621-625.

(45) Godoy, C. A.; de las Rivas, B.; Grazu, V.; Montes, T.; Guisan, J. M.; Lopez-Gallego, F. Glyoxyl-disulfide agarose: a tailor-made support for site-directed rigidification of proteins. *Biomacromolecules* **2011**, *12*, 1800-1809.

(46) Walt, D. R.; Agayn, V. I. The chemistry of enzyme and protein immobilization with glutaraldehyde. *TrAC Trends in Analytical Chemistry* **1994**, *13*, 425-430.

(47) Lopez-Gallego, F.; Guisan, J. M.; Betancor, L. Glutaraldehyde-mediated protein immobilization. *Methods in molecular biology (Clifton, N.J.)* **2013**, *1051*, 33-41.

(48) Singh, B. D.: *Biotechnology: Expanding Horizons*; Kalyani Publishers, 2012.

(49) Aehle, W.: *Enzymes in Industry*; Wiley, 2008.

(50) Axen, R.; Porath, J.; Ernback, S. Chemical Coupling of Peptides and Proteins to Polysaccharides by Means of Cyanogen Halides. *Nature* **1967**, *214*, 1302-1304.

(51) Schnapp, J.; Shalitin, Y. Immobilization of enzymes by covalent binding to amine supports via cyanogen bromide activation. *Biochemical and Biophysical Research Communications* **1976**, *70*, 8-14.

(52) Kavran, J. M.; Leahy, D. J. Coupling Antibody to Cyanogen Bromide-Activated Sepharose. *Methods in enzymology* **2014**, *541*, 27-34.

(53) Lopez-Gallego, F.; Fernandez-Lorente, G.; Rocha-Martin, J.; Bolivar, J. M.; Mateo, C.; Guisan, J. M. Stabilization of enzymes by multipoint covalent immobilization on supports activated with glyoxyl groups. *Methods in molecular biology (Clifton, N.J.)* **2013**, *1051*, 59-71.

(54) Mateo, C.; Palomo, J. M.; Fuentes, M.; Betancor, L.; Grazu, V.; López-Gallego, F.; Pessela, B. C. C.; Hidalgo, A.; Fernández-Lorente, G.;

Fernández-Lafuente, R.; Guisán, J. M. Glyoxyl agarose: A fully inert and hydrophilic support for immobilization and high stabilization of proteins. *Enzyme and Microbial Technology* **2006**, *39*, 274-280.

(55) Santos, J. C. S. d.; Barbosa, O.; Ortiz, C.; Berenguer-Murcia, A.; Rodrigues, R. C.; Fernandez-Lafuente, R. Importance of the Support Properties for Immobilization or Purification of Enzymes. *ChemCatChem* **2015**, *7*, 2413-2432.

(56) Grazu, V.; Betancor, L.; Montes, T.; Lopez-Gallego, F.; Guisan, J. M.; Fernandez-Lafuente, R. Glyoxyl agarose as a new chromatographic matrix. *Enzyme and Microbial Technology* **2006**, *38*, 960-966.

(57) da Silva, E. S.; Gómez-Vallejo, V.; Llop, J.; López-Gallego, F. Structural, kinetic and operational characterization of an immobilized l-aminoacid dehydrogenase. *Process Biochemistry* **2017**.

(58) Barbosa, O.; Torres, R.; Ortiz, C.; Berenguer-Murcia, A.; Rodrigues, R. C.; Fernandez-Lafuente, R. Heterofunctional supports in enzyme immobilization: from traditional immobilization protocols to opportunities in tuning enzyme properties. *Biomacromolecules* **2013**, *14*, 2433-2462.

(59) Tian, J.: *Molecular Imaging: Fundamentals and Applications*; Zhejiang University Press, 2013.

(60) James, M. L.; Gambhir, S. S. A molecular imaging primer: modalities, imaging agents, and applications. *Physiol. Rev.* **2012**, *92*, 897-965.

(61) Townsend, D. W.; Cheng, Z.; Georg, D.; Drexler, W.; Moser, E. Grand challenges in biomedical physics. *Front. Phys.* **2013**, *1*, 1-6.

(62) Levin, C. S. New imaging technologies to enhance the molecular sensitivity of positron emission tomography. *Proceedings of the IEEE* **2008**, *96*, 439-467.

(63) Schmitz, G. Ultrasonic imaging of molecular targets. *Basic Res. Cardiol.* **2008**, *103*, 174-181.

(64) Fass, L. Imaging and cancer: a review. *Mol. Oncol.* **2008**, *2*, 115-152.

(65) Liu, X.; Jia, L. The Conduct of Drug Metabolism Studies Considered Good Practice (I): Analytical Systems and In Vivo Studies. *Curr. Drug Metab.* **2007**, *8*, 815-821.

(66) Sigel, H.: *Metal Ions in Biological Systems: Volume 40: The Lanthanides and Their Interrelations with Biosystems*; Taylor & Francis: Switzerland, 2003.

(67) Miller, P. W.; Long, N. J.; Vilar, R.; Gee, A. D. Synthesis of 11C, 18F, 15O, and 13N radiolabels for positron emission tomography. *Angewandte Chemie (International ed. in English)* **2008**, *47*, 8998-9033.

(68) De Lima, J. J.: *Nuclear Medicine Physics*; CRC Press, 2016.

(69) Miller, P. W.; Long, N. J.; Vilar, R.; Gee, A. D. Synthesis of 11C, 18F, 15O, and 13N Radiolabels for Positron Emission Tomography. *Angewandte Chemie International Edition* **2008**, *47*, 8998-9033.

(70) Llop, J.; Gómez-Vallejo, V.; Bosque, M.; Quincoces, G.; Peñuelas, I. Synthesis of S-[13N]nitrosoglutathione (13N-GSNO) as a new potential PET imaging agent. *Applied Radiation and Isotopes* **2009**, *67*, 95-99.

(71) Gómez-Vallejo, V.; Kato, K.; Oliden, I.; Calvo, J.; Baz, Z.; Borrell, J. I.; Llop, J. Fully automated synthesis of 13N-labeled nitrosothiols. *Tetrahedron Letters* **2010**, *51*, 2990-2993.

(72) Gómez-Vallejo, V.; Kato, K.; Hanyu, M.; Minegishi, K.; Borrell, J. I.; Llop, J. Efficient system for the preparation of [13N]labeled nitrosamines. *Bioorganic & Medicinal Chemistry Letters* **2009**, *19*, 1913-1915.

(73) Gaja, V.; Gomez-Vallejo, V.; Puigivila, M.; Perez-Campana, C.; Martin, A.; Garcia-Osta, A.; Calvo-Fernandez, T.; Cuadrado-Tejedor, M.; Franco, R.; Llop, J. Synthesis and evaluation of 13N-labelled azo compounds for beta-amyloid imaging in mice. *Molecular imaging and biology : MIB : the official publication of the Academy of Molecular Imaging* **2014**, *16*, 538-549.

(74) Joshi, S. M.; de Cozar, A.; Gomez-Vallejo, V.; Koziorowski, J.; Llop, J.; Cossio, F. P. Synthesis of radiolabelled aryl azides from diazonium salts: experimental and computational results permit the identification of the preferred mechanism. *Chemical communications (Cambridge, England)* **2015**, *51*, 8954-8957.

(75) Joshi, S. M.; Gomez-Vallejo, V.; Salinas, V.; Llop, J. Synthesis of 13N-labelled polysubstituted triazoles via Huisgen cycloaddition. *RSC Advances* **2016**, *6*, 109633-109638.

(76) Suzuki, K.; Yoshida, Y. Production of [13N]NH3 with ultra-high specific activity. *Applied Radiation and Isotopes* **1999**, *50*, 497-503.

(77) Krizek, H.; Lembares, N.; Dinwoodie, R.; Gloria, I.; Lathrop, K. A.; Harper, P. V. Production of radiochemically pure 13NH3 for biomedical studies using the $^{16}O(p,a)^{13}N$ reaction. *J. Nucl. Med.* **1973**, 629.

(78) Dence, C. S.; Welch, M. J.; Hughey, B. J.; Shefer, R. E.; Klinkowstein, R. E. Production of [13N]ammonia applicable to low energy accelerators. *Nucl Med Biol* **1994**, *21*, 987-996.

(79) Sobczyk, D. P.; van Grondelle, J.; de Jong, A. M.; de Voigt, M. J. A.; van Santen, R. A. Production of chemically pure gaseous [13N]NH3 pulses for PEP studies using a modified DeVarda reduction. *Applied Radiation and Isotopes* **2002**, *57*, 201-207.

(80) Berridge, M. S.; Landmeier, B. J. In-target production of [13N]ammonia: Target design, products, and operating parameters. *Applied Radiation and Isotopes* **1993**, *44*, 1433-1441.

(81) Kumar, R.; Singh, H.; Jacob, M.; Anand, S. P.; Bandopadhyaya, G. P. Production of nitrogen-13-labeled ammonia by using 11MeV medical cyclotron: our experience. *Hellenic journal of nuclear medicine* **2009**, *12*, 248-250.

(82) Krasikova, R. N.; Fedorova, O. S.; Korsakov, M. V.; Landmeier Bennington, B.; Berridge, M. S. Improved [13N]ammonia yield from the proton irradiation of water using methane gas. *Applied Radiation and Isotopes* **1999**, *51*, 395-401.

(83) Firouzbakht, M. L.; Schlyer, D. J.; Wolf, A. P.; Fowler, J. S. Mechanism of nitrogen-13-labeled ammonia formation in a cryogenic water target. *Nucl Med Biol* **1999**, *26*, 437-441.

(84) Kitsiou, A. N.; Bacharach, S. L.; Bartlett, M. L.; Srinivasan, G.; Summers, R. M.; Quyyumi, A. A.; Dilsizian, V. 13N-Ammonia myocardial blood flow and uptake. *Relation to functional outcome of asynergic regions after revascularization* **1999**, *33*, 678-686.

(85) Xiangsong, Z.; Xinjian, W.; Yong, Z.; Weian, C. 13N-NH3: a selective contrast-enhancing tracer for brain tumor. *Nuclear medicine communications* **2008**, *29*, 1052-1058.

(86) Di Carli, M. F.; Lipton, M. J.: *Cardiac PET and PET/CT Imaging*; Springer New York, 2007.

(87) Gelbard, A. S.; Benua, R. S.; Reiman, R. E.; McDonald, J. M.; Vomero, J. J.; Laughlin, J. S. Imaging of the Human Heart after Administration of L-(N-13)Glutamate. *Journal of Nuclear Medicine* **1980**, *21*, 988-991.

(88) Barrio, J. R.; Baumgartner, F. J.; Henze, E.; Stauber, M. S.; Egbert, J. E.; MacDonald, N. S.; Schelbert, H. R.; Phelps, M. E.; Liu, F.-T. Synthesis and Myocardial Kinetics of N-13 and C-11 Labeled Branched-Chain l-Amino Acids. *Journal of Nuclear Medicine* **1983**, *24*, 937-944.

(89) da Silva, E. S.; Gómez-Vallejo, V.; Baz, Z.; Llop, J.; López-Gallego, F. Efficient Enzymatic Preparation of 13N-Labelled Amino Acids: Towards Multipurpose Synthetic Systems. *Chemistry – A European Journal* **2016**, *22*, 13619-13626.

(90) Baumgartner, F. J.; Barrio, J. R.; Henze, E.; Schelbert, H. R.; MacDonald, N. S.; Phelps, M. E.; Kuhl, D. E. 13N-labeled L-amino acids for in vivo assessment of local myocardial metabolism. *Journal of medicinal chemistry* **1981**, *24*, 764-766.

(91) Lambrecht, R. H. D.; Slegers, G.; Claeys, A.; Gillis, E.; Vandecasteele, C. Enzymatic synthesis of radiopharmaceutically pure 13N-labelled L-glutamate. *Radiochemical and Radioanalytical Letters* **1983**, *58*, 39-48.

(92) Helus, F.; Weber, K.; Zeisler, S.; Maier-Borst, W. An automatic system for the enzymatic synthesis of13N-glutamate. *Journal of Radioanalytical and Nuclear Chemistry* **1991**, *155*, 9-13.

(93) Gelbard, A. S.; Cooper, A. J. L.; Asano, Y.; Nieves, E.; Filc-Dericco, S.; Rosenspire, K. C. Methods for the enzymatic synthesis of tyrosine and phenylalanine labeled with nitrogen-13. *International Journal of Radiation Applications and Instrumentation. Part A. Applied Radiation and Isotopes* **1990**, *41*, 229-233.

(94) Gelbard, A. S.; Kaseman, D. S.; Rosenspire, K. C.; Meister, A. Enzymatic syntheses of phosphate, l-citrulline, and N-carbamyl l-aspartate labeled with either 13N or 11C. *International Journal of Nuclear Medicine and Biology* **1985**, *12*, 235-242.

(95) Cooper, A. J.; Gelbard, A. S. The use of immobilized glutamate dehydrogenase to synthesize 13N-labeled L-amino acids. *Anal Biochem* **1981**, *111*, 42-48.

(96) Elmaleh, D.; Hnatowitch, D.; Kulprathipanja, S. A novel synthesis of 13N-L-aspargine. *Journal of Labelled Compounds and Radiopharmaceuticals* **1979**, *16*, 92-93.

Chapter 2

State-of-art: biocatalysis in radiochemistry

INTRODUCTION

Biocatalysis, although surprisingly underutilized in radiochemistry, constitutes an attractive alternative to conventional chemistry. First, enzymes present an exquisite chemical selectivity and high turnover numbers; second, enzymes were evolved to work under physiological conditions, where the concentration of the metabolites is tightly regulated and are rarely in excess. This scenario resembles the conditions for radiochemical reactions where the concentration of the radioactive precursors is extremely low; third, enzymes are the most sophisticated chiral catalysts yielding enantiopure products in most of the cases. Therefore, by harnessing the enzyme properties in PET radiochemistry, chemists have the opportunity to synthesize radiotracers through fast and selective biosynthetic schemes, while minimizing the formation of side products and preventing the formation of racemic mixtures.

Hitherto, enzymes have been employed to radiosynthesize [^{13}N/^{11}C]amino acids, [^{18}F]nucleoside derivatives and [^{11}C/^{18}F]proteins. Additionally, enzymatic reactions have been employed to regio- and stereospecifically introduce radioactive precursors into a plethora of biological molecules.[1,2] Enzyme immobilization has also been utilized to achieve high radiochemical yields during repeated batch cycles.[3-6] Most of the advances in the application of enzymatic reactions in radiochemistry occurred in the 70′s-80′s, and were summarized by Gelbard in 1981.[7] Since then, to the best of our knowledge, the role of biocatalysis in radiochemistry has never been reviewed again. The aim of this chapter is to provide an overview of the biocatalytic approaches that have been reported during the last four decades for the synthesis of PET radiotracers (see **Figure 2.1**) using nitrogen-13, carbon-11, and fluorine-18.
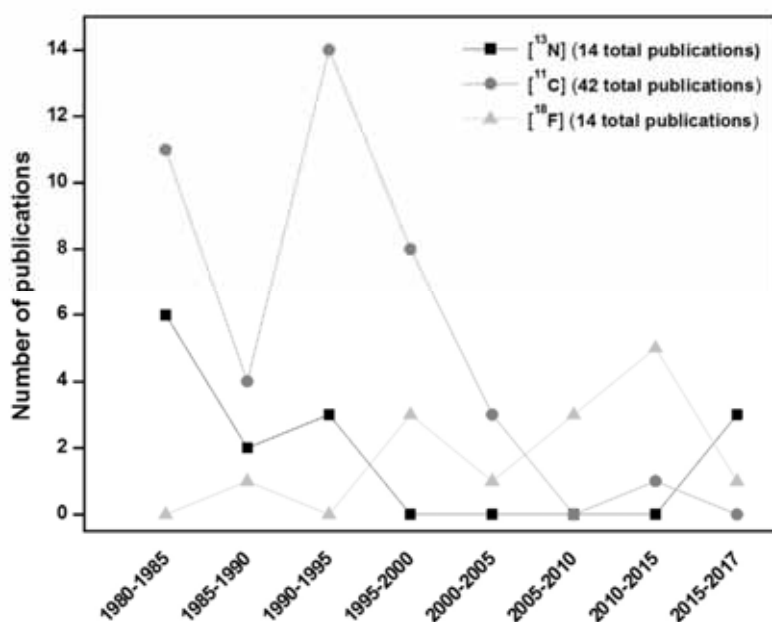
Figure 2.1. Number of scientific publications reporting the application of biocatalysis to radiochemistry since 1980. Data obtained using PubMed, 2015 NLM and Web of Science, 2013 Thomson Reuters.

Nitrogen-13

Nitrogen-13 is the longest-lived radioisotope of nitrogen and has been used mostly under the chemical form $[^{13}N]NH_3$ or $[^{13}N]$amino acids. Nitrogen-13 with high specific activity can be generated by proton irradiation of pure water *via* the $^{16}O(p,\alpha)^{13}N$ nuclear reaction. The nitrogen-13 generated is a mixture of radiolabeled nitrate ($[^{13}N]NO_3^-$), nitrite ($[^{13}N]NO_2^-$) and ammonia ($[^{13}N]NH_3$), being $[^{13}N]NO_3^-$ the major species (approx. 85% of total radioactivity). The $[^{13}N]NO_3^-$ can be reduced to $[^{13}N]NO_2^-$, which can be used as labeling agent for the synthesis of a wide variety of labeled

species, including nitrosothiols, nitrosamines, azo derivatives and triazoles.[8-13] This reduction can be easily performed by chemical methods using cadmium-copper activated columns.[8,14]

As mentioned in the previous chapter, cyclotron produced $[^{13}N]NO_3^-$ can be also reduced to $[^{13}N]NH_3$ by classical or in-target reduction methods.[15] Besides direct application as flow and perfusion marker,[16-18] $[^{13}N]NH_3$ is the main precursor for the synthesis of natural amino acids. In general, $[^{13}N]NH_3$ can be incorporated into amino acids through three main enzymatic routes (**Figure 2.2**): **a)** using amino acid dehydrogenases that catalyze the reductive amination of α-ketoacids using nicotinamide adenine dinucleotide (NADH) as redox cofactor and $[^{13}N]NH_3$ as the amine source;[1,2,19-26] **b)** using amino acid synthetases that catalyze the insertion of $[^{13}N]NH_3$ into the ω-carboxylic group of acidic amino acids by using adenosine triphosphate (ATP);[2,22,23,27] and **c)** using a bi-enzymatic system integrated by an amino acid dehydrogenase (usually glutamate dehydrogenase) that catalyzes the reductive amination of α-ketoglutarate to produce *L*-$[^{13}N]$glutamate, that is concurrently used by a transaminase that transfers the radiolabeled amine group to the target α-ketoacid to form the desired *L*-$[^{13}N]$amino acid.[2,22]
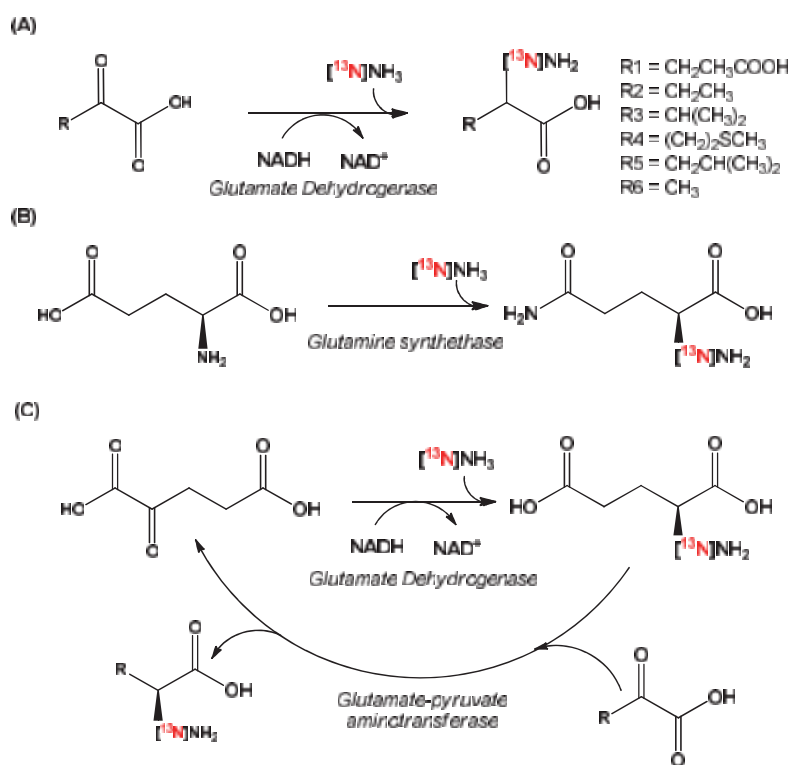
Figure 2.2. Examples of the main enzymatic routes to incorporate $[^{13}N]NH_3$ into amino acids. (**A**) Using amino acid dehydrogenases; (**B**) using amino acid synthetases and (**C**) using a bi-enzymatic system formed by an amino acid dehydrogenase and a transaminase.

These synthetic strategies have been often applied by using soluble enzymes (**Table 2.1**). This, in turn, leads to the potential contamination of the final preparation with pyrogenic enzymes and poses difficulty in the purification process.[7] This problem was smartly solved by immobilizing the enzymes on solid carriers through covalent and irreversible bonds. Several immobilized enzymes, including multi-enzyme systems, have been applied to the heterogeneous synthesis of ^{13}N-labeled amino acids (e.g. glutamine[22], glutamate[1,19,20,22-24], asparagine[27], citrulline[2],

aspartate[2,22], alanine[1,20,22]). These amino acids have been obtained with different radiochemical yields, ranging from 10% for L-[^{13}N]asparagine using an asparagine synthetase,[27] to 95% for L-[^{13}N]glutamate using a glutamate dehydrogenase.[23] The glutamate dehydrogenase proved versatile to synthesize a plethora of L-[^{13}N]amino acids beyond glutamate (see **Figure 2.2A**).[1,20] Some of the above-mentioned amino acids were investigated *in vivo* both in animals and humans in order to assess their biodistribution and metabolism.[19,20] The preparation of L-[^{13}N]glutamate was semi-automated in 1983 by Lambrecht *et al.*,[23] who could synthesize this labeled amino acid with high purity and high specific activity (1.11 GBq.μmol^{-1}) using a glutamate dehydrogenase immobilized on porous glass beads in short times (10 minutes). Later on, the same group adapted this methodology to the fabrication of β-[^{13}N]-nicotinamide adenine dinucleotide ([^{13}N]NAD) and γ-[^{13}N]aminobutyric acid ([^{13}N]GABA).[28,29] Finally, this technology was optimized to manufacture pure L-[^{13}N]glutamate through a full automated system.[24]

Besides amino acids, other biological molecules have been labeled with nitrogen-13 by using [^{13}N]NH$_3$ as the amine source and carbamyl phosphate synthase and carbamoyl transferases as the catalysts. Gelbard *et al.* synthesized [^{13}N]carbamyl phosphate, L-[ω-^{13}N]citrulline and [*carbamyl*-^{13}N]-L-aspartate using carbamyl phosphate synthetase co-immobilized with either aspartate transcarbamylase or ornithine transcarbamylase. These amino acid derivatives were obtained with radiochemical yields of around 15%. Labeled carbamyl phosphate could be obtained using carbamyl phosphate synthetase as the catalyst, [^{13}N]NH$_3$ as the ammonia source, carbamic acid as substrate and ATP as the cofactor; in a concurrent reaction, the corresponding transcarbamylase

transferred the carbamyl group to the ornithine or the aspartate to achieve the corresponding amino acid derivative.[2]

Table 2.1. Literature published on enzymatic reactions (functional group transfer and transformations) applied to nitrogen-13 chemistry since 1980. Entries are ordered chronologically.

Radionuclide	Biosynthetic route	Enzyme family	Reaction	Compound	Ref.
[13N]Ammonia	Asparagine synthetase	EC 6.3.5.4	Acid amide hydrolysis	L-[13N]Asparagine	27
[13N]Ammonia	Glutamate Dehydrogenase (Immobilized)	EC 1.4.1.2	Reductive amination	L-[13N]Glutamate	19,22
[13N]Ammonia	Glutamate Dehydrogenase Glutamate-Pyruvate Transaminase (Immobilized)	EC 1.4.1.2 / EC 2.6.1.2	Reductive amination	L-[13N]Alanine	22
[13N]Ammonia	Glutamine synthethase	EC 6.3.1.2	Acid amide hydrolysis	L-[13N]Glutamine	22
[13N]Ammonia	Aspartate ammonia-lyase	EC 4.3.1.1	Addition	L-[13N]Aspartate	22
[13N]Ammonia	Glutamate Dehydrogenase (immobilized/ semi-automated production method)	EC 1.4.1.2	Reductive amination	L-[13N]Glutamate	23
[13N]Ammonia	Glutamate Dehydrogenase (immobilized)	EC 1.4.1.3	Reductive amination	L-[13N]Glutamate L-α-[13N]Aminobutyrate L-[13N]Valine L-[13N]Methionine L-[13N]Leucine L-[13N]Alanine	1,20
[13N]Ammonia	Carbamyl phosphate synthetase (Co-immobilized)	EC 6.3.5.5	Phosphorylation/ Amination	[13N]Carbamyl phosphate	2
[13N]Ammonia	Ornithine transcarbamylase Carbamyl phosphate synthetase (Co-immobilized)	EC 2.1.3.3 / EC 6.3.5.5	Carbamoylation Phosphorylation/ Amination	L-[ϖ-13N]Citrulline	2
[13N]Ammonia	Aspartate transcarbamylase Carbamyl phosphate synthetase (Co-immobilized)	EC 2.1.3.2 / EC 6.3.5.5	Carbamoylation Phosphorylation/ Amination	[Carbamyl-13N] Carbamyl-L-aspartate	2
[13N]Ammonia	Glutamate dehydrogenase (Immobilized) Aspartate transaminase (Immobilized) Aspartate transcarbamylase (Immobilized)	EC 1.4.1.3 / EC 2.6.1.1 / EC 2.1.3.2	Reductive amination Transamination Carbamoylation	Carbamyl-L-[13N]Aspartate	2
[13N]Ammonia	NAD synthetase (Immobilized)	EC 6.3.1.5	Amide group transfer	[13N]-NAD	28

Radionuclide	Biosynthetic route	Enzyme family	Reaction	Compound	Ref.
[^{13}N]Ammonia	N.D. (two subsequent enzymatic Reaction)	N.D.	N.D.	[^{13}N]-GABA	29
[^{13}N]Ammonia (via L-[^{13}N]Glutamate)	Aspartate aminotransferase (Immobilized)	EC 2.6.1.1	Transamination	L-[^{13}N]Tyrosine	25
[^{13}N]Ammonia	Phenylalanine dehydrogenase (Immobilized)	EC 1.4.1.20	Reductive amination	L-[^{13}N]Phenylalanine L-[^{13}N]Tyrosine	25
[^{13}N]Ammonia	Glutamate Dehydrogenase (automated production method)	EC 1.4.1.2	Reductive amination	L-[^{13}N]Glutamate	24
[^{13}N]Nitrate	Nitrate reductase (Immobilized)	EC 1.7.1.1	Reduction	[^{13}N]Nitrite	30

Carbon-11

Over the last two decades of the 20th century, biocatalysis played an important role in the developments of carbon-11 radiochemistry. Carbon-11 is an attractive and important β^+ emitting radionuclide for the radiolabeling of molecules with biological activity due to the ubiquitous presence of carbon in natural products and drug-like compounds. The cyclotron production of carbon-11 is achieved by proton irradiation of nitrogen-14 *via* the ^{14}N(p,α)^{11}C nuclear reaction. By adding small amounts of O_2 or H_2 to the target, [^{11}C]CO_2 and [^{11}C]CH_4 are produced, respectively. One major drawback in [^{11}C]CO_2 production is the inevitable contamination of the cyclotron target and the gas lines with "cold" CO_2, which leads to a contamination of up to 1000 atoms of stable carbon per one carbon-11 atom produced, and results in low specific activities. This effect is less significant in the case of [^{11}C]CH_4.[31,32] Both [^{11}C]CO_2 and [^{11}C]CH_4 can be chemically derivatized to other ^{11}C-labeled precursors such as [^{11}C]hydrogen cyanide, [^{11}C]acetate, [^{11}C]methanol, [^{11}C]methyl iodide, [^{11}C]propionate and [^{11}C]carbonate. In this context, biocatalysis has exploited those precursors to incorporate carbon-11 into more than 50 biological targets (**Table 2.2**). In carbon-11 radiochemistry, as well as for

nitrogen-13, the use of immobilized enzymes is more popular than the use of their soluble counterparts, because the immobilized enzymes facilitate product purification and enzyme reutilization, as well as allow the enzyme integration into continuous flow reactions.

In a pioneering work in the enzymatic synthesis of ^{11}C-labeled radiotracers, a phosphoenolpyruvate carboxylase (EC$_{4.1.1.31}$) and aspartate transaminase (EC$_{2.6.1.1}$) were separately immobilized on sepharose activated with cyanogen bromide groups and applied for the synthesis of L-[4-^{11}C]aspartic acid using [^{11}C]CO$_2$ as the ^{11}C source.[33] In brief, cyclotron-produced [^{11}C]CO$_2$ and the appropriate substrate (phosphoenolpyruvate) were flushed through a column packed with immobilized carboxylase, generating [4-^{11}C]oxaloacetate that was subsequently contacted with L-glutamate and passed through a second packed column containing an immobilized aspartate transaminase, which enabled the amine transfer from L-glutamate to the [4-^{11}C]oxaloacetic acid to yield L-[4-^{11}C]aspartic acid (**Figure 2.3**). [^{11}C]CO$_2$ was also used as a radioactive precursor for the synthesis of several amino acid derivatives based on the coordinate action of carbamoyl phosphate synthetase and amino acid transaminases. This synthetic strategy has been very valuable for studying the L-glutamate metabolism in a variety of tissues.[2,33,34]
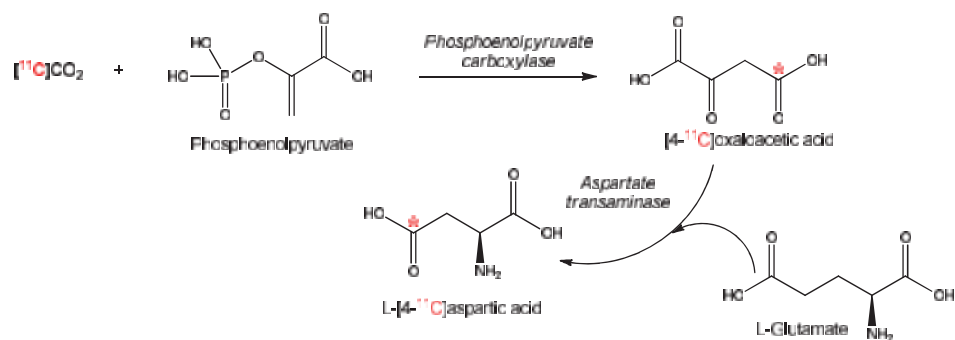
Figure 2.3. Schematic representation of the radiosynthesis of *L*-[4-^{11}C]aspartic acid. This radiosynthesis was performed using a phosphoenolpyruvate carboxylase (EC$_{4.1.1.31}$) and aspartate transaminase (EC$_{2.6.1.1}$) separately immobilized on sepharose activated with cyanogen bromide groups and [^{11}C]CO$_2$ as the ^{11}C source.

Enzymatic carbon-11 radiochemistry has also been applied to other carbon-11 precursors beyond [^{11}C]CO$_2$. For example, [^{11}C]cyanide was used as a radioactive precursor to synthesize *L*-[^{11}C]amino acids and other biological amines.[35] In this reaction scheme, *O*-acetyl-*L*-serine sulfhydrylase and γ-cyano-α-aminobutyric acid synthase (EC$_{2.5.1.49}$) catalyze the nitrilation of O-acetyl-*L*-serine and O-acetyl-*L*-homoserine to yield β-[^{11}C]cyano-*L*-alanine and γ-[^{11}C]cyano-α-amino-*L*-butyric acid, respectively. These intermediate nitriles were further converted into *L*-[4-^{11}C]aspartic acid and *L*-[5-^{11}C]glutamate by alkaline hydrolysis with 50-70% decay corrected radiochemical yields and radiochemical purities higher than 95% (**Figure 2.4**).[36,37] The same chemo-enzymatic route was applied to the synthesis of *L*-[*methyl*-^{11}C]methionine and its analogues [^{11}C]ethionine and [^{11}C]propionine using [^{11}C]cyanide as radioactive precursor and their corresponding *O*-acetyl-protected amino acids.[38]
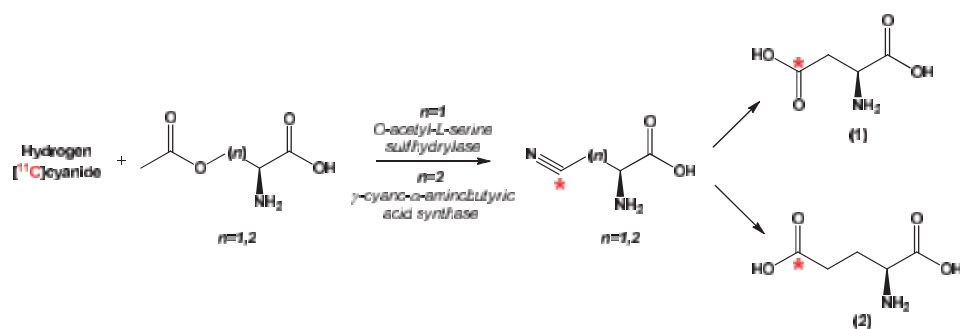
Figure 2.4. Schematic representation of the chemoenzymatic radiosynthesis of *L*-[4-^{11}C]aspartic acid (**1**) and *L*-[5-^{11}C]glutamate (**2**). The synthesis of these compounds was carried out using *O*-acetyl-*L*-serine sulfhydrylase and γ-cyano-α-aminobutyric acid synthase to catalyze the nitrilation of *O*-acetyl-*L*-serine and *O*-acetyl-*L*-homoserine to yield their intermediates β-[^{11}C]cyano-*L*-alanine and γ-[^{11}C]cyano-α-amino-*L*-butyric acid, respectively.

Another carbon-11 precursor that can be directly used by enzymes is [^{11}C]acetate which can be labeled in two different positions (carboxylic and 2-position).[39] [^{11}C]acetate is the main precursor to synthesize [^{11}C]acetyl-CoA,[40,41] one of the main hubs in the central metabolism of cells. [^{11}C]acetyl-CoA can be synthesized through two different enzymatic pathways; (i) a two-step cascade catalyzed by an acetate kinase (EC$_{2.7.2.1}$) that phosphorylates [^{11}C]acetate yielding [^{11}C]acetyl-phosphate, and a phosphotransacetylase (EC$_{2.3.1.8}$) that incorporates the coenzyme A into the phosphorylated intermediate yielding [^{11}C]acetyl-CoA; and (ii) a single-step reaction catalyzed by coenzyme A synthetase (EC$_{6.2.1.1}$) that directly incorporates coenzyme A into [^{11}C]acetate producing [^{11}C]acetyl-CoA. Interestingly, [^{11}C]acetyl-CoA has been used as a general acetylating agent to synthesize a variety of carbon-11 labeled molecules such as [^{11}C]acetyl-

L-carnitine,[41] *L*-[11C]carnitine,[41] [11C]acetyl-*L*-serotonin,[42] and [11C]*N*-acetyl-D-glucosamine[43].

[11C]methanol and [11C]propionate have also been employed sporadically for the enzymatic preparation of 11C-labeled radiotracers. For example, *L*-[11C]serine can be synthesized by an alcohol oxidase co-immobilized with a catalase that oxidizes [11C]methanol to [11C]formaldehyde.[44,45] This radioactive aldehyde is then chemically condensed to tetrahydrofolate forming a methyl-transfer cofactor that is sequentially used by a serine hydroxyl-methyltransferase (EC$_{2.1.2.1}$) to transfer the radiolabeled methyl group to glycine yielding *L*-[11C]serine.[44] Likewise, [11C]formaldehyde has been applied to the synthesis of nucleosides, by using an enzyme system integrated by thymidylate synthase and alkaline phosphatase co-immobilized on membranes fabricated with hollow fibers to yield [11C]thymidine and 2′-Fluoro-5-[11C]-methyl-β-*L*-arabinofuranosyluracyl ([11C]-FMAU).[45,46] Also, [11C]propionate can be enzymatically incorporated into acyl-*L*-carnitine to form [*carbomyl*-11C]propionyl-*L*-carnitine through two different multi-enzyme systems.[47]

Unlike the above-mentioned precursors, [11C]methyl iodide cannot be directly utilized by enzymes but can be efficiently incorporated into *L*-[11C]alanine[48,49] and *L*-[11C]methionine[38,50] through chemical methods. These amino acids can be subsequently utilized by different enzymes to synthesize radiotracers with biomedical interest. For example, *L*-[11C]alanine can be enzymatically converted into [11C]pyruvic acid by the action of alanine racemase and D-amino acid oxidase, leading to quantitative deamination of the amino acid. The dynamic racemization of the amino acid mediated by the racemase allows the D-amino acid oxidase to access 100% of the amino acid in spite of its strict enantioselectivity

towards the D-isomer. The catalase is required in this reaction to *in situ* eliminate hydrogen peroxide, an undesired by-product generated by the oxidase. Alternatively, alanine racemase can be coupled with an alanine dehydrogenase to quantitatively transform *L*-[11C]alanine into [11C]pyruvic acid *via* a NAD$^+$-dependent oxidative deamination catalyzed by an alanine dehydrogenase.[51] The resulting [11C]pyruvic acid can be easily reduced to [11C]lactic acid by adding a NADH-dependent lactate dehydrogenase.[60,62,64,65] From [11C]pyruvate, several aromatic *L*-[11C]amino acids can also be synthesized. For example, by using a transaminase/tyrosinase enzymatic tandem, *L*-tyrosine derivatives such as *L*-[11C]tyrosine and 3,4-dihydroxy-*L*-[11C]phenylalanine (*L*-[11C]DOPA) can be synthesized. Alternatively, the labeled pyruvate can be converted into *L*-[11C]tryptophan or 5-hydroxy-*L*-[11C]tryptophan by using a tryptophanase.[49,52-54] Interestingly, accurate selection of the enzymatic route and the 11C-labeled precursor ([11C]cyanide or [11C]methyl iodide) enables the preparation of *L*-[11C]tryptophan or *L*-[11C]tyrosine labeled in two different positions (carboxylic or β-position; see **Figure 2.5**).[49,52,55-57] The synthesis of these aromatic [11C]amino acids was refined by co-immobilizing the multi-enzyme systems[51] and by automating the procedure[58,59]. Using an automated system, *L*-[11C]DOPA and 5-hydroxy-*L*-[11C]tryptophan could be synthesized with >99% radiochemical purity and 5.3 and 22.0 GBq.µmol^{-1} specific activities, respectively.[58] Advances on the enzymatic routes have allowed the production of these aromatic [11C]amino acids in sufficient amounts to evaluate *in vivo* their biodistribution.[53,60-62]
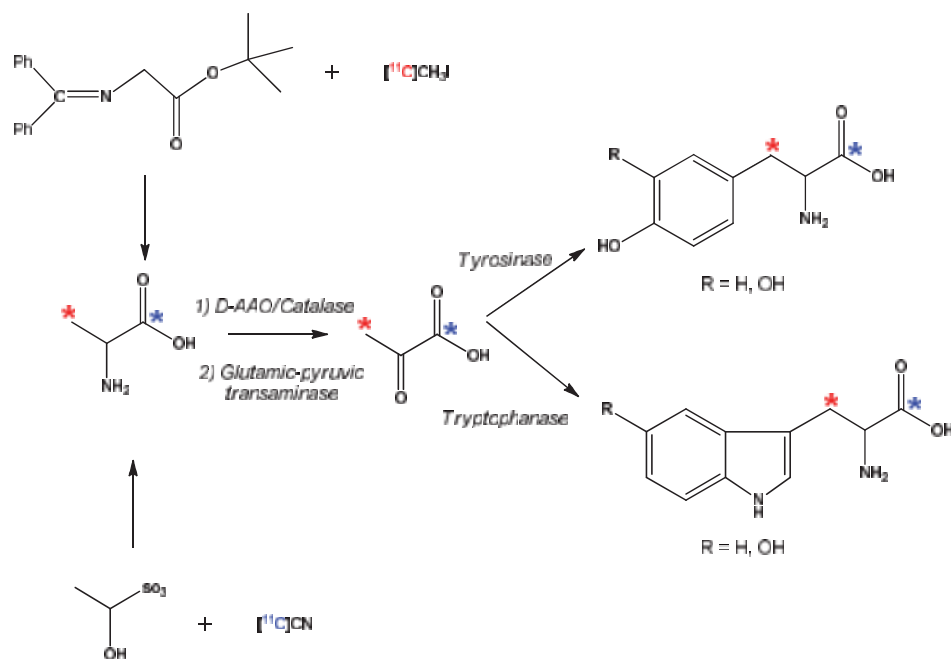
Figure 2.5. Chemo-enzymatic synthesis of aromatic *L*-amino acids labeled with carbon-11 in two different positions.

The chemical synthesis of *L*-[¹¹C]methionine starting from [¹¹C]methyl iodide provides a labeled compound that can be efficiently utilized by several enzymes to efficiently manufacture a plethora of interesting radiotracers. In one example, methionine adenosyltransferase was used to condense *L*-[¹¹C]methionine with ATP to yield *S*-adenosyl-*L*-[¹¹C]-methionine, a methyl-donor cofactor used by methyltransferases in a variety of metabolic reactions.[63] This ¹¹C-labeled methyl-donor cofactor has been exploited to label [¹¹C]epinephrine[64] and [4-methoxy-¹¹C]daunorubicin[50] by the action of different methyl transferases. A more advanced use of *L*-[¹¹C]methionine is its incorporation into proteins by using cell-free protein translation systems. This extraordinary utilization of carbon-11 amino acids has been applied to the synthesis of

[^{11}C]interleukin 8, a chemoattractant cytokine with promising application in chemo- and immunotherapy.[65] The *in vitro* synthesis of labeled proteins is based on cell-free pure preparations of protein synthesis machinery from *E.coli* that contain all the elements required for the sequential transcription and translation of genes into proteins (**Figure 2.6**).[66] With this system, [^{11}C]interleukin 8 was synthesized with a 63% radiochemical yield in only 20 minutes. The [^{11}C]cytokine was further purified by cation exchange and ultrafiltration methods, with a resulting radiochemical purity >95%. This pioneering work opens a promising path to the synthesis of radiotracers based on peptides and biotechnology-derived antibodies, which are becoming increasingly important as a major source of bio-based drugs.[67]
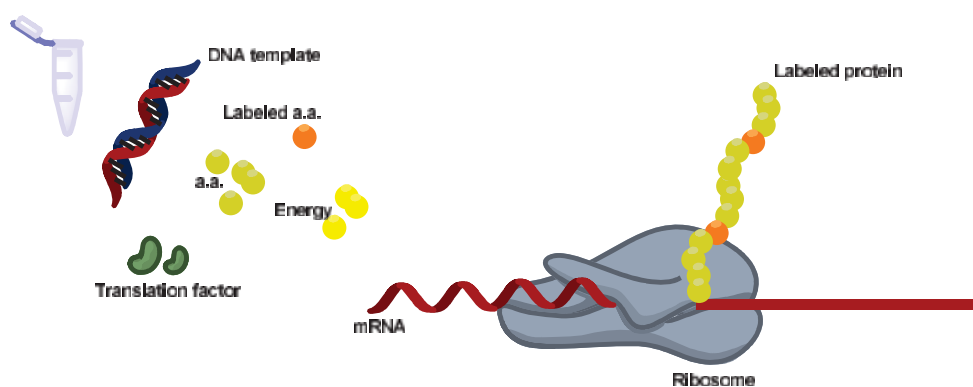
Figure 2.6. Schematic illustration of the proposed labeled protein preparation system using a cell-free translation system.

Table 2.2. Literature published on enzymatic reactions (carbon-carbon bond formation, functional group transfer and transformations) applied in the carbon-11 chemistry since 1980.

Radionuclide	Biosynthetic route	Enzyme family	Reaction	Compound	Ref.
[^{11}C]Carbon dioxide	Phosphoenolpyruvate carboxylase (Immobilized)	EC 4.1.1.31	Decarboxylation	*L*-[4-^{11}C]Aspartic acid	33
	Aspartate transaminase (Immobilized)	EC 2.6.1.1	Transamination		
[^{11}C]Carbon dioxide	Carbamyl phosphate synthetase (Immobilized)	EC 6.3.5.5	Phosphorylation/ Amination	[^{11}C]Carbamyl phosphate	2
[^{11}C]Carbon dioxide	Ornithine transcarbamylase	EC 2.1.3.3	Carbamoylation	*L*-[*ureido*-^{11}C]Citrulline	2
	Carbamyl phosphate synthetase (Co-immobilized)	EC 6.3.5.5	Phosphorylation/ Amination		
[^{11}C]Carbon dioxide	Aspartate transcarbamylase	EC 2.1.3.2	Carbamoylation	[*Carbamyl*-^{11}C]Carbamyl-*L*-aspartate	2
	Carbamyl phosphate synthetase (Co-immobilized)	EC 6.3.5.5	Phosphorylation/ Amination		
[^{11}C]Carbon dioxide	1) Phosphoenol pyruvate carboxylase	1) EC 4.1.1.31	1) Carboxylation	1) [^{11}C]Oxaloacetate	34
	2) Citrate synthase	2) EC 2.3.3.1	2) Addition	2) [^{11}C]Citrate	
	3) Aconitase	3) EC 4.2.1.3	3) Elimination	3) [^{11}C]Isocitrate	
	4) Isocitrate dehydrogenase	4) EC 1.1.1.42	4) Oxidative decarboxylation	4) [α-^{11}C]Ketoglutarate	
	5) Glutamate-pyruvate Transaminase	5) EC 2.6.1.2	5) Transamination	5) *L*-[^{11}C]Glutamate	
[^{11}C]Acetate	1) Acetate kinase	1) EC 2.7.2.1	1) Phosphorylation	[^{11}C]Acetylphosphate	34
	2) Phosphotransacetylase	2) EC 2.3.1.8	2) Acylation	2) [^{11}C]Acetyl-CoA	
	3) Citrate synthase	3) EC 2.3.3.1	3) Addition	3) [^{11}C]Citrate	
	4) Aconitase	4) EC 4.2.1.3	4) Elimination	4) [^{11}C]Isocitrate	
	5) Isocitrate dehydrogenase	5) EC 1.1.1.42	5) Oxidative decarboxylation	5) [γ-^{11}C]Ketoglutarate	
	6) Glutamate-pyruvate Transaminase	6) EC 2.6.1.2	6) Transamination	6) *L*-[^{11}C]Glutamate	
Hydrogen [^{11}C]cyanide	Mandelonitrile lyase	EC 4.1.2.10	Cyanohydrin formation	[^{11}C]Cyanohydrin intermediate for [^{11}C]Octopamine	35
Hydrogen [^{11}C]cyanide	*L*-3-cyanoalanine synthase	EC 4.4.1.9	Elimination (β – replacement)	Intermediate compound for *L*-2,4-Dianino[4-^{11}C]Butyric acid	36
Hydrogen [^{11}C]cyanide	*O*-acetyl-*L*-serine sulfhydrylase	EC 2.5.1.47	Elimination (β – replacement)	Intermediate compound for [4-^{11}C]Aspartic acid	37
Hydrogen [^{11}C]cyanide	γ-cyano-α-aminobutyric acid synthase	EC 2.5.1.49	Elimination (β – replacement)	Intermediate compound for *L*-[5-^{11}C]Glutamate	37
[^{11}C]Methyl iodide	γ-cyano-α-aminobutyric acid synthase (Immobilized)	EC 2.5.1.49	Elimination	*L*-[*methyl*-^{11}C] Methionine	38
[^{11}C]Carbon dioxide	Acetate kinase	EC 2.7.2.1	Quantification by phosphorylation	[1−^{11}C]acetate	39
[1-^{11}C]Acetate	Acetyl CoA synthetase (Immobilized)	EC 6.2.1.1	Acid-thiol ligation	[^{11}C]Acetyl coenzyme A	40
[^{11}C]Acetate	Acetyl CoA synthetase	EC 6.2.1.1	Acid-thiol ligation	*O*-[^{11}C]Acetyl CoA	41
[^{11}C]Acetate	Acetyl CoA synthetase	EC 6.2.1.1	Acid-thiol ligation	*O*-[^{11}C]Acetyl-*L*-Carnitine	41
	Carnitine acetyltransferase	EC 2.3.1.7	Acylation		

Radionuclide	Biosynthetic route	Enzyme family	Reaction	Compound	Ref.
[11C]Acetate	Carnitine acetyltransferase	EC 2.3.1.7	Acylation	L-[11C]Carnitine	41
[1-11C] acetate (*via* [11C]acetylCoA)	Acetyl CoA synthetase Arylamine *N*-acetyltransferase	EC 6.2.1.1 EC 2.3.1.5	Acid-thiol ligation Acylation	[11C]*N*-acetylserotonin	42
[1-11C]acetate (*via* [11C]acetylCoA)	Acetyl CoA synthetase Glucosamine *N*-acetyltransferase	EC 6.2.1.1 EC 2.3.1.3	Acid-thiol ligation Acylation	[11C]*N*-acetyl-D-glucosamine	43
[11C]Methanol	Alcohol oxidase Catalase (co-immobilized) Serine Hydroxyl-methyltransferase	EC 1.1.3.13 EC 1.11.1.6 EC 2.1.2.1	Oxidation Hydroxymethylation	L-[3-11C]Serine	44
[11C]Carbon dioxide	Alcohol oxidase Catalase (co-immobilized)	EC 1.1.3.13 EC 1.11.1.6	Oxidation	[11C]Formaldehyde	45
[11C]Carbon dioxide (*via* [11C]Formaldehyde)	Thymidylate synthase Alkaline phosphatase (immobilized)	EC 2.1.1.45 EC 3.1.3.1	Methylation Dephosphorylation	[11C]Thymidine [11C]2'-Arabino-2'-Fluoro-β-5-MethyI-Urid (FMAU)	46
[11C]Propionate	Acetate kinase Phosphotransacetylase Carnitine acetyltransferase	EC 2.7.2.1 EC 2.3.1.8 EC 2.3.1.7	Phosphorylation Acylation Acylation	NCA [*carbonyl*-11C]Propionyl L-Carnitine	47
[11C]Propionate	Acetyl CoA synthetase Carnitine acetyltransferase	EC 6.2.1.1 EC 2.3.1.7	Acid-thiol ligation Acylation	NCA [*carbonyl*-11C]Propionyl L-Carnitine	47
[11C]Methyl iodide	D-amino acid oxidase / Catalase Glutamic-pyruvic Transaminase	EC 1.4.3.3 / E.C. 1.11.1.6 EC 2.6.1.2	Resolution / Redox reaction Transamination	[3-11C]Pyruvic acid L-[11C]Alanine	48
Hydrogen [11C]cyanide	D-amino acid oxidase / Catalase Glutamic-pyruvic transaminase β-Tyrosinase	EC 1.4.3.3 / E.C. 1.11.1.6 EC 2.6.1.2 EC 4.1.99.2	Resolution / Redox reaction Transamination β – replacement	L- [*carboxy*-11C]Tyrosine L- [*carboxy* -11C]DOPA	49,53
Hydrogen [11C]cyanide	D-amino acid oxidase / Catalase Glutamic-pyruvic transaminase Tryptophanase	EC 1.4.3.3 / E.C. 1.11.1.6 EC 2.6.1.2 EC 4.1.99.1	Resolution / Redox reaction Transamination β – replacement	L- [3-11C]Tryptophan 5-Hydroxy-L-[3-11C]tryptophan	49,54
Hydrogen [11C]cyanide	D-amino acid oxidase / Catalase Glutamic-pyruvic Transaminase	EC 1.4.3.3 / E.C. 1.11.1.6 EC 2.6.1.2	Resolution / Redox reaction Transamination	L-[1-11C]Alanine	49
[*methyL*-11C] Methionine	L-methionine-S-adenosine transferase Carminomycin-4-*O*-methyltransferase	EC 2.1.1.12 EC 2.1.1.292	Methylation Methylation	S-methyl-L-[*methyl*-11C] Methionine [4-methoxy-11C]Daunorobicin	50
[11C]Methyl iodide (*via* [11C]Carbon dioxide)	Alanine racemase/Alanine Dehydrogenase β-tyrosinase (Co-immobilized)	EC 5.1.1.1/ EC 1.4.1.1 EC 4.1.99.2	Isomerization/ Oxidative deamination β – replacement	L-[3-11C]DOPA	51

Radionuclide	Biosynthetic route	Enzyme family	Reaction	Compound	Ref.
[^{11}C]Methyl iodide (via [^{11}C]Carbon dioxide)	Alanine racemase/ Alanine Dehydrogenase	EC 5.1.1.1/ EC 1.4.1.1	Isomerization/ Oxidative deamination	5-Hydroxy-*L*-[3-^{11}C]tryptophan	51
	Tryptophanase (Co-immobilized)	EC 4.1.99.1	β – replacement		
[^{11}C]Methyl iodide (via [^{11}C]Carbon dioxide)	Alanine racemase/D-amino acid oxidase	EC 5.1.1.1/ EC 1.4.3.3	Isomerization/ Resolution	*L*-[3-^{11}C]DOPA	51,58,59
	β-tyrosinase (Co-immobilized)	EC 4.1.99.2	β – replacement		
[^{11}C]Methyl iodide (via [^{11}C]Carbon dioxide)	Alanine racemase/D-amino acid oxidase	EC 5.1.1.1/ EC 1.4.3.3	Isomerization/ Resolution	5-Hydroxy-*L*-[3-^{11}C]tryptophan	51,58,59
	Tryptophanase (Co-immobilized)	EC 4.1.99.1	β – replacement		
[^{11}C]Carbon dioxide	D-amino acid oxidase / Catalase	EC 1.4.3.3 / E.C. 1.11.1.6	Resolution / Redox reaction	*L*- [3-^{11}C]Tyrosine	52,53
	Glutamic-pyruvic transaminase	EC 2.6.1.2	Transamination		
	β-Tyrosinase	EC 4.1.99.2	β – replacement	*L*- [3-^{11}C]DOPA	
[^{11}C]Methyl iodide	D-amino acid oxidase / Catalase	EC 1.4.3.3 / E.C. 1.11.1.6	Resolution / Redox reaction	*L*- [β-^{11}C]Tryptophan	55
	Glutamic-pyruvic Transaminase	EC 2.6.1.2	Transamination	5-Hydroxy-*L*-[β-^{11}C]tryptophan	
	Tryptophanase	EC 4.1.99.1	β – replacement		
[^{11}C]Carbonate	Mutant strain of the *cyanobacterium Synechocystis* PCC 6803	--	Photosynthesis	*L*-[^{11}C]Phenylalanine	56
[^{11}C]Carbon dioxide	Aspartate transaminase (Immobilized)	EC 2.6.1.1	Transamination	[3-^{11}C]Phenylalanine	57
[*methyl*-^{11}C] Methionine	Methionine adenosyltransferase	EC 2.5.1.6	Adenosyl group transfer	[*methyl*-^{11}C]Adenosyl-methionine	63
[*methyl*-^{11}C] Methionine	*L*-methionine-S-adenosine transferase	EC 2.5.1.6	Adenosyl group transfer	[^{11}C]-(-)-Epinephrine	64
	Phenylethanolamine-N-methyl transferase	EC 2.1.1.28	Methylation		
L-[^{11}C] Methionine	Cell-free system	PURESYSTEM	Protein synthesis	[^{11}C]interleukin 8	65
[^{11}C]Carbon dioxide	Pyruvate: ferredoxin 2-oxidoreductase	EC 1.2.7.1	Oxidative decarboxylation	[^{11}C]Pyruvate acid	68
	L-Lactate dehydrogenase	EC 1.1.1.27	Deamination	*L*-[3-^{11}C]Lactic acid	
[^{11}C]Methyl iodide	Glutamate-pyruvate transaminase	EC 2.6.1.2	Transamination		69
	L-Lactate dehydrogenase	EC 1.1.1.27	Deamination	*L*-[3-^{11}C]Lactic acid	
[^{11}C] Hydrogen Cyanide (NCA)	D-amino acid oxidase (Immobilized)	EC 1.4.3.3	Resolution	*L*-[^{11}C]Leucine	70,71
[^{11}C]Carbon dioxide	Green algae *Scenedesmus obtuslusculus Chod.*	--	Photosynthesis	[^{11}C]Glucose	72
[^{11}C] Hydrogen Cyanide (NCA)	D-amino acid oxidase / Catalase (Co-immobilized)	EC 1.4.3.3 / E.C. 1.11.1.6	Resolution / Redox reaction	*L*-[^{11}C]Alanine	73

Radionuclide	Biosynthetic route	Enzyme family	Reaction	Compound	Ref.
[11C] Hydrogen Cyanide (NCA)	D-amino acid oxidase / Catalase (Co-immobilized)	EC 1.4.3.3 / E.C. 1.11.1.6	Resolution / Redox reaction	[1-11C]Pyruvic acid	73
	L-Alanine dehydrogenase	EC 1.4.1.1	Oxidative deamination		
[11C] Hydrogen Cyanide (NCA)	L-Lactate dehydrogenase	EC 1.1.1.27	Reduction	L-[1-11C]Lactic Acid	73
Hydrogen [11C]cyanide	D-amino acid oxidase / Catalase	EC 1.4.3.3 / E.C. 1.11.1.6	Resolution / Redox reaction	[1-11C]pyruvic acid	74
Hydrogen [11C]cyanide	D-amino acid oxidase / Catalase	EC 1.4.3.3 / E.C. 1.11.1.6	Resolution / Redox reaction	L-[1-11C]Lactic Acid	75
	Glutamic-pyruvic transaminase	EC 2.6.1.2	Transamination		
	L-Lactic dehydrogenase	EC 1.1.1.27	Reduction		
[11C]Methyl iodide	D-amino acid oxidase / Catalase	EC 1.4.3.3 / E.C. 1.11.1.6	Resolution / Redox reaction	L-[3-11C]Lactic Acid	75
	Glutamic-pyruvic transaminase	EC 2.6.1.2	Transamination		
	L-Lactic dehydrogenase	EC 1.1.1.27	Reduction		
[11C]Methyl iodide	D-mannitol dehydrogenase	EC 1.1.1.67	Oxidation	D-[16-11C]Fructose	76
[11C]Methyl iodide (via [11C]Carbon dioxide)	Alanine racemase/ Alanine Dehydrogenase	EC 5.1.1.1/ EC 1.4.1.1	Isomerization/ Oxidative deamination	[3-11C]Pyruvic acid	77
	Alanine racemase/D-amino acid oxidase (Co-immobilized)	EC 5.1.1.1/ EC 1.4.3.3			

Fluorine-18

The number of enzymatic applications in fluorine-18 radiochemistry is much lower than in carbon-11 and nitrogen-13 radiochemistry (**Table 2.3**) because the repertoire of enzymatic reactions that use fluorine in nature is very limited. However, incorporation of fluorine-18 into biological molecules is priceless for PET radiochemistry since fluorine-18 has a very convenient half-life for *in vivo* studies, especially in the context of small molecules.[78,79] [18F]fluoride ion ([18F]F-) is cyclotron-generated by irradiation of 18O-enriched water ([18O]H2O) with high-energy protons *via* the 18O(p, n)18F nuclear reaction. The presence of water molecules into the final radioactive solution affects [18F]F- reactivity, which limits direct use in nucleophilic substitution reactions. To overcome this drawback, [18F]Fluoride ions are captured in an anion-exchange resin and further

formulated using a phase transfer catalyst (e.g. Kryptofix [2.2.2]) a polar, non-protic solvents to favor the nucleophilic attack.

Until XXst century, no enzymes capable to directly incorporate cyclotron-produced [^{18}F]F[-] had been reported. Hence, the first ^{18}F-labeling enzymatic reactions reported in the 1980's and 1990's were based on the use of ^{18}F-labeled precursors. For example, 2-deoxy-2-[^{18}F]fluoro-D-glucose ([^{18}F]FDG) was purified from the chemical synthesis by using an hexokinase that selectively phosphorylates D-glucose, facilitating the purification of the radiolabeled sugar.[80] In a more synthetic approach, 6-[^{18}F]fluorodopamine, 4-[^{18}F]catechol and [^{18}F]FDG-1-phosphate were used as substrates of dopamine β-hydroxylase[81], β-tyrosinase[82] and UDP-glucose pyrophosphorylase[83] to synthesize (−)-6-[^{18}F]fluoronorepinephrine, 6-[^{18}F]fluoro-*L*-DOPA and uridine diphospho-2-deoxy-2-[^{18}F]fluoro-α-D-glucose (UDP-[^{18}F]FDG), respectively (**Figure 2.7**).

In 2002, the isolation of a fluorinase (adenosyl-fluoride synthase: $EC_{2.5.1.63}$) from the soil bacterium *Streptomyces cattleya* meant a breakthrough in enzymatic synthesis of fluorinated compounds. The structural and biochemical characterization of this enzyme opened new prospects for the direct ^{18}F-radiofluorination of biological molecules.[84-87] Nature has specialized fluorinases to convert S-adenosyl-*L*-methionine (SAM) to 5'-fluoro-5'-deoxyadenosine (FDA)[86] through a nucleophilic attack of the fluorine ions on the methionine derivative. Since enzymes work by default under aqueous conditions, it was anticipated that cyclotron-produced [^{18}F]F[-] could be used to directly form [18]F−C bonds. Indeed, fluorinases have been later exploited to tackle the [^{18}F]fluorination of several organic molecules.[88,89]
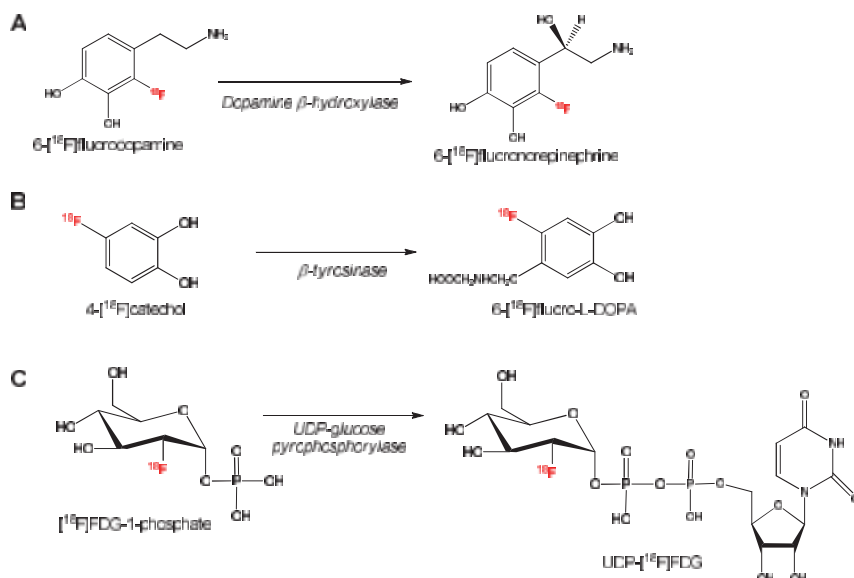
Figure 2.7. Schematic representation of the enzymatic reaction to synthesize (−)-6-[^{18}F]fluoronorepinephrine (**A**), 6-[^{18}F]fluoro-*L*-DOPA (**B**) and UDP-[^{18}F]FDG (**C**). The radiosynthesis of these molecules was achieved starting from the respective ^{18}F-labeled substrates using dopamine β-hydroxylase, β-tyrosinase and UDP-glucose pyrophosphorylase, respectively.

In a first attempt, the fluorinase purified from *Streptomyces cattleya* was applied to the preparation of [^{18}F]FDA from SAM and [^{18}F]F⁻, although poor yields could be achieved (approx. 1%).[90] However, when this enzyme was recombinantly overexpressed in *E.coli* and coupled with a *L*-amino acid oxidase (*L*-AAO), the radiochemical yield was greatly increased.[91] In this multi-enzyme system, the fluorinase catalyzes a nucleophilic attack of [^{18}F]F⁻ ion to SAM, with the release of one molecule of *L*-methionine. This molecule of *L*-methionine is concurrently deaminated by *L*-AAO, preventing the reversible reaction. By using this combination of enzymes, up to 95% radiochemical yield was achieved for the synthesis of [^{18}F]FDA. Harnessing the benefits of the enzyme immobilization, fluorinase was

immobilized to perform the synthesis of [^{18}F]FDA more efficiently.[92] Furthermore, Sergeev *et al*. have broadened the substrate scope of the fluorinase, which is able to accept SAM analogues to synthesize [^{18}F]FDA with 32% radiochemical yield in 3h.[93]

The high-yield synthesis of [^{18}F]FDA accomplished by this two-enzyme system has paved the way for the enzymatic incorporation of fluorine-18 to a plethora of molecules. For example, the deamination of [^{18}F]FDA catalyzed by a 5′-adenylic acid deaminase results in the formation of 5'-[^{18}F]fluoro-5'-deoxyinosine (5'-[^{18}F]FDI). By using bi-enzymatic systems comprising an immobilized purine nucleotide phosphorylase and phytase, the transfer of ^{18}F-fluorinated adenine from [^{18}F]FDA to the 5-deoxy-1-phosphoribose and the concurrent dephosphorylation of the carbon-1 yielding 5′-deoxy-5'-[^{18}F]fluoro-D-ribose (5'-[^{18}F]FDR) could be achieved. After 4 hours reaction, the different enzymatic routes resulted in 75% and 45% radiochemical yields for 5'-[^{18}F]FDI and 5'-[^{18}F]FDR, respectively.[91] Recently, the synthesis of 5'-[^{18}F]FDR from [^{18}F]F^{-} through a four-enzyme/one-pot system (fluorinase, *L*-AAO, purine nucleotide phosphorylase and phytase) was significantly improved, resulting in 80% radiochemical conversion in 2 hours (see **Figure 2.8**). The amount of the radiolabeled monosaccharide was sufficient to be tested in PET imaging.[93-95] The multi-enzyme cascade was varied to synthesize 5'-deoxy-5'-[^{18}F]fluorouridines ([^{18}F]FDU) from [^{18}F]fluoride using [^{18}F]FDA as intermediate. In the cascade, the phytase was replaced by a thymidine phosphorylase that incorporates one uracil nitrogen base into the carbon 1 of the fluorinated sugar to yield fluorinated uridines. Using different uracil derivatives, the multi-enzyme system was used to synthesize the corresponding uridines with decent radiochemical conversions (13-33%) in 1-2h time.
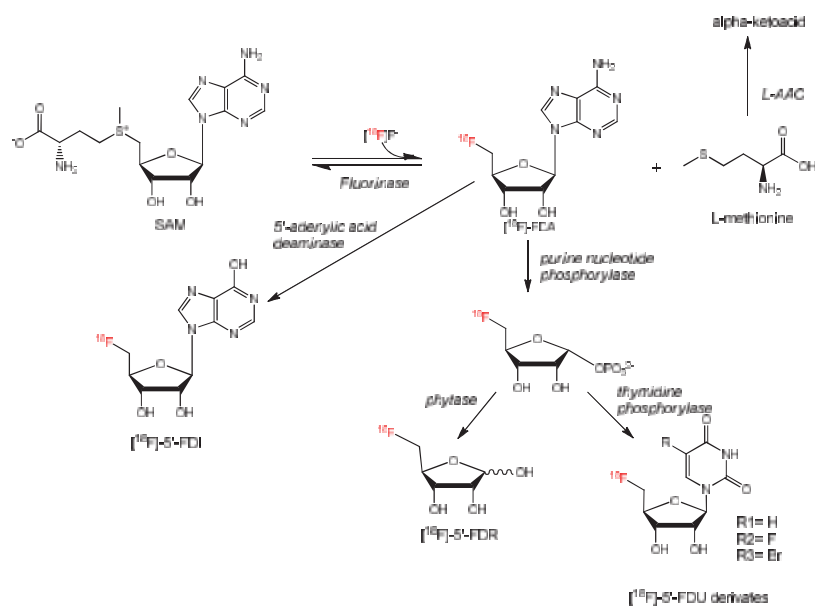
Figure 2.8. Schematic representation of the reported fluorinase multi-coupled enzyme systems for the synthesis of ^{18}F-labeled compounds.

As in the case of carbon-11, enzymatic reactions have also been employed to the synthesis of ^{18}F-labeled proteins using a cell-free approach.[65] Considering the slow pharmacokinetics of macromolecules, the ^{18}F-labeled proteins are more interesting than the ^{11}C-labeled analogues since the longer half-life of ^{18}F enables longer scanning times. By using pure transcription and translation machinery of *Escherichia coli* and 4-[^{18}F]fluoro-*L*-proline, Harada *et al.* have reported the synthesis of [^{18}F]interleukin-8 in overall production time of 120 minutes with 1.5% radiochemical conversion with respect to the fluorinated amino acid.

Radiochemical conversion is lower than that achieved with *L*-[^{11}C]methionine because the aminoacyl-tRNAs synthases are dramatically

less efficient using non-natural amino acids, limiting the pool of tRNAs loaded with 4-[^{18}F]fluoro-*L*-proline.

Table 2.3. Enzymatic radiofluorination and biotechnological developments of the fluorinase and other enzymatic transformations using in the fluorine-18 chemistry reported since the 80's.

Radionuclide	Biosynthetic route	Enzyme family	Reaction	Compound	Ref.
[^{18}F]Fluoride ion	Hexokinase	EC 2.7.1.1	Purification	2-Deoxy-2-[^{18}F]fluoroglucose	80
[^{18}F]Fluoride ion (*via* 6-[^{18}F]Fluorodopamine)	Dopamine β-hydroxylase	EC 1.14.17.1	Reduction	(−)-6-[^{18}F]Fluoronorepinephrine	81
[^{18}F]Fluoride ion	UDP-glucose pyrophosphorylase	EC 2.7.7.9	Nucleotidyl group transfer	Uridine diphospho-2-deoxy-2-[^{18}F]Fluoro-α-D-glucose	83,96
[^{18}F]Fluoride ion (*via* 4-[^{18}F]Fuorocatechol)	β-Tyrosinase	EC 4.1.99.2	β – replacement	6-[^{18}F]Fuoro-*L*-dopa	82
[^{18}F]Fluoride ion	Fluorinase	EC 2.5.1.63	Halogenation	[^{18}F]-5'-fluoro-5'-Deoxyadenosine	90
[^{18}F]Fluoride ion	Fluorinase / *L*-amino acid oxidase	EC 2.5.1.63/ EC 1.4.3.2	Halogenation / Oxidation	[^{18}F]-5'-fluoro-5'-Deoxyadenosine (Intermediate for [^{18}F]-fluoroacetate)	91,97
[^{18}F]Fluoride ion (*via* [^{18}F]-5'-fluoro-5'-Deoxyadenosine)	5'-Adenylic Acid Deaminase (coupled with Fluorinase / *L*-amino acid oxidase)	EC 3.5.4.6	Deamination	[^{18}F]-5'-Fluoro-5'-deoxyinosine	91
[^{18}F]Fluoride ion (*via* [^{18}F]-5'-fluoro-5'-Deoxyadenosine)	Fluorinase / *L*-amino acid oxidase	EC 2.5.1.63/ EC 1.4.3.2	Halogenation / Oxidation	5'-deoxy-5'-[^{18}F]Fluoro-D-ribose	91
	Purine nucleoside phosphorylase (Immobilized)	EC 2.4.2.1	Pentosylation		
	Phytase	EC 3.1.3.1	Hydrolysis of phosphoric ester		

Radionuclide	Biosynthetic route	Enzyme family	Reaction	Compound	Ref.
[18F]Fluoride ion	Fluorinase / L-amino acid oxidase	EC 2.5.1.63 / EC 1.4.3.2	Halogenation / Oxidation	5'-deoxy-5'-[18F]Fluorouridines	98
	Purine nucleoside phosphorylase	EC 2.4.2.1	Pentosylation		
	Thymidine phosphorylase	EC 2.4.2.4	Pentosylation		
[18F]Fluoride ion	Fluorinase	EC 2.5.1.63	Halogenation	5'-deoxy-5'-[18F]Fluoro-D-ribose	94,95
	Nucleoside Hydrolase (TvNH)	EC 3.2.2.1	Hydrolysis of N-glycosyl bond		
[18F]Fluoride ion	Fluorinase	EC 2.5.1.63	Halogenation	[18F]-5'-fluoro-5'-deoxyadenosine	93
[18F]Fluoride ion	Fluorinase (Immobilized)	EC 2.5.1.63	Halogenation	[18F]-5'-fluoro-5'-deoxyadenosine	92
	L-amino acid oxidase	EC 1.4.3.2			
4-[18F]fluoro-L-proline	Cell-free system	PURExpress	Protein synthesis	[18F]interleukin 8	99

SUMMARY AND FUTURE PERSPECTIVES

The application of biosynthetic methods in radiosynthesis has proven efficient for the preparation of labeled compounds that would be difficult to label using chemical methods. Enzymes exhibit high regio-, chemo- and stereo-selectivity and high catalytic versatility, and can be used either in their free form (in solution) or immobilized on a solid carrier.

The understanding of the precise mechanisms underlying biocatalytic reactions in radiochemistry opens new avenues for the preparation of radiolabeled compounds in multiple biomedical applications. Thanks to the advances in bioengineering, old approaches are finding new applications. Moreover, new approaches are currently being developed, as exemplified by the most recent work from O'Hagan *et al.* with enzymatic fluorination of sugar and nucleoside derivatives[88,89] or the elegant strategy from Harada *et al.* for the preparation of [11C]/[18F]-labeled proteins using cell-free translation systems.[74,108]

A recurrent apprehension regarding the use of biological catalysts for the preparation of injectable solutions is often mentioned as a drawback for the incorporation of PET radionuclides into molecules by enzymatic methods. However, several factors may open a second era in the enzymatic preparation of radiopharmaceuticals: first, a legislative evolution has occurred in the last decades; second, protein engineering and improvement of industrialized and commercial methods for the preparation of enzymes have brought a new safety paradigm compatible with GMP practices.[100,101] Unlike in the past, where these biomolecules were often synthesized and isolated *in situ* for further use, nowadays they can be purchased through certified companies that ensure biological safety and absence of pyrogens or cell-derived residues; third, improvements in immobilization techniques and the availability of a wide range of spin or membrane filters facilitate purification steps. In this context, it can be expected that enzymatic synthesis will progressively find more and more applications both in the pre-clinical and clinical settings. The execution of the experimental work reported in this PhD thesis (see chapters 4-6) has resulted in a significant contribution to the development of novel strategies for the radiosynthesis of ^{13}N-labeled compounds using enzymatic catalysis.

REFERENCES

(1)   Cooper, A. J.; Gelbard, A. S. The use of immobilized glutamate dehydrogenase to synthesize 13N-labeled L-amino acids. *Anal Biochem* **1981**, *111*, 42-48.

(2)   Gelbard, A. S.; Kaseman, D. S.; Rosenspire, K. C.; Meister, A. Enzymatic syntheses of phosphate, l-citrulline, and N-carbamyl l-aspartate labeled with either 13N or 11C. *International Journal of Nuclear Medicine and Biology* **1985**, *12*, 235-242.

(3)   Datta, S.; Christena, L. R.; Rajaram, Y. R. S. Enzyme immobilization: an overview on techniques and support materials. *3 Biotech* **2013**, *3*, 1-9.

(4)   Sheldon, R. A.; van Pelt, S. Enzyme immobilisation in biocatalysis: why, what and how. *Chem Soc Rev* **2013**, *42*, 6223-6235.

(5)   Homaei, A. A.; Sariri, R.; Vianello, F.; Stevanato, R. Enzyme immobilization: an update. *Journal of Chemical Biology* **2013**, *6*, 185-205.

(6)   Hartmann, M.; Kostrov, X. Immobilization of enzymes on porous silicas - benefits and challenges. *Chemical Society Reviews* **2013**, *42*, 6277-6289.

(7)   Gelbard, A. S. Biosynthetic methods for incorporating positron-emitting radionuclides into compounds of biomedical interest. *Journal of Labelled Compounds and Radiopharmaceuticals* **1981**, *18*, 933-945.

(8)   Llop, J.; Gómez-Vallejo, V.; Bosque, M.; Quincoces, G.; Peñuelas, I. Synthesis of S-[13N]nitrosoglutathione (13N-GSNO) as a new potential PET imaging agent. *Applied Radiation and Isotopes* **2009**, *67*, 95-99.

(9)   Gómez-Vallejo, V.; Kato, K.; Oliden, I.; Calvo, J.; Baz, Z.; Borrell, J. I.; Llop, J. Fully automated synthesis of 13N-labeled nitrosothiols. *Tetrahedron Letters* **2010**, *51*, 2990-2993.

(10)   Gómez-Vallejo, V.; Kato, K.; Hanyu, M.; Minegishi, K.; Borrell, J. I.; Llop, J. Efficient system for the preparation of [13N]labeled nitrosamines. *Bioorganic & Medicinal Chemistry Letters* **2009**, *19*, 1913-1915.

(11)   Gaja, V.; Gomez-Vallejo, V.; Puigivila, M.; Perez-Campana, C.; Martin, A.; Garcia-Osta, A.; Calvo-Fernandez, T.; Cuadrado-Tejedor, M.; Franco, R.; Llop, J. Synthesis and evaluation of 13N-labelled azo compounds for beta-amyloid imaging in mice. *Molecular imaging and biology : MIB : the official publication of the Academy of Molecular Imaging* **2014**, *16*, 538-549.

(12)   Joshi, S. M.; de Cozar, A.; Gomez-Vallejo, V.; Koziorowski, J.; Llop, J.; Cossio, F. P. Synthesis of radiolabelled aryl azides from diazonium salts: experimental and computational results permit the identification of the preferred mechanism. *Chemical communications (Cambridge, England)* **2015**, *51*, 8954-8957.

(13)   Joshi, S. M.; Gomez-Vallejo, V.; Salinas, V.; Llop, J. Synthesis of 13N-labelled polysubstituted triazoles via Huisgen cycloaddition. *RSC Advances* **2016**, *6*, 109633-109638.

(14)   Long, N.; Wong, W. T.: *The Chemistry of Molecular Imaging*; Wiley, 2014.

(15)   Suzuki, K.; Yoshida, Y. Production of [13N]NH3 with ultra-high specific activity. *Applied Radiation and Isotopes* **1999**, *50*, 497-503.

(16)   Kitsiou, A. N.; Bacharach, S. L.; Bartlett, M. L.; Srinivasan, G.; Summers, R. M.; Quyyumi, A. A.; Dilsizian, V. 13N-Ammonia myocardial blood flow and uptake. *Relation to functional outcome of asynergic regions after revascularization* **1999**, *33*, 678-686.

(17) Xiangsong, Z.; Xinjian, W.; Yong, Z.; Weian, C. 13N-NH3: a selective contrast-enhancing tracer for brain tumor. *Nuclear medicine communications* **2008**, *29*, 1052-1058.

(18) Di Carli, M. F.; Lipton, M. J.: *Cardiac PET and PET/CT Imaging*; Springer New York, 2007.

(19) Gelbard, A. S.; Benua, R. S.; Reiman, R. E.; McDonald, J. M.; Vomero, J. J.; Laughlin, J. S. Imaging of the Human Heart after Administration of L-(N-13)Glutamate. *Journal of Nuclear Medicine* **1980**, *21*, 988-991.

(20) Barrio, J. R.; Baumgartner, F. J.; Henze, E.; Stauber, M. S.; Egbert, J. E.; MacDonald, N. S.; Schelbert, H. R.; Phelps, M. E.; Liu, F.-T. Synthesis and Myocardial Kinetics of N-13 and C-11 Labeled Branched-Chain l-Amino Acids. *Journal of Nuclear Medicine* **1983**, *24*, 937-944.

(21) da Silva, E. S.; Gómez-Vallejo, V.; Baz, Z.; Llop, J.; López-Gallego, F. Efficient Enzymatic Preparation of 13N-Labelled Amino Acids: Towards Multipurpose Synthetic Systems. *Chemistry – A European Journal* **2016**, *22*, 13619-13626.

(22) Baumgartner, F. J.; Barrio, J. R.; Henze, E.; Schelbert, H. R.; MacDonald, N. S.; Phelps, M. E.; Kuhl, D. E. 13N-labeled L-amino acids for in vivo assessment of local myocardial metabolism. *Journal of medicinal chemistry* **1981**, *24*, 764-766.

(23) Lambrecht, R. H. D.; Slegers, G.; Claeys, A.; Gillis, E.; Vandecasteele, C. Enzymatic synthesis of radiopharmaceutically pure 13N-labelled L-glutamate. *Radiochemical and Radioanalytical Letters* **1983**, *58*, 39-48.

(24) Helus, F.; Weber, K.; Zeisler, S.; Maier-Borst, W. An automatic system for the enzymatic synthesis of13N-glutamate. *Journal of Radioanalytical and Nuclear Chemistry* **1991**, *155*, 9-13.

(25) Gelbard, A. S.; Cooper, A. J. L.; Asano, Y.; Nieves, E.; Filc-Dericco, S.; Rosenspire, K. C. Methods for the enzymatic synthesis of tyrosine and phenylalanine labeled with nitrogen-13. *International Journal of Radiation Applications and Instrumentation. Part A. Applied Radiation and Isotopes* **1990**, *41*, 229-233.

(26) da Silva, E. S.; Gómez-Vallejo, V.; Llop, J.; López-Gallego, F. Structural, kinetic and operational characterization of an immobilized l-aminoacid dehydrogenase. *Process Biochemistry* **2017**.

(27) Elmaleh, D.; Hnatowitch, D.; Kulprathipanja, S. A novel synthesis of 13N-L-aspargine. *Journal of Labelled Compounds and Radiopharmaceuticals* **1979**, *16*, 92-93.

(28) Lambrecht, R. H. D.; Slegers, G.; Claeys, A.; Vandecasteele, C. Enzymatic synthesis of 13N-β-nicotinamide adenine dinucleotide. *International*

Atomic Energy Agency, Vienna (Austria); Proceedings series **1985**, 321-330.

(29) Lambrecht, R. H. D.; Slegers, G.; Mannens, G.; Claeys, A. Enzymatic synthesis of 13N-labeled γ-amino-butyric acid *Journal of Labelled Compounds and Radiopharmaceuticals* **1986**, *23*, 1114-1115.

(30) da Silva, E. S.; Gomez-Vallejo, V.; Llop, J.; Lopez-Gallego, F. Efficient nitrogen-13 radiochemistry catalyzed by a highly stable immobilized biocatalyst. *Catalysis Science & Technology* **2015**.

(31) Vallabhajosula, S.: *Molecular Imaging: Radiopharmaceuticals for PET and SPECT*; Springer Berlin Heidelberg, 2009.

(32) Gómez-Vallejo, V.; Vijay, G.; Jacek, K.; Jordi, L.: Specific Activity of 11C-Labelled Radiotracers: A Big Challenge for PET Chemists. In *Positron Emission Tomography - Current Clinical and Research Aspects*; InTech, 2012; pp 183-210.

(33) Barrio, J. R.; Egbert, J. E.; Henze, E.; Schelbert, H. R.; Baumgartner, F. J. L-[4-11C]aspartic acid: enzymatic synthesis, myocardial uptake, and metabolism. *J. Med. Chem.* **1982**, *25*, 93-96.

(34) Cohen, M. B.; Spolter, L.; Chia, C. C.; Behrendt, D.; Cook, J.; MacDonald, N. S. The varying tissue distribution of L-glutamic acid labelled at three different sites. *The International Journal of Applied Radiation and Isotopes* **1982**, *33*, 613-617.

(35) Maeda, M.; Koga, Y.; Fukumura, T.; Kojima, M. [11C]octopamine synthesis using [11C]cyanide: Chemical and enzymatic approaches for the [11C]cyanohydrin synthesis. *International Journal of Radiation Applications and Instrumentation. Part A. Applied Radiation and Isotopes* **1990**, *41*, 463-469.

(36) Antoni, G.; Omura, H.; Bergström, M.; Furuya, Y.; Moulder, R.; Roberto, A.; Sundin, A.; Watanabe, Y.; Långström, B. Synthesis of L-2,4-diamino[4-11C]butyric acid and its use in some in vitro and in vivo tumour models. *Nuclear medicine and biology* **1997**, *24*, 595-601.

(37) Antoni, G.; Omura, H.; Ikemoto, M.; Moulder, R.; Watanabe, Y.; Långström, B. Enzyme catalysed synthesis of L-[4-11C]aspartate and L-[5-11C]glutamate. *Journal of Labelled Compounds and Radiopharmaceuticals* **2001**, *44*, 287-294.

(38) Kaneko, S.; Ishiwata, K.; Ishii, S.-I.; Omura, H.; Senda, M. Enzymatic synthesis of carbon-11 labeled methionine and its derivatives with immobilized γ-cyano-α-aminobutyric acid synthase. *Appl. Radiat. Isot.* **1999**, *51*, 285-291.

(39) Pike, V. W.; Eakins, M. N.; Allan, R. M.; Selwyn, A. P. Preparation of [1−11C]acetate—An agent for the study of myocardial metabolism by

positron emission tomography. *The International Journal of Applied Radiation and Isotopes* **1982**, *33*, 505-512.

(40)   Mannens, G.; Slegers, G.; Lambrecht, R.; Goethals, P. Enzymatic synthesis of carbon-11 acetyl coenzyme A. *J. Labelled Compd. Radiopharmaceut.* **1988**, *25*, 695-705.

(41)   Jacobson, G. B.; Watanabe, Y.; Valind, S.; Kuratsune, H.; Langstrom, B. Synthesis of O-[11C]Acetyl CoA, O-[11C]Acetyl-L-carnitine, and L-[11C]carnitine labelled in specific positions, applied in PET studies on rhesus monkey. *Nucl Med Biol* **1997**, *24*, 471-478.

(42)   Mannens, G.; Slegers, G.; Goethals, P. Enzymatic synthesis of [11C]N-acetylserotonin. *Journal of Labelled Compounds and Radiopharmaceuticals* **1990**, *28*, 311-320.

(43)   Mannens, G.; Slegers, G.; Goethals, P.; Claeys, A. Enzymatic synthesis of carbon-11 N-acetyl-D-glucosamine. *J. Labelled Compd. Radiopharmaceut.* **1990**, *28*, 53-64.

(44)   Svärd, H.; Jigerius, S.; Långström, B. The Enzymatic synthesis of L-3-11C-serine. *Appl. Radiat. Isotop.* **1990**, *41*, 587-591.

(45)   Hughes, J. A.; Jay, M. Preparation of [11C]formaldehyde using a hollow fiber membrane bioreactor. *Nuclear medicine and biology* **1995**, *22*, 105-109.

(46)   Hughes, J. A.; Hartman, N. G.; Jay, M. Preparation of [11C]-thymidine and [11C]-2′-arabino-2′-fluoro-β-5-methyl-uridine (FMAU) using a hollow fiber membrane bioreactor system. *Journal of Labelled Compounds and Radiopharmaceuticals* **1995**, *36*, 1133-1145.

(47)   Davenport, R. J.; Pike, V. W.; Dowsett, K.; Turton, D. R.; Poole, K. Automated chemoenzymatic synthesis of no-carrier-added [carbonyl-11C]propionyl l-carnitine for pharmacokinetic studies. *Appl. Radiat. Isot.* **1997**, *48*, 917-924.

(48)   Bjurling, P.; Watanabe, Y.; Långström, B. The synthesis of [3-11C]pyruvic acid, a useful synthon, via an enzymatic route. *International Journal of Radiation Applications and Instrumentation. Part A. Applied Radiation and Isotopes* **1988**, *39*, 627-630.

(49)   Bjurling, P.; Antoni, G.; Watanabe, Y.; Langstrom, B. Enzymatic synthesis of carboxy-11C-labelled L-tyrosine, L-DOPA, L-tryptophan and 5-hydroxy-L-tryptophan. *Acta Chem. Scand.* **1990**, *44*, 178-182.

(50)   Eriks-Fluks, E.; Elsinga, P. H.; Hendrikse, N. H.; Franssen, E. J. F.; Vaalburg, W. Enzymatic synthesis of [4-methoxy-11C]daunorubicin for functional imaging of P-glycoprotein with PET. *Appl. Radiat. Isot.* **1998**, *49,* 811-813.

(51)   Ikemoto, M.; Sasaki, M.; Haradahira, T.; Yada, T.; Omura, H.; Furuya, Y.; Watanabe, Y.; Suzuki, K. Synthesis of L-[β-11C]amino acids using immobilized enzymes. *Appl. Radiat. Isot.* **1999**, *50*, 715-721.

(52)   Bjurling, P.; Watanabe, Y.; Oka, S.; Nagasawa, T.; Yamada, H.; Långström, B. Multi-enzymatic synthesis of 11 C-labelled L-tyrosine and l-DOPA. *Acta Chem. Scand.* **1990**, *44*, 183-188.

(53)   Hartvig, P.; Agren, H.; Reibring, L.; Tedroff, J.; Bjurling, P.; Kihlberg, T.; Langstrom, B. Brain kinetics of L-[beta-11C]dopa in humans studied by positron emission tomography. *J Neural Transm Gen Sect* **1991**, *86*, 25-41.

(54)   Hartvig, P.; Lindner, K. J.; Tedroff, J.; Andersson, Y.; Bjurling, P.; Langstrom, B. Brain kinetics of 11 C-labelled L-tryptophan and 5-hydroxy-L-tryptophan in the rhesus monkey. A study using positron emission tomography. *J. Neural Transm. Gen. Sect.* **1992**, *88*, 1-10.

(55)   Bjurling, P.; Watanabe, Y.; Tokushige, M.; Oda, T.; Langstrom, B. Syntheses of [small beta]-11C-labelled L-tryptophan and 5-hydroxy-L-tryptophan using a multi-enzymatic reaction route. *J. Chem. Soc., Perkin Trans. 1* **1989**, 1331-1334.

(56)   Labarre, J.; Donie, P.; Crouzel, C. The biosynthesis of L-[11C]phenylalanine using a mutant strain of a cyanobacterium (Synechocystis PCC 6803). *Applied Radiation and Isotopes* **1991**, *42*, 659-663.

(57)   Halldin, C.; Längström, B. Synthesis of [3-11C]phenylpyruvic acid and its use in an enzymatic transamination to [3-11C]phenylalanine. *J. Labelled Compd. Radiopharmaceut.* **1986**, *23*, 715-722.

(58)   Harada, N.; Nishiyama, S.; Sato, K.; Tsukada, H. Development of an automated synthesis apparatus for l-[3-11C] labeled aromatic amino acids. *Applied Radiation and Isotopes* **2000**, *52*, 845-850.

(59)   Sasaki, M.; Ikemoto, M.; Mutoh, M.; Haradahira, T.; Tanaka, A.; Watanabe, Y.; Suzuki, K. Automatic synthesis of l-[β-11C]amino acids using an immobilized enzyme column. *Applied Radiation and Isotopes* **2000**, *52*, 199-204.

(60)   Tedroff, J.; Aquilonius, S. M.; Hartvig, P.; Bredberg, E.; Bjurling, P.; Langstrom, B. Cerebral uptake and utilization of therapeutic [beta-11C]-L-DOPA in Parkinson's disease measured by positron emission tomography. Relations to motor response. *Acta neurologica Scandinavica* **1992**, *85*, 95-102.

(61)   Tedroff, J.; Aquilonius, S. M.; Hartvig, P.; Lundqvist, H.; Bjurling, P.; Langstrom, B. Estimation of regional cerebral utilization of [11C]-L-3,4-dihydroxy-phenylalanine (DOPA) in the primate by positron emission tomography. *Acta neurologica Scandinavica* **1992**, *85*, 166-173.

(62) Bergström, M.; Lu, L.; Marquez, M.; Johan Fasth, K.; Bjurling, P.; Watanabe, Y.; Eriksson, B.; Långström, B. Modulation of organ uptake of 11C-labelled L-DOPA. *Nuclear Medicine and Biology* **1997**, *24*, 15-19.

(63) Gueguen, P.; Morgat, J.-L.; Maziere, M.; Berger, G.; Comar, D.; Maman, M. Enzymatic synthesis of 11C-labelled S-adenosylmethionine. *Journal of Labelled Compounds and Radiopharmaceuticals* **1982**, *19*, 157-170.

(64) Soussain, R.; Gueguen, P.; Morgat, J.-L.; Maziere, M.; Berger, G.; Comar, D. Enzymatic synthesis of 11C-labelled (−)-epinephrine. *Journal of Labelled Compounds and Radiopharmaceuticals* **1984**, *21*, 203-222.

(65) Harada, R.; Furumoto, S.; Yoshikawa, T.; Ishikawa, Y.; Shibuya, K.; Okamura, N.; Iwata, R.; Yanai, K. Synthesis of [11C]interleukin 8 using a cell-free translation system and L-[11C]methionine. *Nucl Med Biol* **2012**, *39*, 155-160.

(66) Spirin, A. S.: *Cell-Free Translation Systems*; Springer Berlin Heidelberg, 2012.

(67) Carlson, E. D.; Gan, R.; Hodgman, C. E.; Jewett, M. C. Cell-Free Protein Synthesis: Applications Come of Age. *Biotechnology advances* **2012**, *30*, 1185-1194.

(68) Cohen, M. B.; Spolter, L.; Chang, C. C.; Cook, J. S.; Macdonald, N. S. Enzymatic synthesis of 11C-pyruvic acid and 11C-L-lactic acid. *The International Journal of Applied Radiation and Isotopes* **1980**, *31*, 45-49.

(69) Kloster, G.; Laufer, P. Enzymatic synthesis and chromatographic purification of L-3-[11C]-lactic acid via D, L-3-[11C]-alanine. *J. Labelled Compd. Radiopharmaceut.* **1980**, *17*, 889-894.

(70) Barrio, J. R.; Phelps, M. E.; Huang, S.-C.; Keen, R. E.; MacDonald, N. S. 1-(C-11)L-leucine and the principle of metabolic trapping for the tomographic measurement of cerebral protein synthesis in man. *J. Labelled Compd. Radiopharmaceut.* **1982**, *19*, 1271-1272.

(71) Barrio, J. R.; Keen, R. E.; Ropchan, J. R.; MacDonald, N. S.; Baumgartner, F. J.; Padgett, H. C.; Phelps, M. E. L-[1-11C]Leucine: Routine Synthesis by Enzymatic Resolution. *J. Nucl. Med.* **1983**, *24*, 515-521.

(72) Ehrin, E.; Stone-Elander, S.; Nilsson, J. L. G.; Bergström, M.; Blomqvist, G.; Brismar, T.; Eriksson, L.; Greitz, T.; Jansson, P. E.; Litton, J.-E.; Malmborg, P.; af Ugglas, M.; Widén, L. C-11-Labeled Glucose and its Utilization in Positron-Emission Tomography. *J. Nucl. Med.* **1983**, *24*, 326-331.

(73) Ropchan, J. R.; Barrio, J. R. Enzymatic synthesis of [1-11C]pyruvic acid, L-[1-11C]lactic acid and L-[1-11C]alanine via DL-[1-11C]alanine. *J. Nucl. Med.* **1984**, *25*, 887-892.

(74) Takahashi, T.; Någren, K.; Aho, K. An alternative synthesis of DL-[1-11C]Alanine from [11C]HCN. *International Journal of Radiation Applications and Instrumentation. Part A. Applied Radiation and Isotopes* **1990**, *41*, 1187-1191.

(75) Bjurling, P.; Långström, B. Synthesis of 1- and 3-11C-labelled L-lactic acid using multi-enzyme catalysis. *J. Labelled Compd. Radiopharmaceut.* **1990**, *28*, 427-432.

(76) Ögren, M.; Långström, B. ChemInform Abstract: Synthesis of D-[1-11C]Mannitol and Its Enzymatic Oxidation to D-[1/6-11C]Fructose. *Acta Chem. Scand.* **1998**, *52*, 1137-1140.

(77) Ikemoto, M.; Sasaki, M.; Haradahira, T.; Okamoto, E.; Omura, H.; Furuya, Y.; Watanabe, Y.; Suzuki, K. A new synthesis of [3-11C]pyruvic acid using alanine racemase. *Applied Radiation and Isotopes* **1998**, *49*, 1557-1562.

(78) Wangler, C.; Kostikov, A.; Zhu, J.; Chin, J.; Wangler, B.; Schirrmacher, R. Silicon-[18F]Fluorine Radiochemistry: Basics, Applications and Challenges. *Applied Sciences* **2012**.

(79) Schirrmacher, R.; Wangler, C.; Schirrmacher, E. Recent Developments and Trends in 18F-Radiochemistry: Syntheses and Applications. *Mini Rev. Org. Chem.* **2007**, *4*, 317-329.

(80) Gatley, S. J.; Brown, S. G.; Thompson, C. M. Rapid, Inexpensive Quality Control of fluorine-18 2-Deoxy-2-Fluoro-D-Glucose Preparations Using the Hexokinase Reaction In Vitro. *J. Nucl. Med.* **1988**, *29*, 1443-1447.

(81) Lui, E.; Chirakal, R.; Firnau, G. Enzymatic synthesis of (−)-6-[18F]-fluoronorepinephrine from 6-[18F]-fluorodopamine by dopamine β-hydroxylase. *J Label Compd Radiopharm* **1998**, *41*, 503–521.

(82) Kaneko, S.; Ishiwata, K.; Hatano, K.; Omura, H.; Ito, K.; Senda, M. Enzymatic synthesis of no-carrier-added 6-[18F]fluoro-l-dopa with β-tyrosinase. *Applied Radiation and Isotopes* **1999**, *50*, 1025-1032.

(83) Prante, O.; Hamacher, K.; Coenen, H. H. Chemo-enzymatic n.c.a. synthesis of the coenzyme uridine diphospho-2-deoxy-2-[18F]fluoro-α-D-glucose (Abstract). *J Label Compd Radiopharm* **1999**, *42*, S111-S112.

(84) Deng, H.; O'Hagan, D.; Schaffrath, C. Fluorometabolite biosynthesis and the fluorinase from Streptomyces cattleya. *Natural Product Reports* **2004**, *21*, 773-784.

(85) Zhu, X.; Robinson, D. A.; McEwan, A. R.; O'Hagan, D.; Naismith, J. H. Mechanism of Enzymatic Fluorination in Streptomyces cattleya. *Journal of the American Chemical Society* **2007**, *129*, 14597-14604.

(86) O'Hagan, D.; Schaffrath, C.; Cobb, S. L.; Hamilton, J. T. G.; Murphy, C. D. Biochemistry: Biosynthesis of an organofluorine molecule. *Nature* **2002**, *416*, 279-279.

(87) Dong, C.; Huang, F.; Deng, H.; Schaffrath, C.; Spencer, J. B.; O'Hagan, D.; Naismith, J. H. Crystal structure and mechanism of a bacterial fluorinating enzyme. *Nature* **2004**, *427*, 561-565.

(88) O'Hagan, D.; Deng, H. Enzymatic Fluorination and Biotechnological Developments of the Fluorinase. *Chemical Reviews* **2015**, *115*, 634-649.

(89) Onega, M.; Winkler, M.; O'Hagan, D. Fluorinase: a tool for the synthesis of 18F-labeled sugars and nucleosides for PET. *Future Medicinal Chemistry* **2009**, *1*, 865-873.

(90) Martarello, L.; Schaffrath, C.; Deng, H.; Gee, A. D.; Lockhart, A.; O'Hagan, D. The first enzymatic method for C–18F bond formation: the synthesis of 5′-[18F]-fluoro-5′-deoxyadenosine for imaging with PET. *Journal of Labelled Compounds and Radiopharmaceuticals* **2003**, *46*, 1181-1189.

(91) Deng, H.; Cobb, S. L.; Gee, A. D.; Lockhart, A.; Martarello, L.; McGlinchey, R. P.; O'Hagan, D.; Onega, M. Fluorinase mediated C-18F bond formation, an enzymatic tool for PET labelling. *Chem. Commun.* **2006**, 652-654.

(92) Sergeev, M. E.; Morgia, F.; Javed, M. R.; Doi, M.; Keng, P. Y. Polymer-immobilized fluorinase: Recyclable catalyst for fluorination reactions. *Journal of Molecular Catalysis B: Enzymatic* **2013b**, *92*, 51-56.

(93) Sergeev, M. E.; Morgia, F.; Javed, M. R.; Doi, M.; Keng, P. Y. Enzymatic radiofluorination: Fluorinase accepts methylaza-analog of SAM as substrate for FDA synthesis. *J. Mol. Catal. B: Enzym.* **2013a**, *97*, 74-79.

(94) Dall'Angelo, S.; Bandaranayaka, N.; Windhorst, A. D.; Vugts, D. J.; van der Born, D.; Onega, M.; Schweiger, L. F.; Zanda, M.; O'Hagan, D. Tumour imaging by Positron Emission Tomography using fluorinase generated 5-[18F]fluoro-5-deoxyribose as a novel tracer. *Nuclear Medicine and Biology*, *40*, 464-470.

(95) Onega, M.; Domarkas, J.; Deng, H.; Schweiger, L. F.; Smith, T. A. D.; Welch, A. E.; Plisson, C.; Gee, A. D.; O'Hagan, D. An enzymatic route to 5-deoxy-5-[18F]fluoro-d-ribose, a [18F]-fluorinated sugar for PET imaging. *Chemical Communications* **2010**, *46*, 139-141.

(96) Prante, O.; Hamacher, K.; Coenen, H. H. Chemoenzymatic n.c.a synthesis of the coenzyme UDP-2-deoxy-2-[18F]fluoro-α-D-glucopyranose as substrate of glycosyltransferases. *Journal of Labelled Compounds and Radiopharmaceuticals* **2007**, *50*, 55-63.

(97) Li, X.-G.; Domarkas, J.; O'Hagan, D. Fluorinase mediated chemoenzymatic synthesis of [18F]-fluoroacetate. *Chem. Commun.* **2010**, *46*, 7819-7821.

(98) Winkler, M.; Domarkas, J.; Schweiger, L. F.; O'Hagan, D. Fluorinase-Coupled Base Swaps: Synthesis of [18F]-5′-Deoxy-5′-fluorouridines. *Angew. Chem. Int. Ed.* **2008**, *47*, 10141-10143.

(99) Harada, R.; Furumoto, S.; Yoshikawa, T.; Ishikawa, Y.; Shibuya, K.; Okamura, N.; Ishiwata, K.; Iwata, R.; Yanai, K. Synthesis and Characterization of [18F]-Interleukin-8 Using a Cell-Free Translation System and 4-[18F]-Fluoro-L-Proline. *Journal of nuclear medicine : official publication, Society of Nuclear Medicine* **2016**, *57*, 634-639.

(100) Gouveia, B. G.; Rijo, P.; Gonçalo, T. S.; Reis, C. P. Good manufacturing practices for medicinal products for human use. *Journal of Pharmacy & Bioallied Sciences* **2015**, *7*, 87-96.

(101) EudraLex - Good Manufacturing Practice (GMP) guidelines. DIRECTORATE-GENERAL, E. C. H. A. C., Ed., 2012; Vol. Vol. 4.

Chapter 3

Background and objectives

BACKGROUND

Emerging PET applications, together with the need for better, more efficient and even personalized diagnostic tools, have resulted in a boost in the demand for new molecular probes for biological targets currently inaccessible to this technique. The development of such molecular probes (radiotracers) requires a multidisciplinary vision and approach, which should start at target identification, structure design and development/implementation of radiolabeling strategies, followed by exhaustive *in vitro* and *in vivo* testing, ultimately leading to radiotracer validation.

The radiochemistry associated with the synthesis of radiotracers is far from trivial, especially for short half-lived radionuclides. Because of the limited availability of training programs in this field, PET centres and (radio)pharmaceutical companies compete for a limited pool of talent. This gap was identified by Prof. V. Gouverneur (University of Oxford), coordinator of the Marie-Curie FP7-PEOPLE-ITN action **RADIOMI** (2012-2016). In this initiative, six academic and two industrial partners, all of them leading experts in the areas of chemistry and radiochemistry, pooled their expertises to implement a coordinated, first-class training program to produce new talent in PET radiochemistry, focused on the development of innovative radiolabeling strategies for the preparation of small molecules labeled with short-lived positron emitters, namely fluorine-18, carbon-11 and nitrogen-13, while spanning over a wide range of molecular formats. Besides establishing a cutting-edge, scientifically sound research program, this successful initiative aimed to provide transnational and cross-sectorial training to 15 ESRs and 3 ERs, covering different aspects of radiolabeling using positron emitters.

CIC biomaGUNE, a research institution located in San Sebastian and where the experimental part of the current PhD thesis was conducted, participated in such initiative. Due to the previous work and tracked experience of Dr. Llop's group in the field of ^{13}N-radiochemistry, the specific role of CIC biomaGUNE team within the project was to develop innovative labeling strategies using nitrogen-13. With that aim, two PhD students were selected. One of them, Sameer M. Joshi, was focused on the development of novel strategies for the preparation of ^{13}N-labeled compounds using the labeling agent $[^{13}N]NO_2^-$. The project for the second PhD student, myself, Eunice S. Da Silva, author of the work presented here, should focus on developing innovative enzymatic strategies for the preparation of radiolabeled amino acids. In the experimental work, I was able to merge radiochemistry and biocatalysis to access valuable radiotracers in a more efficient manner thanks to the close collaboration established with the group of Heterogeneous biocatalysis from CIC biomaGUNE and led by Dr. Fernando López Gallego, who is the co-supervisor of this thesis together with Dr. Jordi Llop. This fruitful collaboration, which started at the beginning of the thesis and is still active nowadays, and aims to apply biocatalytic solutions in radiochemistry. This thesis is a clear example of how to succeed bringing together two different areas to develop a multi-disciplinary project.

Besides conducting the experimental work and getting involved in a cutting-edge research program at the local level, participation in the **RADIOMI** initiative provided me with the opportunity to collaborate with other different fields such as cancer research in collaboration with Prof. Arkaitz Carracedo (Animal studies), and to attend periodic meetings and different workshops, schools and international conferences, which have contributed to my overall education.

In this context, the first goal of the current PhD was the investigation of the work published in the field of enzymatic catalysis applied to radiochemistry. This investigation was focused on the work published since 1980 when the last review describing the applications of enzymatic methods in radiochemistry for the synthesis of PET radionuclides was published. All the literature found in this area was reviewed and the manuscript has been submitted to a scientific peer-reviewed journal (*Journal of Labelled Compounds and Radiopharmaceuticals*). Hence, the state-of-art of the enzymatic methods in radiochemistry was the basis of the work presented in the previous **Chapter 2**.

Considering the potential of the enzymes observed within this literature revision, the first experimental goal of the present PhD was to develop biocatalytic strategies for the preparation of pure ^{13}N-nitrite, which can be used as suitable labeling precursor for the subsequent preparation of ^{13}N-labeled molecules of interest. The results obtained were published in *Catalysis Science & Technology* (*Catal. Sci. Technol.*, 2015, **5**, 2705-2713 **DOI:** 10.1039/C5CY00179J) and are the basis of **Chapter 4** of this PhD thesis.

The successful application of enzymes in nitrogen-13 radiochemistry obtained in the first experimental work aroused our interest in the development of other enzymatic strategies to label small biomolecules. For example, amino acids could be very interesting tracers for the detection of some types of cancer. Enantioselective chemical synthesis of amino acids is also problematic and very hard to achieve. The use of enzymes could help, thanks to their fast reaction rates and unique enantio- and chemo-selectivity. *L*-alanine dehydrogenase from *Bacillus subtilis* was the selected enzyme for the synthesis of amino acids which use ammonia as

substrate. This biocatalyst was firstly tested and characterized under non-radioactive conditions. After optimization of the experimental conditions, the experimental setup was then applied to the synthesis of a variety of ^{13}N-labeled amino acids (L-[^{13}N]alanine, [^{13}N]glycine, and L-[^{13}N]serine). The enzymatically radiolabeled amino acids were further analyzed regarding their *in vivo* biodistribution in healthy (wild-type) mice. The capacity to selectively accumulate in the tumor was assessed in a prostate cancer mouse model kindly provided by Prof. Carracedo. This work, which is the basis of **Chapter 5** of the current PhD thesis, was published in *Chemistry - A European Journal* (*Chem. Eur. J. 2016, 22, 13619.* **DOI:** 10.1002/chem.201602471).

The third experimental part of the PhD thesis consisted in the stabilization of L-Alanine dehydrogenase from *Bacillus subtillis* into a solid carrier. This enzyme has been intensively exploited in biocatalysis but its immobilized form is rarely used. The immobilization of L-Alanine dehydrogenase from *Bacillus subtillis* was essayed on three different agaroses. After optimization of the experimental conditions and selection of the best catalyst, the experimental set up was then applied to the synthesis of labeled amino acids. This work, which is described in **Chapter 6** of the current PhD thesis, was published in *Process Biochemistry* (*Proc. Biochemistry. 2017.* **DOI:** 10.1016/j.procbio.2017.03.005).

OBJECTIVES

The general objective of this PhD thesis was the development of enzymatic strategies for the preparation of ^{13}N-labeled of radiotracers. To achieve this goal, the following specific objectives were defined:

1- To acquire a solid knowledge about the potential of the biocatalysis in radiochemistry in order to design enzymatic strategies for efficient synthetic routes of relevant radiotracers.

2- To develop an immobilized biocatalyst-based on a NADPH-dependent nitrate reductase for the one-pot preparation and one-step purification of $[^{13}N]NO_2^-$, to be used as a radioactive precursor for the subsequent chemical synthesis of *S*-$[^{13}N]$nitrosoglutathione.

3- To select and produce a suitable NADH-dependent L-amino acid dehydrogenase to synthesize enantiopure ^{13}N-labeled amino acids using $[^{13}N]NH_3$ as the primary labeling agent and α-ketoacids as starting materials.

4- To integrate a recycling enzyme (formate dehydrogenase) to the synthetic process developed in objective 3, in order to *in situ* replenish the pool of NADH.

5- To assess the biodistribution of the ^{13}N-labeled amino acids synthesized in objective 3 in healthy mice; to evaluate the potential of these ^{13}N-labeled amino acids as radiotracers for the diagnostic of prostate cancer in animals with Pten deletion.

6- To stabilize the amino acid dehydrogenase selected in objective 3 by immobilizing this enzyme on solid carriers using different immobilization chemistries; to fabricate and characterise a robust
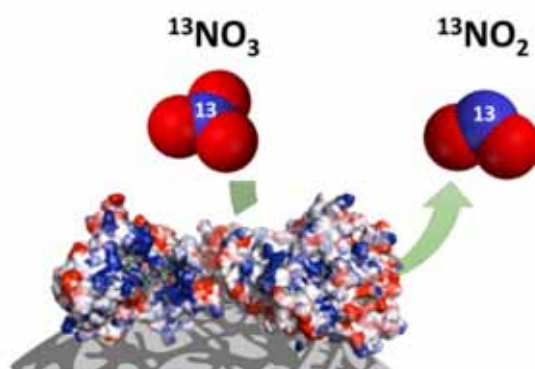
heterogenous biocatalysts in order to run consecutive cycles of radiochemical synthesis of ^{13}N-labeled amino acids.

Chapter 4

Efficient [^{13}N]nitrate reduction catalyzed by a highly stable immobilized biocatalyst

In the present chapter, an unprecedented strategy for the reduction of [^{13}N]NO$_3^-$ to [^{13}N]NO$_2^-$ using a heterogeneous biocatalyst will be presented. A eukaryotic nitrate reductase from *Aspergillus niger* was immobilized on different carriers. Optimal immobilization yield and recovered activities were obtained when this enzyme was immobilized on porous agarose beads activated with positively charged tertiary amino group (Ag-DEAE). The optimal immobilized preparation was 12-fold more thermostable than the soluble enzyme. Biochemical characterization of the immobilized enzyme showed an interesting thermal-induced hyperactivation driven by the interaction between the enzyme and the carrier. The best heterogeneous biocatalyst could be re-used up to 7 reaction cycles preserving its initial activity. Finally, to demonstrate the potential of this heterogeneous biocatalyst in the context of radiochemistry, a chemo-enzymatic radiosynthesis of *S*-[^{13}N]nitrosoglutathione was approached using enzymatically produced [^{13}N]NO$_2^-$ as the labeling precursor.

INTRODUCTION

As recently shown by our research group, the labeling agent $[^{13}N]NO_2^-$ is a useful precursor for the preparation of a wide range of labeled compounds such as S-$[^{13}N]$nitrosothiols[1,2], S-$[^{13}N]$nitrosamines[3], ^{13}N-labeled azo derivatives[4,5], ^{13}N-labeled azides[6] and ^{13}N-labeled triazoles[7], and further applications are currently being investigated[8]. Unfortunately, direct production of $[^{13}N]NO_2^-$ in the cyclotron is not feasible and it is usually obtained by reduction of $[^{13}N]NO_3^-$ to $[^{13}N]NO_2^-$ using a typical column containing activated cadmium.[9] Besides the inherent toxicity of cadmium, which may hamper the translation of the technology to the clinical field, this experimental setting presents several technological pitfalls.

Inspired by the biological cycle of nitrogen[10], we reasoned that eukaryotic nitrate reductase (eNR)[11] may efficiently catalyze the reduction of $[^{13}N]NO_3^-$ to the more convenient labeling agent $[^{13}N]NO_2^-$. The enzyme eNR is a homodimer which contains three different domains per monomer: one N-terminus domain that binds NADPH and FAD^+ as redox cofactors (NADPH-domain), a second cytochrome b domain containing a Fe-heme cofactor (heme-domain) and a third C-terminus domain that binds a molybdopterin cofactor (MOCO-domain). All these cofactors are required during the catalytic cycle; while FAD^+, heme and MOCO cofactors are stably bound to the enzymes, NADPH must be exogenously added to the reaction media. The enzyme mechanism relies on the large conformational change that approaches the NADPH/FAD^+ and heme domains to the MOCO domain, allowing the electron transfer from

NADPH to molybdenum via the heme group to reduce nitrate to nitrite (**Figure 4.1**).[12]
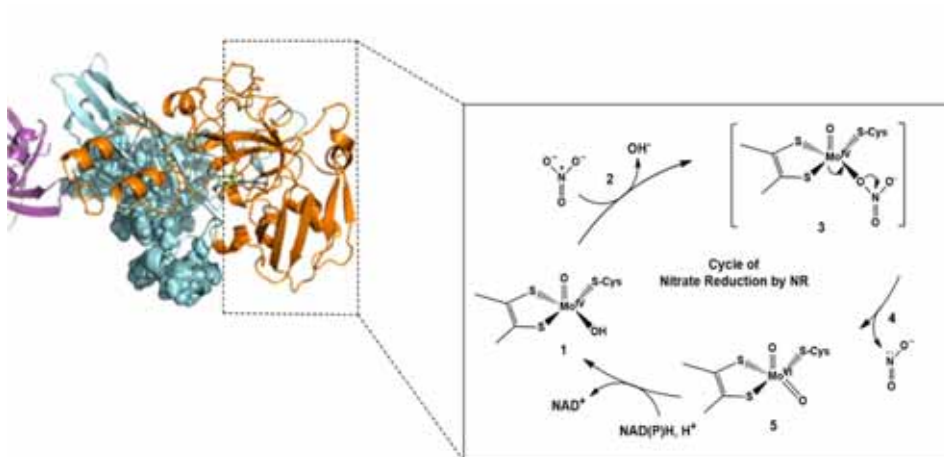
Figure 4.1. Hypothetical reaction cycle of nitrate reduction by NR. The reaction starts with the reduced Mo[IV] form (**1**). Then, nitrate binds to the active site (**2**) and replaces the equatorial hydroxo/water ligand, forming an intermediate (**3**). The bond between the nitrate oxygen and nitrogen is broken and nitrite is released (**4**); consequently, the Mo center is oxidized to Mo[VI] (**5**). After completion of the reductive half-reaction, the Mo is regenerated [Mo(IV)] for the next cycle. Adapted from the reference[12].

Nitrate reductase has been mainly applied for the detection and determination of nitrate in different sources. Nitrate is a typical inorganic pollutant in environmental, food, industrial and physiological systems[13,14], therefore, various methods for detection and determination of nitrate have been reported, involving spectroscopic, chromatographic, electrochemical detection methods, etc.[15,16] Although, spectroscopic and chromatographic methods are accurate and reliable, they require bulky, delicate and

expensive equipment which is not suitable for *in situ* applications. Over the past decades, the immobilization of nitrate reductase has been quite exploited in biosensors based on immobilization methods, consisting of another option for optical[17] and electrochemical[18-21] biosensing applications. However, the immobilization of this enzyme is rather challenging since restrictions in the conformational flexibility required for the catalysis may compromise the reducing capacity. This structural complexity may explain the low recovered activity of immobilized eNRs reported elsewhere.[22] In our work, we pretend to stabilize and make use of the nitrate reductase not for nitrate detection but to incorporate it in radiochemical synthetic routes. To the extent of our knowledge, the nitrate reductase has been not tested in any synthetic approaches.

In the present chapter, we will present the unprecedented use of eNR as an efficient heterogeneous biocatalyst for the reduction of $[^{13}N]NO_3^-$ to $[^{13}N]NO_2^-$. The immobilization chemistry was optimized to yield active and stable preparations of immobilized eNR on porous agarose beads. As a proof of concept of the applicability of the experimental set up to the preparation of PET tracers, the ^{13}N-labeled nitrosothiol *S*-$[^{13}N]$nitrosoglutathione ($[^{13}N]GSNO$) was prepared with an excellent radiochemical conversion.

EXPERIMENTAL SECTION

Materials

Agarose beads activated with a primary amine group (Ag-MANAE)[23], coated with 25 KDa polyethyleneimine (Ag-PEI)[24] and coated with dextran-sulphate (Ag-DS)[25] were prepared as described elsewhere. Cyanogen bromide-activated-Sepharose® 4B (Ag-CB) was purchased from Sigma-Aldrich Química S.A. (Madrid, Spain) and diethyl-aminoethyl Sepharose (Ag-DEAE) was purchased from GE healthcare (Pittsburgh, USA). Nitrate reductase from *Aspergillus niger* and reduced β-Nicotinamide adenine dinucleotide 2′-phosphate tetrasodium salt (β-NADPH; purity >97%) were purchased from Roche Life Science (Barcelona, Spain). Sodium nitrite ($NaNO_2$, ACS reagent, Ph. Eur.), sodium nitrate ($NaNO_3$, ACS reagent), sodium phosphate dibasic (Na_2HPO_4, for molecular biology, purity ≥98.5%), sodium phosphate monobasic (NaH_2PO_4, purity ≥99.0%), glutathione (GSH, purity ≥99%), *S*-nitrosoglutathione (GSNO, purity ≥97%), hydrochloric acid (HCl, 1 M standard solution), sodium hydroxide (NaOH, ACS reagent), trifluoroacetic acid (CF_3COOH, HPLC grade) and acetonitrile (CH_3CN, HPLC grade) were purchased from Sigma-Aldrich Química S.A. (Madrid, Spain) and used without further purification. Bio-Rad Protein Assay Dye Reagent Concentrate was purchased from BIO-RAD (Madrid, Spain). Additive for ionic chromatography mobile phase (P/N 5062-2480) was purchased from Agilent Technologies (Madrid, Spain). All others reagents were of analytical grade unless otherwise specified.

METHODS

Structural modeling of nitrate reductase from *Aspergillus niger*. Structural homology models complexed with molybdenum, NADPH, FAD^+ and heme cofactors were built by using different structural templates and aided by the homology-modeling server from Expasy.[26] The modeling server selected the nitrate reductase from *Pichia pastoris* (2BIH) complexed with molybdopterin as template to model the molybdenum binding domain with 56% identity (**Figure 4.2A**). However, the server modeled both cytochrome and $NADPH/FAD^+$ domains by using NADH-dependent cytochrome B5 reductase from rat (1IB0) complexed with both FAD^+ and NAD^+ as a template showing 39% identity (**Figure 4.2B**).
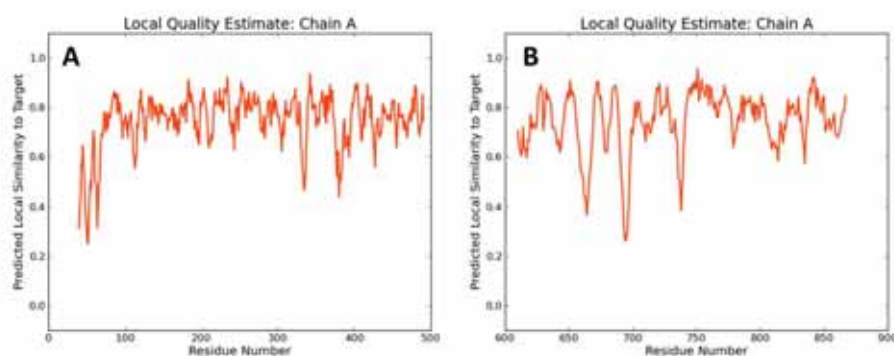
Figure 4.2. Plot showing predicted local similarity for the MOCO domain (**A**) and the NADPH binding domain (**B**) of eNR enzyme model by the homology-modeling server from Expasy (predicted local similarity versus residue number).

Structures are validated by comparison of an atomic model with their amino acid sequences and assignment from 1 (high reliability) to 0 (poor

reliability) for each amino acid positions. The model for the domain that binds NADPH, FAD$^+$ and heme has a very good compatibility score, while the model for the molybdenum binding domain presented very low score mainly due to the low compatibility of its *N*-terminus that was highly flexible and consequently hard to model. Protein models were visualized and aligned with their template structure by using PyMol 0.99 developed by DeLano Scientific LLC (San Francisco, CA). The electrostatic potential was calculated by using Bluues server.[27]

Determination of the enzyme activity and protein concentration. The activities of both free and immobilized nitrate reductase from *Aspergillus niger* were determined by measuring the decrease in absorbance at 340 nm, resulting from NADPH oxidation during the enzymatic conversion of nitrate to nitrite. A sample of enzyme solution of 10 μL was incubated in a multi-well plate with 190 μL reaction mixture with a final concentration of 10 mM sodium phosphate buffer, 0.21 mM NADPH and 4.25 mM NaNO$_3$ at 25°C and pH 7.5 under mild shaking. When indicated, different temperatures and pH values were used. One activity unit was defined as the amount of enzyme required to oxidize 1 μmol of NADPH under the above-described conditions. The protein concentration of all soluble eNR samples was measured by using Bradford's method[28] and bovine serum albumin (BSA) as a protein standard.

Kinetic parameters. The kinetic parameters were calculated from the initial rate values determined with different concentrations of NADPH (0-2 mM) and nitrate (0-20 mM). Results were fitted to Michaelis-Menten equation by non-linear regression and K_m and k_{cat} were calculated using OriginPro 8.0 software.

Enzyme Immobilization. The eNR was immobilized on agarose beads activated with cyanogen bromide groups (Ag-CB), on agarose beads activated with either positively charged mono-aminoethyl groups (Ag-MANAE) or diethyl-aminoethyl groups (Ag-DEAE) and coated with positively charged poly-ethylenimine (Ag-PEI), and on agarose beads coated with negatively charged dextran-sulphate (Ag-DS).

Generally, all the immobilizations were carried out by adding 200mg of the corresponding carrier (Ag-CB, Ag-DEAE, Ag-MANAE, Ag-PEI and Ag-DS) to 1mL of soluble eNR (1-5U/mL) in 10 mM sodium phosphate at pH 7.5. The suspension was kept under mild stirring at 25°C. Periodically, samples of the supernatants and the carrier-enzyme suspensions were withdrawn and analyzed to evaluate the progress of the immobilization process. In parallel, a blank of the soluble enzyme (without a carrier) was also analyzed. After immobilization, enzyme preparations were washed with an excess of distilled water and immobilization buffer to eliminate any non-bound protein molecule.

The immobilization on Ag-CB requires a pre-activation of the carrier; thus, 0.2 g of the lyophilized carrier was washed and swell with 10mL HCl 1 mM during 30 min, followed by gentle filtration between successive additions of water. Then, the washed carrier was equilibrated with 100 mM $NaHCO_3$ in 0.5 M NaCl, pH 8.3. eNR was incubated with the support under mild stirring at room temperature. The support containing the immobilized eNR was washed with Tris–HCl using 0.1 M HCl, pH 8.0, followed by 0.1 M acetic acid/sodium acetate containing 0.5 M NaCl, pH 4.0 (3 cycles of alternating pH buffers) to block any remaining active groups.

Thermal stability of soluble and immobilized eNR. All enzyme preparations (both soluble and immobilized), were incubated in 10mM sodium phosphate buffer (pH 7.5) at different temperatures (25-55°C) for 15 min. As previously described, the eNR activities were assayed at 25 ºC. In a different experiment, soluble and immobilized preparations were incubated at 40ºC, and samples were withdrawn at different times and assayed at 25ºC to determine the residual activity. The inactivation constant is calculated by fitting the thermal inactivation curve to first-order kinetics equation ($A/A_o = e^{-k*t}$) considering that the enzyme becomes completely inactivated after a certain time. The fitting was carried out by using OriginPro 8.

Loading capacity. For the best immobilization chemistry, Ag-DEAE, loading capacity studies were carried out. Different amounts of *Aspergillus niger* eNR preparation (0.0075; 0.0107; 0.0143; 0.0255; 0.0349 mg protein) were offered to 200 mg of Ag-DEAE suspended in 1 mL of 10 mM sodium phosphate buffer at pH 7.5. The amount of protein bound to the carrier was determined as the difference between the initial and the residual protein concentration in the supernatants. This loading capacity was also monitored by analyzing both initial and residual enzyme activity in the supernatant. For each enzyme load, recovered activity of the immobilized eNR was measured upon the immobilization process.

Fluorescence Spectroscopy studies. Fluorescence measurements were carried out in a Varioskan Flash fluorescence spectrophotometer (Thermo Scientific), monitoring the intrinsic fluorescence of soluble and immobilized *Aspergillus niger* eNR on Ag-DEAE, using an excitation wavelength of 280nm with excitation and emission bandwidths of 5 nm and recording fluorescence emission spectrum between 300 and 600nm.

All spectroscopic measurements were made in 10 mM sodium phosphate at pH 7.5 and 25°C.

Activity-pH profile of eNR soluble and immobilized on Ag-DEAE. The effect of pH on the activity of the enzyme preparations was determined by measuring the residual activities of eNR at the different pH values (5<pH<10) and 25°C. The expressed activity was measured as described before. Different 10 mM buffer solutions were used to set the right pH value; acetate buffer was used for pH 5-6; sodium phosphate buffer for pH 7-8 and sodium bicarbonate buffer for pH 9-10.

Production of the radioactive precursor [^{13}N]NO$_2^-$ by enzyme catalysis: general procedure

Nitrogen-13 was produced in an IBA Cyclone 18/9 cyclotron via the ^{16}O(p,α)^{13}N nuclear reaction. The target system consisted of an aluminum insert (2 mL) covered with havar foil (thickness 25 μm, Ø 29 mm) and with an aluminum vacuum foil (thickness 25 μm, Ø 23 mm). The target (containing 1.75 mL of ultrapure water, Type I water, ISO 3696) was irradiated with 18MeV protons. The beam current was maintained at 20 μA (pressure in the range 5–10 bar into the target during bombardment) to reach the desired integrated currents (0.1-0.5 μAh). The resulting solution was transferred to a 10mL vial and the activity was measured in a dose calibrator (Capintec CRC®-25 PET, New Jersey, USA). The final activities (corrected to the end of irradiation) were in the range 333-1110 MBq (9-30 mCi).

Enzymatic reduction of [^{13}N]NO$_3^-$ to [^{13}N]NO$_2^-$ was carried out with 6.72 mU of immobilized eNR packed into a plastic column. This insoluble preparation was incubated with 90 μL of cyclotron produced ^{13}N solution

(which contained $[^{13}N]NO_3^-$) in the presence of 10μL of 2.1 mM NADPH (0.21 mM final concentration) in 500 mM sodium phosphate buffer (50 mM final concentration; pH 7.5) under mild conditions (25°C and pH 7.5) for 4 min. Relative amounts of $[^{13}N]NH_4^+$, $[^{13}N]NO_2^-$ and $[^{13}N]NO_3^-$ were measured by radio-HPLC. An Agilent 1200 series HPLC equipped with a quaternary pump, a multiple wavelength detector and a radiometric detector (Gabi, Raytest) was used. An HP Asahipak ODP-50 (5 μm, 125x4 mm, Teknokroma, Spain) was used as stationary phase, and a solution containing additive for ionic chromatography (15 mL) in 1L of a mixture water/acetonitrile (86:14) basified to pH 8.6 with 1M sodium hydroxide solution was used as the mobile phase at a flow rate of 1 mL/min. Simultaneous UV ($\lambda = 254$ nm) and isotopic detection were used.

Recycling of eNR immobilized on Ag-DEAE. Reusability of eNR immobilized on Ag-DEAE was evaluated by performing consecutive catalytic cycles at 25°C using nitrate (both non-radioactive and radioactive) and NADPH as substrates. In some experiments, the immobilized enzyme was incubated with a solution 1.0 mM NADPH and the nitrate reduction was carried out without adding exogenous NADPH. After each cycle, the immobilized preparation was washed and the enzymatic activity towards non-radioactive nitrate was determined by spectrophotometry, while the final yield towards radioactive nitrate was determined by radio-HPLC.

Two-step chemo-enzymatic synthesis of *S*-[^{13}N]nitrosoglutathione ([^{13}N]GSNO)

The preparation of [^{13}N]GSNO followed the synthetic protocol previously reported,[2] but the $[^{13}N]NO_2^-$ used as the labeling agent was enzymatically synthesized. A radioactive solution (300 μL) containing cyclotron

produced $[^{13}N]NO_3^-$ was incubated in a packed column equilibrated with 1 mM NADPH loaded with 175µg eNR per g of carrier (22mU of immobilized eNR determined as previously described) for 4 min; the resulting supernatant containing $[^{13}N]NO_2^-$ was diluted with 1 mL of 10 mM sodium phosphate buffer (pH=7.5) and then flushed through an anion exchange cartridge (Sep-Pak® Accell Plus QMA, Waters) to selectively retain $[^{13}N]NO_2^-$. The column was further washed with distilled water (2 mL) and the QMA cartridge was dried with nitrogen gas for 15s. An acidic solution of the precursor glutathione (0.5 mL; 1 mM) was loaded into the cartridge and the nitrosation reaction was allowed to occur; the reaction mixture was finally eluted directly into a collection vial. The identification of $[^{13}N]GSNO$ was performed by co-elution with reference standard using the same HPLC system described above; in this case, a Mediterranean SeaRP-18 column (5µm, 150 x 4.6mm, Teknokroma, Spain) was used as stationary phase and aqueous TFA solution/acetonitrile (95:5) was used as the mobile phase at a flow rate of 1 mL/min. Simultaneous UV ($\lambda = 220$ nm) and isotopic detection were used.

RESULTS AND DISCUSSION

Immobilization of eNR on functionalized porous agarose beads

Eukaryotic nitrate reductase from *Aspergillus niger* was immobilized through different immobilization chemistries on a survey of agarose-based matrixes: i) irreversibly immobilized through its *N*-terminus on agarose beads activated with cyanogen bromide groups (Ag-CB); ii) reversibly immobilized through its acid amino acid richest regions on agarose beads activated with either positively charged mono aminoethyl

groups (Ag-MANAE) or diethyl aminoethyl groups (Ag-DEAE) and coated with positively charged polyethylenimine (Ag-PEI); and iii) through its basic amino acid-richest regions on agarose beads coated with negatively charged dextran sulphate (Ag-DS), see **Table 3.1**.

Table 4.1. Parameters of *Aspergillus niger* nitrate reductase immobilization onto agarose carrier via different chemistries.

CARRIER	Reactive group	μmol of amines per gram of carrier	Immobilization chemistry	Immobilized Activity Ai (mU/g)[a]	Immobilization yield ψ (%)[b]	Expressed Activity Ae (mU/g)[c]/ (%)[d]
Ag-CB	Cyanogen Bromide	-	Covalent bond through the eNR Nt	964±32	96±3	26±4 / (3)
Ag-DEAE	Diethyl-aminoethyl	150	Ionic adsorption through the most acid eNR regions	995±10	99±1	210±60 / (21)
Ag-PEI	Poly-ethylenimine	3448		982±12	98±1	155±25 / (16)
Ag-MANAE	Mono-aminoethyl	5		820±24	82±2	192±41 / (23)
Ag-DS	Dextran-sulphate	-	Ionic adsorption through the most basic eNR regions	750	75	58 / (8)

The initial offered activity was always 1000mU per gram. [a]Ai=The activity immobilized on 1 gram of carrier after the immobilization process. This activity was calculated as the difference between the offered activity and the activity in the supernatant after incubation with the carrier for 1h. [b]Immobilization yield (ψ) = (immobilized activity/offered activity) x 100. [c]The expressed activity (Ae) is defined as the measured activity of the immobilized enzyme after washing. [d]Relative expressed activity (Ae) = (expressed activity/immobilized activity) x 100.

As it can be seen at **Table 4.1**, all carriers were able to efficiently immobilize eNR (immobilization yields >75% in all cases), although low values of expressed activity were achieved after immobilization when compared to the free enzyme. Irreversible immobilization and cationic exchange on Ag-CB and Ag-DS led to a dramatic decrease in the expressed activity (26±4 and 58 mU/g, respectively). On the other hand, ionic immobilization of eNR on positively charged carriers yielded values of expressed activity in the range 155-210 mU/g, resulting in up to 23% of

relative expressed activity. Noteworthy, although the chemistry that drove the immobilization on Ag-MANAE, Ag-DEAE and Ag-PEI was the same, Ag-MANAE offered lower immobilization yields ($82\pm2\%$) than Ag-DEAE ($99\pm1\%$) and Ag-PEI ($98\pm1\%$). This fact may be explained because Ag-MANAE surface presents a lower density of positively charged groups than Ag-DEAE and Ag-PEI surfaces, see **Table 4.1**.

In order to explain the functional discrepancies obtained with the different immobilized preparations, we further studied the eNR surface to understand how the protein orientation on the carrier surface may affect its functionality. Unfortunately, X-ray structure of eNR from *A. niger* has not been solved yet, and hence its 3D-structural homology model containing the NADPH-domain, the heme-domain and the MOCO-domain was built (**Figure 4.3A**) and the electrostatic surface potential was calculated in order to determine the spatial charge distribution across the enzyme surface (**Figure 4.3B and 4.3C**). The analysis of this structural model reveals an acidic belt on the MOCO-domain located at the opposite face regarding the active site. The model also shows that heme, FAD^+, NAD^+ and molybdenum binding sites are surrounded by basic amino acids (**Figure 4.3C**).
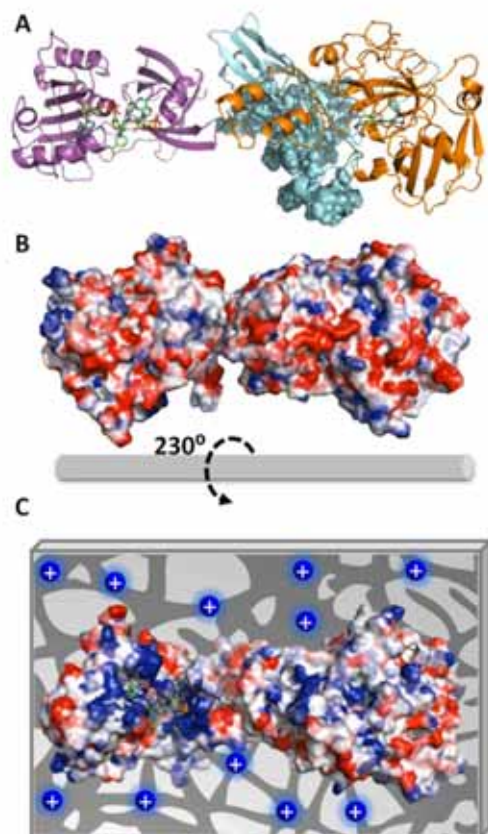
Figure 4.3. Structural model of a monomer of eNR from *Aspergillus niger*. (**A**) Cartoon representation of 3D-structural homology model by using the X-ray structures of eNR from Pichia pastoris and cytochrome B5 from rat complexed with both FAD^+ and NAD^+ as templates for molybdenum domain (*N*-terminus) (orange) and cytochrome domain (C-terminus) (purple) respectively. The sphere representation colored in cyan depicts the dimerization domain of the eNR. Green sticks represent the cofactors NAD^+, FAD^+ and molydopterin. (**B**) Surface electrostatic potential of eNR calculated by Bluues server (back face of active site) and (**C**) proposed orientation of eNR monomer on porous Ag-DEAE surface. The blue circles represent the tertiary amine groups located on the carrier surface. The surface electrostatic potential is depicted with a red-blue gradient that corresponds to the acid-basic gradient. All the images were prepared by using Pymol 0.99v.

These structural observations suggest that eNR immobilized on Ag-DS is oriented through its active site (basic region), hampering the accessibility of both NADPH and nitrate to the catalytic pocket with a consequent decrease in catalytic efficiency. Nevertheless, the eNR orientation onto positively charged carriers seems to occur through one acidic region located far away from the binding pockets. Therefore, active centres remain fairly accessible for the substrates, resulting in significantly higher relative expressed activity values for such immobilized preparations (**Figure 4.3C**). Moreover, such orientation seems to negligibly affect dimmer stability because the dimerization domain is not involved in the protein-carrier interaction. In fact, when eNR immobilized on Ag-DEAE was incubated under high ionic strength conditions, the enzyme was quantitatively eluted to the supernatant, demonstrating the ionic character and the reversibility of this immobilization chemistry.

The values of expressed activity shown in **Table 4.1** have been determined by using NADPH as a cofactor; such values are relatively high when compared with previous results obtained using immobilization protocols based on porous hydrogels. For example, eNR from *Aspergillus niger* immobilized on a porous vinyl polymeric matrix expressed less than 2% of its expressed activity by using NADPH as cofactor.[22] The high structural complexity of eNR might be the main reason for the low expressed activity achieved in this previous work. This enzyme requires enough structural flexibility for efficient electron transfer between both the cytochrome and the molybdenum domains. Hence, immobilization chemistries that highly rigidify the 3D structure of eNR (covalent immobilization), may hinder the catalytic conformational changes or promote wrong protein orientations that limit either the electron transfer

105

or the substrate accessibility, resulting in a low expressed activity of the immobilized preparation.

Effects of the temperature on both activity and stability of soluble and immobilized eNR

The thermal stabilities of immobilized and soluble eNR were tested at different temperatures. **Figure 4.4A** shows the inactivation courses of the three different immobilized preparations incubated at pH 7.5 and 25°C. The half-life time of eNR immobilized on Ag-DEAE was estimated 30-fold and 6-fold higher than eNR immobilized on Ag-MANAE and Ag-PEI, respectively, suggesting that the thermal stability of the immobilized enzymes relies on the chemical nature and density of the amine groups located on the surface of the carrier. The surface of Ag-DEAE containing 150 μmol/g of tertiary amine groups seems to establish more favourable interactions with the acidic protein regions than the Ag-MANAE surface, which presents low density of primary amine groups (5 μmol/g), and the Ag-PEI surface coated by a polymeric bed with a high density of primary, secondary and tertiary amine groups (3448 μmol/g). Ag-PEI has been suggested as an excellent carrier to stabilize multimeric enzymes, because the basic polymeric bed establishes 3D-protein-polymer interactions[24] that attach all the subunits to the carrier, resulting in a stabilization of the quaternary structure of the protein. Unexpectedly, in this study, eNR immobilized on Ag-PEI was less stable than eNR immobilized on Ag-DEAE. This unexpected result may be explained because the flexibility of the polymer may generate additional interactions with the protein over time. Such enhancement of the spatial reactivity may lead to undesired interactions between both cytochrome and molybdenum domains and the

polymeric brushes, reducing the enzyme flexibility required for the electron transfer, and consequently decreasing the nitrate reduction activity over time. Those negative interactions would not be possible to the much less flexible Ag-DEAE surface formed by a 2D-monolayer of tertiary amine groups. Hence, our results suggest that the interaction between eNR and the positively charged carriers must be strong enough to guarantee the stabilizing immobilization effect and flexible enough to enable the conformation changes required for the catalysis.
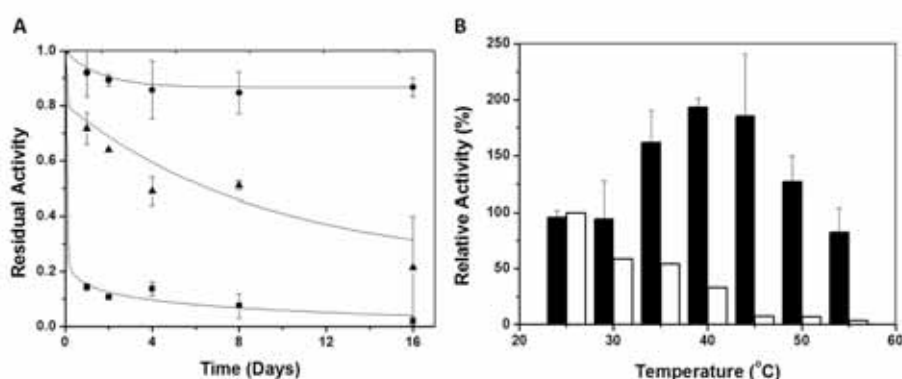
Figure 4.4. Stability of eNR. (**A**) Inactivation course of different eNR immobilized preparations at 25°C and pH 7.5. eNR was immobilized on Ag-DEAE (●); Ag-PEI (▲); Ag-MANAE (■). Values are normalized to starting the activity. (**B**) Inactivation of eNR soluble (white bars) and immobilized on Ag-DEAE (black bars) at different temperatures. Soluble and immobilized preparations were incubated 15 minutes at different temperatures and then activities were assayed at 25 ºC.

As it can be seen in the **Figure 4.4B**, the enzyme immobilized on Ag-DEAE was much more stable than its soluble counterpart under a broad

range of temperatures, between 30-55°C. Surprisingly, when such immobilized biocatalyst was incubated for only 15 minutes in the range of 40-45°C, a 2-fold activity enhancement (hyperactivation) was observed with respect to the non-thermally treated enzyme.
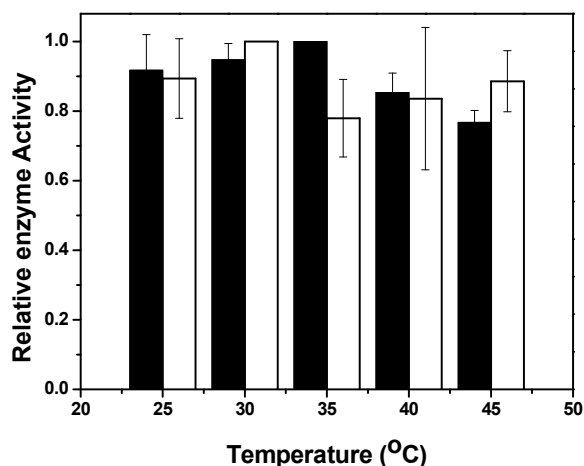
Figure 4.5. Activity/temperature profile of both soluble and immobilized eNR. Reductase activity of eNR immobilized on Ag-DEAE (white bars) and soluble eNR (black bars) was assayed at different temperatures at pH 7.5.

Such hyperactivation effect was not observed with the soluble enzyme, which decreased its initial activity after incubation at temperatures higher than 25°C due to thermal inactivation. Interestingly, both the soluble and immobilized enzymes showed similar activity/temperature profiles. **Figure 4.5** displays that the activity of soluble and immobilized enzymes at different temperatures is very similar: both preparations showed a maximum of activity in the range of 25-50. These results point out that the

temperature does have a differential effect on the conformational stability of the immobilized enzyme compared to the soluble one, but it does similarly affect their catalytic properties under different reaction temperatures. The optimal temperature of eNR, both for its soluble and immobilized forms, ranges 25-30ºC, which agrees with the optimal temperature of other mesophilic enzymes. Hence, these results suggest that the aforementioned hyperactivation effect can only be attributed to the carrier and that is not related to the effect of the temperature on the catalysis itself.

Inactivation kinetics studies of the hyperactivated immobilized enzyme at conditions of pH 7.5 and 40°C proved an enhanced stability with respect to its soluble counterpart under the same conditions (**Figure 4.6**). The inactivation courses for both soluble and immobilized enzyme follow first-order kinetics where the inactivation rate depends on the inactivation constant. The immobilized enzyme showed a thermal inactivation constant (ki) of $(1.31\pm0.63)x10^{-5}$ (s^{-1}) at 40°C, while the ki value of the soluble enzyme was $(15.3\pm2.3)x10^{-5}$ (s^{-1}). These findings confirm that the immobilization process results in an increased half-life time ($t_{1/2}$) of eNR up to 883 minutes; 12 times longer than the $t_{1/2}$ of the soluble enzyme.

The thermal-hyperactivation and thermal-stabilization effects observed for eNR immobilized on Ag-DEAE may be explained by some beneficial enzyme-carrier interactions triggered by the temperature and that drive to some local structural re-organization in the enzyme, resulting in a more efficient electron transfer between the NADPH and the MOCO domains. Those interactions may stabilize a more beneficial conformation for eNR, which explains the 2-fold more active and 12-fold more stable enzyme compared to its soluble counterpart. These carrier- and temperature-

assisted conformational changes were further investigated by fluorescence studies.
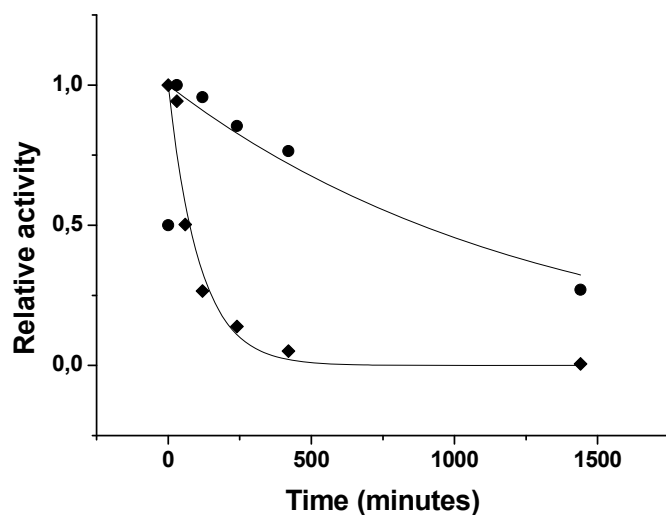

Figure 4.6. Thermal inactivation courses of *Aspergillus niger* nitrate reductase immobilized onto Ag-DEAE at 40°C. The preparation of *A. niger* eNR insoluble derivative was carried out as described in Section Material and Methods. Each insoluble and soluble preparations were incubated in 10mM sodium phosphate at pH 7.5 and 40ºC. The *A. niger* eNR preparations used to perform these studies were: immobilized on Ag-DEAE (●) and soluble (♦).

Fluorescence spectrum analyzed at 25 ºC was obtained for soluble eNR and immobilized eNR on Ag-DEAE with or without incubation at 40ºC during 15 minutes.

As can be observed in **Figure 4.7**, the fluorescence spectrum of the soluble enzyme remained unaltered after the thermal incubation at 40ºC in spite of

the activity decay induced by the thermal treatment. However, a deep change in the fluorescence spectrum of the thermal incubated eNR immobilized on Ag-DEAE was observed. The temperature-incubated immobilized enzyme showed higher fluorescence intensity at 314 nm; λ_{max} (maximum emission wavelength) for the tryptophan (Trp), and lower fluorescence intensity at 532 nm; λ_{max} for FAD than the non-incubated and immobilized enzyme. Additionally, the enzyme immobilized on Ag-DEAE presented a 10 nm-shift of the Trp- λ_{max} (324 nm) with respect to the soluble enzyme (314 nm), but when incubated at 40º C, such Trp- λ_{max} shifted back 10 nm to the UV, showing the same value than the soluble enzyme. These results point out that the immobilization of eNR promotes some conformational changes where the tryptophan residues are surrounded by a less polar environment than that one in their native conformation in solution. After a temperature-induced conformational change, the local environment of the tryptophan in the immobilized enzyme changes its polarity, becoming more polar as indicated by the observed red-shifting of Trp-λ_{max} after thermal incubation.[29] Moreover, the thermal incubation seems to trigger the shielding of the FAD cofactor because its fluorescence was quenched after thermal incubation. Therefore, the shift of Trp- λ_{max} and the differences in the Trp and FAD^+ fluorescence intensities reveal that the immobilization itself causes some structural rearrangement; interestingly, the temperature also induces further structural reorganization in the immobilized enzyme that can explain the enhancement in both activity and stability of the immobilized eNR incubated at 40ºC. Hereby, the temperature seems to act as an external stimulus that induces an optimal fitting between the surfaces of the enzyme and the carrier, resulting in a suitable geometric congruence for the catalysis. Despite the nature of this thermally-induced more active

conformation is not clear at present, it is worth mentioning that similar effects have been described for other soluble enzymes[30-32]. In any case, we put forth one of the few experimental demonstrations of thermal hyperactivation and stabilization assisted by the carrier surface, which is not only acting as a scaffold to stabilize eNR but also as an active surface that induces temperature-triggered positive conformational changes on the enzyme.
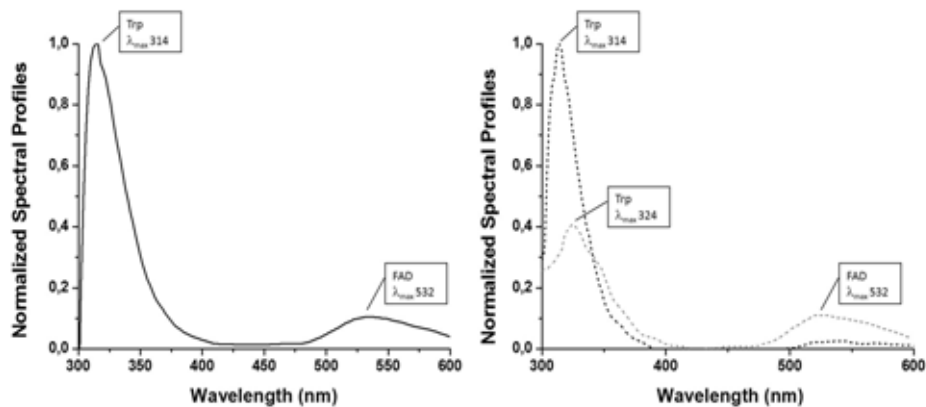
Figure 4.7. Emission fluorescence spectra of *A. niger* eNR (soluble and insoluble). (**A**) Fluorescence spectra of *A. niger* eNR soluble. The fluorescence spectrum of soluble enzyme incubated 15 minutes at 40º C perfectly overlapped to the non-incubated enzyme. (**B**) The fluorescence spectra of *A. niger* eNR immobilized on Ag-DEAE activated (dash black) and no-activated (dash grey). The preparation of *A. niger* eNR insoluble derivative was carried out as described in Section Material and Methods. Both insoluble and soluble preparations were incubated in 10mM sodium phosphate at pH 7.5 and 25ºC and 40ºC.

Kinetic parameters and loading capacity of eNR immobilized on Ag-DEAE

Considering the high stability and satisfactory catalytic efficiency of eNR immobilized on Ag-DEAE, we selected this heterogeneous biocatalyst to carry out the sustainable reduction of $[^{13}N]NO_3^-$ to $[^{13}N]NO_2^-$ in aqueous media under mild conditions. Nevertheless, before applying this biocatalyst to radiochemistry, we carried out its kinetic characterization. To this aim, Michaelis-Menten parameters were determined for soluble and the immobilized eNRs towards the substrates: nitrate and NADPH.

Table 4.2. Kinetic characterization of free and immobilized *Aspergillus niger* eNRs.

		Km (mM)	kcat (s^{-1})	Kcat/Km (s^{-1} • mM^{-1})
NaNO₃	NR soluble	0.27±0.07	30.33	111.23
	NR Ag-DEAE	0.06±0.03	11.97	199.44
NADPH	NR free	0.07±0.03	27.93	399.05
	NR Ag-DEAE	1.86±0.82	N.D.	N.D.

The steady-state kinetics parameters were measured at pH 7.5 and 25°C (see Section *Material and Methods*).

As it can be seen in **Table 4.2**, the kinetic studies provided interesting data that helped us to understand the activity decrease resulting from the immobilization process. In a first glance, the immobilized preparation showed a 26-fold $K_{m[NADPH]}$ higher than the soluble enzyme. Contrarily, $K_{m[NO3]}$ was 4.5 times smaller for the immobilized eNR than for the soluble preparation. These results confirm that immobilization of eNR on Ag-DEAE negatively affected the enzyme binding towards NADPH, which explains the low expressed activity after the immobilization process. The high $K_{m[NADPH]}$ values for the immobilized preparation may due to two

main reasons: *i*) Conformational changes induced by the carrier during the immobilization process that diminishes the enzyme affinity towards NADPH, or *ii*) mass transfer issues that hamper NADPH diffusivity from the bulk solution to the active sites of the immobilized eNR molecules.
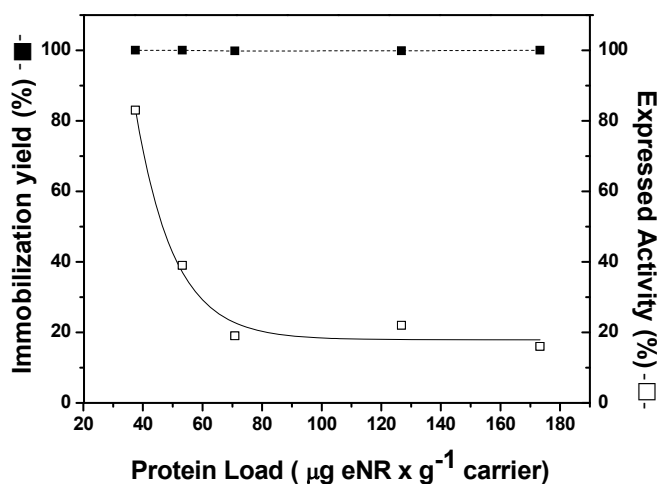
Figure 4.8. Enzyme-loading capacity of Ag-DEAE. The experiment was carried out offering different protein concentrations to 200mg of the carrier at pH 7.5 and 25°C. Immobilization yield (full square) and relative expressed activity (open square) were determined for each enzyme load. Immobilization yield and expressed activity were calculated as was previously described.

In order to elucidate which reason has more contribution to the low expressed activity, the effect of the enzyme loading on both immobilization yield and expressed activity after the immobilization was tested. **Figure 4.8** shows that the immobilization was always quantitative regardless the enzyme load. However, the relative expressed activity

presented a strong negative logarithmic correlation with the enzyme load. Under very low enzyme loads (37.5 $\mu g_{eNR}/g_{\ carrier}$) the relative expressed activity was 85%, while the value decreased to approximately 20% at loads higher than 75 $\mu g_{eNR}/g_{carrier}$.

This experiment demonstrates that immobilization chemistry does not promote inactive enzyme conformations that intrinsically diminish its specific activity after the immobilization process. In such scenario, the expressed activity should be always low regardless of the enzyme load. So, it is plausible to think that mass transfer limitations of substrate and cofactors are the main reason to explain the low expressed activity of the immobilized eNR. Contextualizing these results together with the high $K_{m[NADPH]}$ values for the immobilized preparation, we suggest that the cofactor undergoes severe mass transfer limitations to diffuse across the Ag-DEAE microstructure to reach the enzyme active sites. Under high enzyme loads, NADPH does not efficiently diffuse into the porous microstructure of the carrier to saturate all active sites immobilized on such carrier. On the contrary, under very low enzyme loads, the vast majority of the eNR molecules are saturated with the NADPH. These results are in good agreement with previous data[18], which showed that eNR from *A. niger* covalently immobilized on non-porous particles expresses more than 90% of its specific activity after immobilization. Moreover, these data strongly suggest that low specific activity of eNR immobilized on positively charged agarose beads is due to limited NADPH diffusion rather than inaccurate protein orientation, because positively charged porous carrier seem to immobilize eNR through an optimal orientation according to the protein surface analysis (see **Figure 4.3C**).

pH-profile of soluble and immobilized eNR on Ag-DEAE

It is well-known that the immobilization can improve the pH tolerance of enzymes. Here, the activities of soluble and immobilized eNR on Ag-DEAE under different pH conditions were also evaluated (**Figure 4.9**).
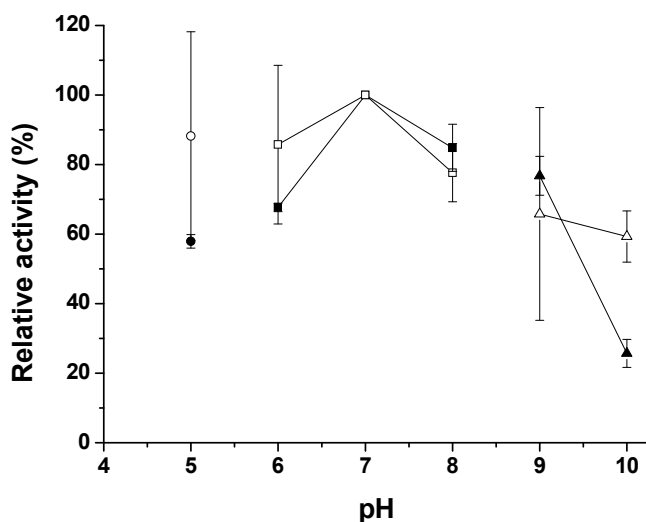
Figure 4.9. Effects of pH on NR immobilized onto Ag-DEAE activity. The NR preparations used to perform these studies were: immobilized on Ag-DEAE (open symbols) and soluble (filled symbols). The 10mM buffer solutions used in this essay were: sodium acetate pH 5 (circles); sodium phosphate pH 6, 7 and 8 (squares) and bicarbonate pH 9 and 10 (triangles).

The soluble and immobilized preparation showed optimal activity at pH value of 7 (**Figure 4.9**); such activity significantly decreased at pH lower than 7 for the immobilized enzyme. However, the effect of the acidic pH on the activity of the soluble enzyme was more dramatic reducing close to

116

50% of its initial activity. Under basic conditions, the soluble enzyme undergoes a dramatic inactivation as reflected in its activity-pH profile; such inactivation can be moderated by immobilizing eNR on Ag-DEAE. This data demonstrated that immobilized eNR performs more efficiently in a wider pH range (5 to 10) than the soluble enzyme.

Reduction of radiolabeled nitrate catalyzed by eNR immobilized on Ag-DEAE. Reusability of the immobilized biocatalyst

eNR immobilized on Ag-DEAE was used to reduce $[^{13}N]NO_3^-$ to $[^{13}N]NO_2^-$. The reaction was carried out in batch mode and the immobilized biocatalyst was re-used for several reaction cycles. As it can be seen in **Figure 4.10**, the immobilized enzyme only yielded 60% of $[^{13}N]NO_2^-$ in 4 minutes in the first cycle, while the soluble enzyme reduced 96% of $[^{13}N]NO_3^-$ to $[^{13}N]NO_2^-$. Surprisingly, in the second cycle, the immobilized enzyme reduced up to 93% of $[^{13}N]NO_3^-$ to $[^{13}N]NO_2^-$. We suggest that differences in NADPH effective concentration inside the carrier pores might cause that intriguing effect.

We hypothesize that during the first reaction cycle some negatively charged NADPH molecules are ionically absorbed to the positively charged carrier surface. However, such molecules would present an association/dissociation equilibrium that would simultaneously provide one fraction of soluble NADPH available for the enzyme catalysis and the second fraction of NADPH trapped into the intra-pore space of the carrier surface that would be available for consecutive cycles. In this scenario, the effective concentration of NADPH in the second and successive cycles will be higher, explaining the higher yield observed in the second cycle compared to the first one. In order to demonstrate this ionic interaction

between NADPH and Ag-DEAE, we equilibrated the eNR immobilized on Ag-DEAE with NADPH (same concentration and time as a typical reaction) in solution before triggering the first reaction cycle.
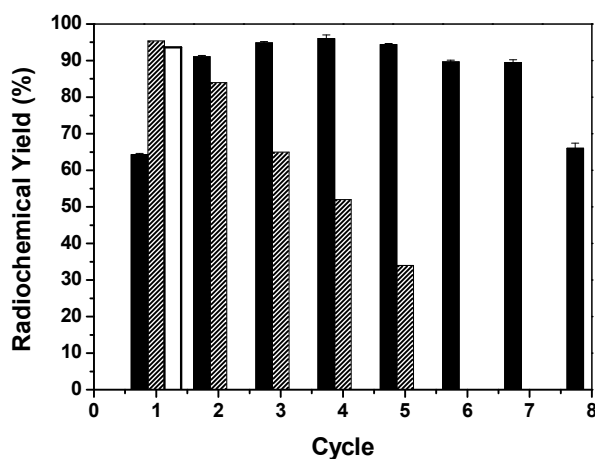
Figure 4. 10. Reusability of eNR immobilized on Ag-DEAE. Soluble eNR (white bar), eNR immobilized on Ag-DEAE without NADPH equilibration (black bars) and eNR immobilized on Ag-DEAE equilibrated with NADPH (stripped bars) were used to catalyze the reduction from $[^{13}N]NO_3^-$ to $[^{13}N]NO_2^-$ at 25° C, pH 7.5. Reactions catalyzed by soluble and non-equilibrated immobilized eNR were carried out by adding exogenous NADPH, while the reactions catalyzed by equilibrated immobilized eNR were carried out without exogenous NADPH.

The equilibrated heterogeneous biocatalyst was able to reduce 96% of $[^{13}N]NO_3^-$ to $[^{13}N]NO_2^-$ from the first cycle (**Figure 4.10**). This finding confirms that a fraction of NADPH is ionically trapped into the carrier surface, increasing the internal concentration of NADPH that results in higher reduction yields. In fact, we also confirmed that when the radiochemical reduction was carried out with the NADPH-equilibrated

immobilized enzyme, the heterogeneous biocatalyst was able to catalyze the radiolabeled nitrate reduction for 5 cycles with more than 30% yield without exogenous addition of NADPH (**Figure 4.10)**. This experiment provides evidence that NADPH molecules are reversibly bound to the carrier surface providing an internal cofactor concentration that was sufficient for the immobilized eNR to catalyze the radiochemical reduction with the maximum yield during the first cycle, and proportionally lower yields with the consecutive cycles. The lower reduction yield along the cycles agrees with the fact that NADPH is oxidized to $NADP^+$ decreasing the pool of NADPH trapped into the carrier porous structure. Therefore, along the consecutive cycles, immobilized eNR suffers from a lower availability of the reduced NADPH, explaining the lower yields along the operational cycles. Contrarily, when reduction was carried out by adding exogenous NADPH in each reaction cycle, the maximum yield was maintained during 7 cycles, demonstrating the excellent operational stability of the immobilized biocatalyst (**Figure 4.10**). To the best of our knowledge, this is the first evidence of a heterogeneous biocatalyst where the carrier plays an important role in supplying the corresponding cofactor to the enzyme. Furthermore, it was confirmed by SDS-page with silver staining (**Figure 4.11**) that this optimal heterogeneous biocatalyst, offers a clean final product without any significant protein contamination, even during the recycling process, confirming once again that ionic interactions between eNR and Ag-DEAE are quite strong in spite of their reversible nature.
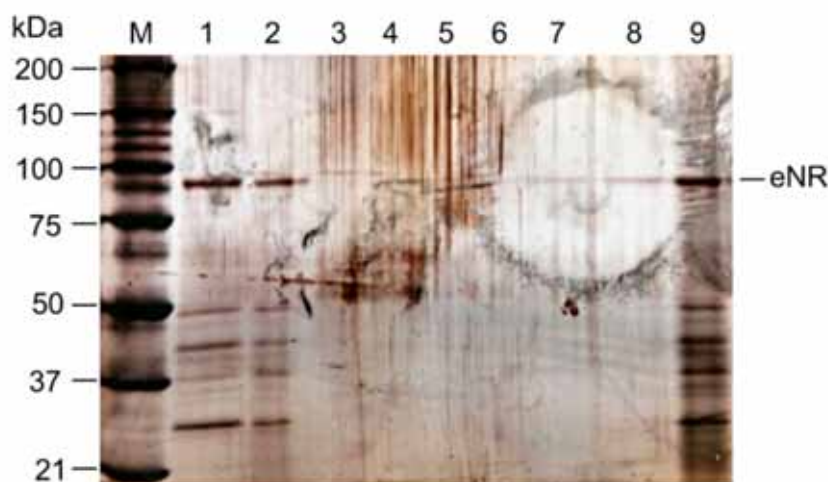
Figure 4.11. SDS-PAGE/silver staining of *Aspergillus niger* nitrate reductase. Lane M: molecular weight marker; Lane 1: eNR soluble; lane 2: eNR immobilized before any reaction; lane 3: non-bound protein after immobilization; lane 4: cycle 1; lane 5: cycle 2; lane 6: cycle 3; lane 7: cycle 4; lane 8: cycle 5; and lane 9: eNR immobilized after 5 reaction cycles.

Two step chemo-enzymatic solid-phase synthesis of *S*-[^{13}N]GSNO

To proof the concept that the enzymatically synthesized [^{13}N]NO$_2^-$ can be directly integrated into a radiochemical synthetic cascade, we coupled the optimal eNR immobilized on Ag-DEAE to the two-step chemo-enzymatic synthesis of *S*-[^{13}N]GSNO (**Figure 4.12**).

[^{13}N]NO$_3^-$ was enzymatically reduced to [^{13}N]NO$_2^-$ in the presence of NADPH. The supernatant of such reaction was passed through an anion exchange cartridge in order to trap the enzymatically produced [^{13}N]NO$_2^-$. Then, an acidic solution of *S*-glutathione (1 mM) was also passed through the same anion exchange cartridge enabling the solid-phase *S*-nitrosation of glutathione. The resulting product was finally desorbed from the resin

120

by elution with distilled water. 95% of the enzymatically yielded [¹³N]NO$_2$⁻ was converted to *S*-[¹³N]GSNO, similar to the radiochemical conversion obtained in previous works conducted in our research group using Cd-reduced [¹³N]NO$_2$⁻.[1] This result confirms that the redox cofactor needed for the enzymatic reactions does not interfere with the next chemical step. Therefore, the radioactive nitrite produced by this heterogeneous biocatalyst is suitable to be used in radiochemical reactions.
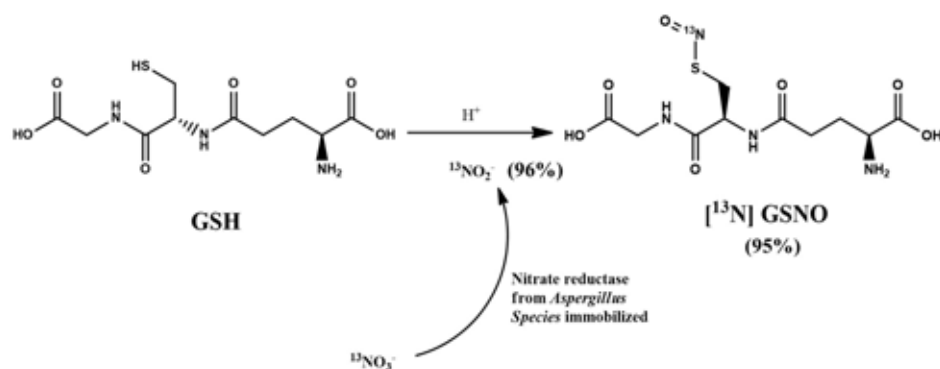
Figure 4.12. [¹³N]GSNO synthesis using [¹³N]NO$_2^-$ produced by enzymatic catalysis.

CONCLUSION

In this chapter, an unprecedented strategy for the reduction of [¹³N]NO$_3$⁻ to [¹³N]NO$_2$⁻ using an efficient heterogeneous biocatalyst was successfully applied. The use of one eukaryotic nitrate reductase immobilized on a solid carrier to a radiochemical process is for the first time published. This immobilized enzyme has been able to selectively reduce [¹³N]NO$_3$⁻ to [¹³N]NO$_2$⁻ aided by NADPH as redox cofactor. Likewise, by controlling

the immobilization chemistry and physicochemical properties of the carrier, optimal heterogeneous biocatalysts with high potential in synthetic chemistry were achieved. Noteworthy, this work is one of the few examples where an immobilized enzyme has been applied for a radiochemical process and the first report so far of a two-step chemo-enzymatic route to synthesize model radiotracers starting from a precursor ($[^{13}N]NO_3^-$) directly produced in the cyclotron.

From this experimental work, we can also conclude that immobilized enzymes are highly active and stable, and simplify the process work-up, and have great potential to be applied in radiochemistry to yield pure radiotracers that can be directly used for biomedical purposes. Hence, they can be anticipated as ideal tools for the preparation of radiotracers labeled with short-lived radionuclides. Moreover, we have faced the challenge to immobilize an enzyme whose catalytic mechanism depends on several cofactors and conformational changes recovering enough activity and increasing its stability to catalyze several reaction cycles.

The success of this work will so far open the doors to a new application of enzymes in radiochemistry and will potentiate the use of other chemo-enzymatic designs for the synthesis of novel radiotracers, even using short-lived isotopes. Successful enzyme immobilization will contribute to develop in flow radiochemical processes as well as to integrate radiochemical synthesis on-chip.[33-36]

REFERENCES

(1)   Llop, J.; Gómez-Vallejo, V.; Bosque, M.; Quincoces, G.; Peñuelas, I. Synthesis of S-[13N]nitrosoglutathione (13N-GSNO) as a new potential PET imaging agent. *Applied Radiation and Isotopes* **2009**, *67*, 95-99.

(2)   Gómez-Vallejo, V.; Kato, K.; Oliden, I.; Calvo, J.; Baz, Z.; Borrell, J. I.; Llop, J. Fully automated synthesis of 13N-labeled nitrosothiols. *Tetrahedron Letters* **2010**, *51*, 2990-2993.

(3)   Gómez-Vallejo, V.; Kato, K.; Hanyu, M.; Minegishi, K.; Borrell, J. I.; Llop, J. Efficient system for the preparation of [13N]labeled nitrosamines. *Bioorganic & Medicinal Chemistry Letters* **2009**, *19*, 1913-1915.

(4)   Gaja, V.; Gomez-Vallejo, V.; Puigivila, M.; Perez-Campana, C.; Martin, A.; Garcia-Osta, A.; Calvo-Fernandez, T.; Cuadrado-Tejedor, M.; Franco, R.; Llop, J. Synthesis and evaluation of (13)N-labelled azo compounds for beta-amyloid imaging in mice. *Mol. Imaging Biol.* **2014**, *16*, 538-549.

(5)   Gomez-Vallejo, V.; Borrell, J. I.; Llop, J. A convenient synthesis of 13N-labelled azo compounds: a new route for the preparation of amyloid imaging PET probes. *Eur. J. Med. Chem.* **2010**, *45*, 5318-5323.

(6)   Joshi, S. M.; de Cozar, A.; Gomez-Vallejo, V.; Koziorowski, J.; Llop, J.; Cossio, F. P. Synthesis of radiolabelled aryl azides from diazonium salts: experimental and computational results permit the identification of the preferred mechanism. *Chemical Communications* **2015**, *51*, 8954-8957.

(7)   Joshi, S. M.; Gomez-Vallejo, V.; Salinas, V.; Llop, J. Synthesis of 13N-labelled polysubstituted triazoles via Huisgen cycloaddition. *RSC Advances* **2016**, *6*, 109633-109638.

(8)   Joshi, S. M.; Mane, R. B.; Gomez-Vallejo, V.; Llop, J.; Rode, C. Microwave assisted synthesis of 5-substituted 1H-tetrazoles via [3+2] cycloaddition over heterogeneous Cu based catalyst: Application to the preparation of 13N-labelled tetrazoles. *submitted* **2017**.

(9)   Margeson, J. H.; Suggs, J. C.; Midgett, M. R. Reduction of nitrate to nitrite with cadmium. *Analytical Chemistry* **1980**, *52*, 1955-1957.

(10)   Bernhard, A. The Nitrogen Cycle: Processes, Players, and Human Impact. . *Nature Education Knowledge* **2010**, *3*, 25.

(11)   Krappmann, S.; Braus, G. H. Nitrogen metabolism of Aspergillus and its role in pathogenicity. *Medical mycology* **2005**, *43 Suppl 1*, S31-40.

(12)   Fischer, K.; Barbier, G. G.; Hecht, H.-J.; Mendel, R. R.; Campbell, W. H.; Schwarz, G. Structural Basis of Eukaryotic Nitrate Reduction: Crystal Structures of the Nitrate Reductase Active Site. *The Plant Cell* **2005**, *17*, 1167-1179.

(13)   Arauzo, M. Vulnerability of groundwater resources to nitrate pollution: A simple and effective procedure for delimiting Nitrate Vulnerable Zones. *Science of The Total Environment* **2017**, *575*, 799-812.

(14)   Zhai, Y.; Zhao, X.; Teng, Y.; Li, X.; Zhang, J.; Wu, J.; Zuo, R. Groundwater nitrate pollution and human health risk assessment by using

HHRA model in an agricultural area, NE China. *Ecotoxicology and Environmental Safety* **2017**, *137*, 130-142.

(15) Moorcroft, M. J.; Davis, J.; Compton, R. G. Detection and determination of nitrate and nitrite: a review. *Talanta* **2001**, *54*, 785-803.

(16) Wang, Q.-H.; Yu, L.-J.; Liu, Y.; Lin, L.; Lu, R.-g.; Zhu, J.-p.; He, L.; Lu, Z.-L. Methods for the detection and determination of nitrite and nitrate: A review. *Talanta* **2017**, *165*, 709-720.

(17) W. Aylott, J.; J. Richardson, D.; A. Russell, D. Optical Biosensing of Nitrate Ions Using a Sol-Gel Immobilized Nitrate Reductase. *Analyst* **1997**, *122*, 77-80.

(18) Sachdeva, V.; Hooda, V. A new immobilization and sensing platform for nitrate quantification. *Talanta* **2014**, *124*, 52-59.

(19) Cosnier, S.; Da Silva, S.; Shan, D.; Gorgy, K. Electrochemical nitrate biosensor based on poly(pyrrole-viologen) film-nitrate reductase-clay composite. *Bioelectrochemistry (Amsterdam, Netherlands)* **2008**, *74*, 47-51.

(20) Quan, D.; Shim, J. H.; Kim, J. D.; Park, H. S.; Cha, G. S.; Nam, H. Electrochemical Determination of Nitrate with Nitrate Reductase-Immobilized Electrodes under Ambient Air. *Analytical Chemistry* **2005**, *77*, 4467-4473.

(21) Madasamy, T.; Pandiaraj, M.; Balamurugan, M.; Bhargava, K.; Sethy, N. K.; Karunakaran, C. Copper, zinc superoxide dismutase and nitrate reductase coimmobilized bienzymatic biosensor for the simultaneous determination of nitrite and nitrate. *Biosensors & bioelectronics* **2014**, *52*, 209-215.

(22) Mellor, R. B.; Ronnenberg, J.; Campbell, W. H.; Diekmann, S. Reduction of nitrate and nitrite in water by immobilized enzymes. *Nature* **1992**, *355*, 717-719.

(23) Fernandez-Lafuente, R.; Rosell, C. M.; Rodriguez, V.; Santana, C.; Soler, G.; Bastida, A.; Guisan, J. M. Preparation of activated supports containing low pK amino groups. A new tool for protein immobilization via the carboxyl coupling method. *Enzyme Microb. Technol.* **1993**, *15*, 546-550.

(24) Mateo, C.; Abian, O.; Fernandez-Lafuente, R.; Guisan, J. M. Reversible enzyme immobilization via a very strong and nondistorting ionic adsorption on support–polyethylenimine composites. *Biotechnol. Bioeng.* **2000**, *68*, 98-105.

(25) Fuentes, M.; Pessela, B. C. C.; Maquiese, J. V.; Ortiz, C.; Segura, R. L.; Palomo, J. M.; Abian, O.; Torres, R.; Mateo, C.; Fernández-Lafuente, R.; Guisán, J. M. Reversible and Strong Immobilization of Proteins by Ionic

Exchange on Supports Coated with Sulfate-Dextran. *Biotechnol. Prog.* **2004**, *20*, 1134-1139.

(26) Arnold, K.; Bordoli, L.; Kopp, J.; Schwede, T. The SWISS-MODEL workspace: a web-based environment for protein structure homology modelling. *Bioinformatics* **2006**, *22*, 195-201.

(27) Walsh, I.; Minervini, G.; Corazza, A.; Esposito, G.; Tosatto, S. C. E.; Fogolari, F. Bluues server: electrostatic properties of wild-type and mutated protein structures. *Bioinformatics* **2012**, *28*, 2189-2190.

(28) Bradford, M. M. A rapid and sensitive method for the quantitation of microgram quantities of protein utilizing the principle of protein-dye binding. *Analytical Biochemistry* **1976**, *72*, 248-254.

(29) Ghisaidoobe, A. B.; Chung, S. J. Intrinsic tryptophan fluorescence in the detection and analysis of proteins: a focus on Forster resonance energy transfer techniques. *International journal of molecular sciences* **2014**, *15*, 22518-22538.

(30) Wedler, F. C.; Hoffmann, F. M. Glutamine synthetase of Bacillus stearothermophilus. I. Purification and basic properties. *Biochemistry* **1974**, *13*, 3207-3214.

(31) Facchiano, F.; Ragone, R.; Porcelli, M.; Cacciapuoti, G.; Colonna, G. Effect of temperature on the propylamine transferase from Sulfolobus solfataricus, an extreme thermophilic archaebacterium. *Eur. J. Biochem.* **1992**, *204*, 473-482.

(32) Rocha-Martin, J.; Vega, D.; Bolivar, J.; Godoy, C.; Hidalgo, A.; Berenguer, J.; Guisan, J.; Lopez-Gallego, F. New biotechnological perspectives of a NADH oxidase variant from Thermus thermophilus HB27 as NAD+-recycling enzyme. *BMC Biotechnol.* **2011**, *11*, 101.

(33) Rensch, C.; Lindner, S.; Salvamoser, R.; Leidner, S.; Bold, C.; Samper, V.; Taylor, D.; Baller, M.; Riese, S.; Bartenstein, P.; Wangler, C.; Wangler, B. A solvent resistant lab-on-chip platform for radiochemistry applications. *Lab on a Chip* **2014**, *14*, 2556-2564.

(34) Zhang, H.; Cantorias, M. V.; Pillarsetty, N.; Burnazi, E. M.; Cai, S.; Lewis, J. S. An improved strategy for the synthesis of [(18)F]-labeled arabinofuranosyl nuclosides. *Nucl. Med. Biol.* **2012**, *39*, 1182-1188.

(35) Lu, S.; Chun, J.-H.; Pike, V. W. Fluorine-18 chemistry in micro-reactors. *J. Labelled Comp. Radiopharm.* **2010**, *53*, 234-238.

(36) Keng, P. Y.; Chen, S.; Ding, H.; Sadeghi, S.; Shah, G. J.; Dooraghi, A.; Phelps, M. E.; Satyamurthy, N.; Chatziioannou, A. F.; Kim, C.-J. C.; van Dam, R. M. Micro-chemical synthesis of molecular probes on an electronic microfluidic device. *Proc. Natl. Acad. Sci. U. S. A.* **2012**, *109*, 690-695.

Chapter 5

Enzymatic preparation of ^{13}N-labeled amino acids and their Biological assessment in prostate tumor models
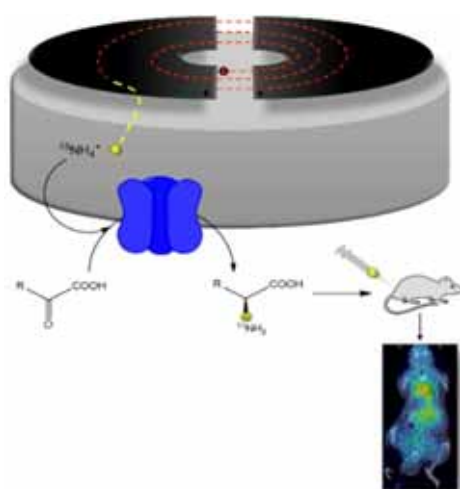
In the present chapter, the one-pot, enzymatic and non-carrier-added synthesis of a variety of ^{13}N-labeled amino acids (L-[^{13}N]alanine, [^{13}N]glycine, and L-[^{13}N]serine) is presented. To this aim, L-alanine dehydrogenase from *Bacillus subtilis*, an enzyme that catalyzes the reductive amination of α-keto acids has been assayed, using nicotinamide adenine dinucleotide (NADH) as the redox cofactor and ammonia as the amine source. In addition, the integration of both L-alanine dehydrogenase and formate dehydrogenase from *Candida boidinii* in the same reaction vessel allows the *in situ* regeneration of NADH during the radiochemical synthesis of the amino acids. The enzymatically labeled amino acids have been used to analyze their *in vivo* biodistribution in healthy (wild-type) mice. The capacity to selectively accumulate in the tumor has been assessed in a prostate cancer mouse model (prostate-specific Pten deletion) by using dynamic PET-CT imaging.

INTRODUCTION

Amino acids labeled with nitrogen-13 are attractive because these are very difficult to label using other isotopes. Additionally, amino acids could be very interesting tracers for the detection of some types of cancer when [^{18}F]FDG does not work. Enantioselective chemical synthesis of amino acids is also very hard. The use of enzymes can help, thanks to their fast reaction rates and unique enantio- and chemo-selectivity.

As already mentioned before (*Chapter 2*), the utilization of enzymes for the preparation of ^{13}N-labeled amino acids was first described in the 70's.[1] For example, *L*-[^{13}N]glutamate was synthesized by incubation of α-ketoglutarate (α-KG) with [^{13}N]NH$_3$ in the presence of the enzyme *L*-glutamate dehydrogenase and NADH as the redox cofactor.[2,3] Likewise, *L*-[^{13}N]glutamine was synthesized by glutamine synthethase using glutamic acid as the substrate and adenosine triphosphate (ATP) as the cofactor.[3,4] These two amino acids were synthesized with incorporation values close to 90% in 15 minutes of incubation. Other amino acids such as *L*-[^{13}N]valine, *L*-[^{13}N]methionine, *L*-[^{13}N]leucine and *L*-[^{13}N]alanine have been produced by a one-pot/two-step or two-pot/two-step processes by coupling glutamate dehydrogenase and transaminases. These methodologies have allowed 16-90% chromatographic yields of the corresponding *L*-[^{13}N]amino acid.[5,6]

Amino acid dehydrogenases (AADH) are a class of enzymes which have been extensively used in biocatalysis as main enzymes for the production of enantiomerically pure α-amino acids,[7,8] as cofactor recycling enzymes to replenish the NADH or NAD$^+$ pool utilized by alcohol dehydrogenases[9] and as donor enzymes to provide ω-transaminases with the suitable amine donors using ammonia as the amine source.[10] Interestingly, *L*-alanine

amine dehydrogenases (*L*-AlaDHs) are a special type of AADH that have low sequence similarities with other AADH (glutamate dehydrogenase, leucine dehydrogenases, phenylalanine dehydrogenases…) and some important mechanistic differences.[11,12] *L*-Alanine dehydrogenase, *L*-AlaDH, is an oxidoreductase ($EC_{1.4.1.1}$) which catalyzes the reversible deamination of *L*-alanine yielding pyruvate and ammonia. In this reaction, the alanine is oxidized at the enzyme active site with concomitant reduction of NAD^+ to NADH by hydride transfer.[11,13] The kinetic properties of *L*-AlaDHs from different microbial sources have been extensively investigated, and some of these enzymes have been cloned in heterologous hosts.[14] Although the physiological role of *L*-AlaDH remains controversial, it has been reported that this enzyme is involved in the utilization of alanine as an energy source during the germination process of *Bacillus* species.[15,16]

In continuation of our previous work related to the application of enzyme-mediated reactions to ^{13}N-radiochemistry,[17] we describe in this chapter a one-pot/one-step radiosynthesis of *L*-[^{13}N]alanine, [^{13}N]glycine, and *L*-[^{13}N]serine catalyzed by a versatile *L*-alanine dehydrogenase (*L*-AlaDH) from *Bacillus subtilis* (**Figure 5.1a**). In contrast with the well reported glutamate dehydrogenase that needs to be coupled to transaminase, *L*-AlaDH is self-sufficient to incorporate [^{13}N]NH$_3$ into a broad scope of organic precursors to yield the corresponding *L*-[^{13}N]amino acids with an exquisite selectivity.

One of the major drawbacks of utilizing amino acid dehydrogenase is the necessity of adding an exogenous redox cofactor to the reaction mixture. This may require the product purification before administration in order to avoid toxicological or side effects. In biocatalysis, the recycling of the

redox cofactor has been elegantly solved by using secondary enzymes, whose mission is to replenish the pool of the cofactors during the reaction. In this scenario, a lower amount of cofactor can be used, with the consequent positive impact in the process-costs. There are different enzymes that have been exploited to regenerate the cofactor.[18,19] Glucose dehydrogenase,[20,21] sulfite dehydrogenase,[22,23] and formate dehydrogenase (FDH)[24] are some examples.
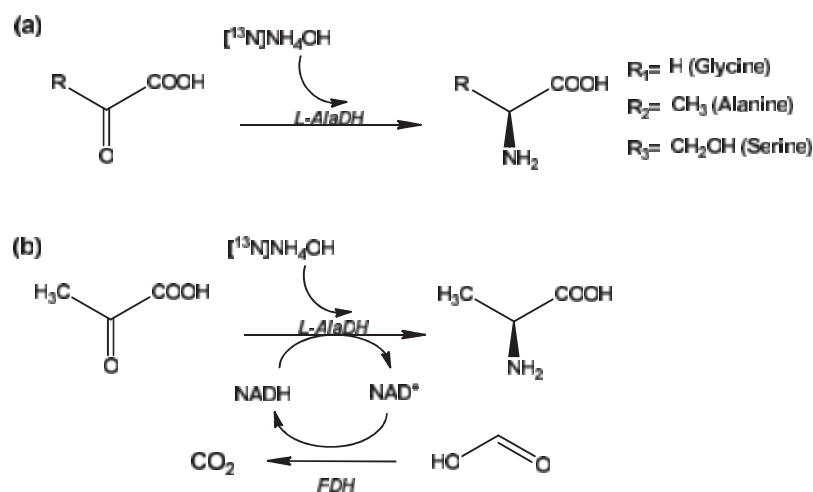
Figure 5.1. Schematic representation of: (**a**) Enzyme-mediated preparation of *L*-[^{13}N]alanine, [^{13}N]glycine, and *L*-[^{13}N]serine using *L*-alanine dehydrogenase (*L*-AlaDH) from *Bacillus subtilis* as the enzyme; (**b**) one-pot, multi-enzyme reaction for the preparation of *L*-[^{13}N]alanine with regeneration of NADH.

In the current work, coupling *L*-AlaDH with FDH from *Candida boidinii* has allowed us *in situ* recycling of NADH by using formate buffer as the substrate without compromising reaction rates (**Figure 5.1b**). Since FDH can be recombinantly produced in the laboratory obtaining high yields, and

it uses a soluble and low-cost substrate - formic acid - which is oxidized to carbon dioxide as product (which is easily evaporated shifting the equilibrium towards the oxidation reaction), this enzyme was designated for the regeneration of NADH in our experiment.[24]

The present synthetic strategy resulted in ready-to-inject ^{13}N-labeled amino acids in sufficient amount to approach *in vivo* studies in small healthy and diseased rodents, and paves the way towards future solid-supported, multi-purpose, in flow synthetic processes.

EXPERIMENTAL SECTION

Materials

The genes of *L*-alanine dehydrogenase (*L*-AlaDH) from *Bacillus subtilis* (*L*-alanine: NAD oxidoreductase, EC$_{1.4.1.1}$) and formate dehydrogenase (FDH) from *Candida boidinii* (Formate: NAD$^+$ oxidoreductase, EC$_{1.2.1.2}$) were synthesized and cloned into pET28b by GenScript company (Piscataway, USA). β-Nicotinamide adenine dinucleotide, reduced disodium salt hydrate (β-NADH; purity >97%), pyruvic acid (CH$_3$COCOOH, purity ≥98%), ammonium chloride (NH$_4$Cl, for molecular biology, purity ≥99.5%), sodium phosphate dibasic (Na$_2$HPO$_4$, for molecular biology, purity ≥98.5%), sodium phosphate monobasic (NaH$_2$PO$_4$, purity ≥99.0%), *L*-alanine (purity ≥98%), *D*-alanine (purity ≥98%), glycine (purity ≥99%), *L*-serine (purity ≥99.5%), *D*-serine (purity ≥98%), *L*-phenylalanine (purity ≥98%), *D*-phenylalanine (purity ≥98%), *L*-norvaline, and *D*-norvaline (purity ≥99%) were purchased from Sigma Chemical Co. (St. Louis, IL, USA) and used without further purification. TALON resin was purchased from Clontech (Saint-Germain-en-Laye,

132

France). Bio-Rad Protein Assay Dye Reagent Concentrate was purchased from Bio-Rad Laboratories (Madrid, Spain). All other reagents were of analytical grade.

Production of *L*-AlaDH and FDH in *E. Coli.* *Expression.* A total of 1ml of an overnight culture of *E. coli* BL21 transformed with the corresponding plasmid (pET28b-Bs*L*-AlaDH or pET28b-CbFDH) was inoculated in a 50ml of Luria-Bertani (LB) broth containing kanamycin (final concentration of 30 μg mL^{-1}). To overexpress *L*-AlaDH, the resulting culture was incubated at 37°C with energetic shaking until the OD$_{600nm}$ reached 0.6. Then, 1-thio-β-d-galactorpyranoside (IPTG) was added to the culture to a final concentration of 1 mM to induce protein synthesis. Cells were grown at 37 °C for 3h and then harvested by centrifugation at 1290*g* for 30 min. To overexpress FDH, the culture was incubated at 21°C with energetic shaking until the OD$_{600nm}$ reached 0.6. Then, 1-thio-β-d-galactorpyranoside (IPTG) was added to the culture to a final concentration of 1 mM to induce protein synthesis. Cells were grown at 21°C for 18h and then harvested by centrifugation at 1290*g* for 30 min. *Purification.* Both FDH and *L*-AlaDH were purified as follows: the resulting pellet from 50 mL culture was resuspended in 5 mL of binding buffer (25 mM sodium phosphate buffer solution, pH 7). Cells were broken by sonication (LABSONIC P, Sartorius Stedim biotech) at amplitude 30% for 5min. The resulting suspensions were centrifuged at 10528*g* for 30min. The supernatant containing the enzyme was collected and passed through a TALON resin equilibrated with binding buffer. Following the protein binding to the column, the flow through was discarded and the resin was washed three times with binding buffer prior to the protein elution with elution buffer (binding buffer supplemented with 300 mM imidazole). The eluted protein was gel-filtered by using a

centrifugal filter of 10KDa (Millipore, Merck) to remove the imidazole and exchange the enzyme buffer to 25 mM sodium phosphate 7, and the enzyme was stored under such conditions at 4 ºC. Samples were analyzed by 12 % SDS-PAGE (Sodium dodecyl sulphate-Polyacrylamide gel electrophoresis) (Coomassie Blue staining) after each protein production to determine the purity of the enzymes. The studies of the oligomeric state of this protein were carried out through a gel filtration process performed by Fast protein liquid chromatography (FLPC) using a Superdex TM 200, 10/300 GL.

Protein and enzyme colorimetric assays. *Determination of the protein concentration.* The protein concentration of soluble *L*-AlaDH and FDH were measured as described in Chapter 4 for eNR. *Determination of enzyme activity.* The enzymatic activities were spectrophotometrically measured in 96-well plates by monitoring the absorbance at 340 nm, which varied depending on the concomitant production or consumption of NADH. *L-AlaDH*: The reductive amination was assayed using 10µL of L-AlaDH, 190 µL of 0.5mM NADH, and 75 mM pyruvic acid (or other α-keto acids) which were incubated in 450 mM ammonium chloride at pH 5-10 and 25ºC. On the other hand, for the oxidative deamination (inverse reaction) 10 µL of L-AlaDH, 200 µL of 1mM NAD^+ and 10 mM L/D amino acids (alanine, glycine, serine, norvaline and phenylalanine) were incubated in 300 mM sodium phosphate buffer at pH 8 and 25ºC. *FDH*: To measure the enzyme activity of FDH, 200 µL of 1 mM NAD^+ and 100 mM formic acid in 25 mM sodium phosphate buffer at pH 7 were incubated with 5 µL of the enzymatic solution at 25ºC. One unit of activity was defined as the amount of enzyme that was needed to either reduce or oxidize 1 µmol of the corresponding nicotinamide cofactor at 25ºC and the corresponding pH.

Enzyme kinetic parameters. The kinetic parameters, Michaelis constant value (K_m) and maximum rate (V_{max}), were determined by activity colorimetric assay at pH 8 (pH 9 for serine) and 25ºC following the method described above for L-AlaDH, using 0-1.8M ammonium chloride as amine source.

Production of the radiolabeling agent [¹³N]NH₃. Nitrogen-13 (^{13}N) was produced in an IBA Cyclone 18/9 cyclotron via the $^{16}O(p,\alpha)^{13}N$ nuclear reaction as explained in chapter 4, but 5 mM EtOH solution in pure water was irradiated. Integrated currents in the range 0.1-1 µAh were used. The resulting solution was transferred to a 10 mL vial and the activity was measured in a dose calibrator (Capintec CRC®-25 PET, New Jersey, USA).

Synthesis of L-[¹³N]amino acids. *General procedure.* Radioactive enzymatic reactions of the amino acids were carried out by adding 100µL of a mixture containing 0.5 mM NADH, 75mM α-keto acid and 300 mM sodium phosphate buffer solution at pH 8 to a solution of 20 µL containing L-AlaDH (15-300 µg/mL in reaction) and 100µL of [¹³N]NH₃ (20-450 MBq). Reactions were conducted in tubes with 50 KDa cut-off membranes. For the preparation of L-[¹³N]serine, sodium bicarbonate buffer (300 mM, pH 9) was used instead. The mixture was incubated at 25ºC under mild stirring for 2.5-20 min, and subsequently filtered under centrifugation to separate the enzyme from the radiolabeled products.

Enzymatic cascade reactions for regeneration of the cofactor. The reactions were conducted as above, but FDH at 5:1 (FDH:L-AlaDH) molar ratio and formic acid (100 mM) were added. 100µL of this soluble preparation were incubated with cyclotron produced [¹³N]NH₃ solution (100 µL). All the reactions were carried out in tubes with 50 KDa cut-off

membranes to easily separate the enzymes from the final products by fast centrifugation.

HPLC and radio-HPLC analysis. The determination of all radioactive/non-radioactive compounds was carried out by HPLC using an Agilent 1100 Series system equipped with a quaternary pump and a variable wavelength UV detector connected in series with a radiometric detector (Gabi, Raytest, Straubenhardt, Germany). A chiral column, (Phenomenex Chirex®3126 column, 50 x 4.6mm; Micron Phenomenex, Madrid, Spain) was used as stationary phase. As the mobile phase, 1 mM $CuSO_4$ solution at 1 ml min^{-1} was used for alanine, glycine and norvaline; 2mM $CuSO_4$ solution at 0.2 ml min^{-1} was used for serine; and 2mM $CuSO_4$/methanol solution (70:30) at 1 ml min^{-1} was used for phenylalanine. Pure commercial enantiomers were used as standards.

For the determination of the specific activity of L-[^{13}N]alanine, the concentration of amino acid in the purified fraction was carried out by HPLC-MS, using an AQUITY UPLC separation module coupled to a LCT TOF Premier XE mass spectrometer (Waters, Manchester, UK). An Acquity UPLC Glycan BEH amide column (1.7 μm, 50 mm, 2.1 mm) was used as stationary phase. The elution buffers were A (acetonitrile) and B (0.1 M ammonium formate). The column was eluted with a linear gradient of B: t=0 min, 95%; t=3 min, 50%; t=3.5 min, 95%; t=5 min, 95%. Total run was 5 min, injection volume was 10 μL and the flow rate 0.5 mL/min. The detection was carried out in positive ion mode, monitoring the most abundant isotope peaks from the mass spectra. Alanine was detected as protonated molecule (m/z = 90) with a retention time of 1.81 min.

Animal experimentation

General considerations. Animals were maintained in a temperature and humidity-controlled room with a 12 h light-dark cycle. Food and water were available *ad libitum*. Animals were cared for and handled in accordance with the Guidelines for Accommodation and Care of Animals (European Convention for the Protection of Vertebrate Animals Used for Experimental and Other Scientific Purposes), and ethical protocols were approved by the internal Ethical Committee and by regional authorities.

In vivo **studies.** PET studies were performed using an eXploreVista-CT small animal PET-CT system (GE Healthcare). Healthy mice (20-22 g, C57BL/6JRJ, Janvier, France; n=2 per amino acid) were used to assess the biodistribution of the labeled amino acids. Prostate cancer mice (22-26 g, prostate-specific Pten deletion; n=2 per amino acid) kindly provided by Prof. Arkaitz Carracedo (CIC bioGUNE, Bilbao, Spain) were used to evaluate tumor uptake. In all cases, mice were anesthetized with a mixture of 3-4% isoflurane in O_2 for induction, and reduced to 1-1.5% for maintenance. A nose cone was used to facilitate regular breathing, monitored by a SA Instrument Inc. (NY, USA) pressure sensor. Respiration and body temperature were monitored throughout the scan. The temperature, measured rectally, was maintained at 37±1ºC using a water heating blanket (Homeothermic Blanket Control Unit; Bruker, Germany). For administration of ^{13}N-labeled amino acids, the tail vein was catheterized with a C10SS-MTV1301 29-gauge catheter (Instech, Laboratories Inc., Plymouth Meeting, PA, USA) and 16.5±3.1 MBq (approximately 100 µL) were injected in tandem with the start of a PET dynamic acquisition. The cannula was then rinsed with a physiologic saline solution (50µL) and dynamic images (33 frames: 8x5 s, 6x15 s, 6x30

s, 6x60 s, 7x120 s) were acquired in 2-bed positions in the 400-700 keV energy window, with a total acquisition time of 50min and 20s. After each PET scan, CT acquisitions were also performed, providing anatomical information as well as the attenuation map for later image reconstruction. Dynamic acquisitions were reconstructed (decay, random and CT-based attenuation corrected) with OSEM-2D (2 iterations, 16 subsets). PET images were visually analyzed using PMOD image analysis software (PMOD Technologies Ltd, Zürich, Switzerland).

RESULTS AND DISCUSSION

The aim of this chapter was to develop an efficient synthetic procedure for the preparation of ^{13}N-labeled amino acids for the *in vivo* assessment of tumor uptake in a mouse model of prostate cancer. The natural amino acids *L*-alanine, *L*-serine and glycine are biosynthetically linked and together provide the essential precursors for the synthesis of proteins, nucleic acids, and lipids that are crucial to cancer cell growth.[26,27] Hence, these three amino acids were identified as the priority target compounds.

Selection, expression and purification of an active *L*-AlaDH in *E. coli*

The inspection of different data bases (BRENDA, KEEGG, MetaCyc) suggests that *L*-AlaDH from *Bacillus subtilis* and *Bacillus sphaericus* may enable the preparation of different ^{13}N-labeled amino acids since they present a broad substrates scope for the reductive amination of α-keto acids. Among *L*-AlaDHs, the *L*-AlaDH from *Bacillus subtilis* was selected here due to its better kinetic properties for a wider variety of amino acids.

The enzyme was expressed in *E. coli* BL21 and purified by affinity chromatography based on the histidine tag inserted at its *N*-terminus (**Figure 5.2**). According to the literature,[14,28] the pure *L*-AlaDH is a hexamer with a subunit mass of 44 KDa which results in a total mass of 264 KDa (**Figure 5.2**). This result was confirmed by SDS-PAGE gel and gel filtration analysis. The pure *L*-AlaDH showed a specific enzyme activity of 106±5 U/mg towards pyruvate.

Synthesis of amino acids under non-radioactive conditions

The amination activity towards α-keto acids with different side chains was first tested in non-radioactive conditions. With that aim, the synthesis of *L*-alanine, glycine, and *L*-serine was approached by incubating the appropriate substrates with ammonium chloride in the presence of NADH as cofactor and *L*-AlaDH from *Bacillus subtilis* as a biocatalyst. Despite this work was focused in these three amino acids, two more amino acids (*L*-phenylalanine and *L*-norvaline) were tested just to evaluate the scope of the application of our method.

Expectedly, the highest activity was observed towards pyruvic acid, but the enzyme also catalyzed the reductive amination of other α-keto acids such as glycolic acid, 3-hydroxypyruvic acid, 2-oxopentanoic acid and 2-phenylpyruvic acid to yield glycine, serine, norvaline and phenylalanine, respectively (**Table 5.1**). The specific enzyme activity towards these α-keto acids ranged from 17 to 32% of the maximum specific enzyme activity measured with pyruvic acid. Generally, bulky α-keto acids were worse substrates than small ones, as previously observed for the vast majority of the previously studied *L*-AlaDHs.[29-31]
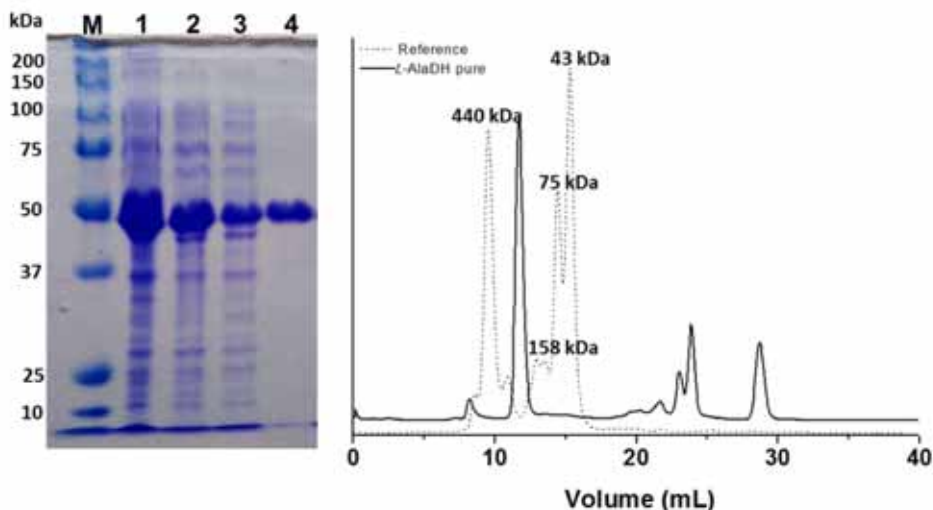
Figure 5.2. (Left) SDS-PAGE analysis of expression and purification of *L*-AlaDH from *Bacillus subtillis* in BL21 *E.coli.* Lane M shows molecular weight references. Lane 1 represents a crude extract of after sonication. Lane 2 represents soluble protein fraction after sonication and removal of cell debris and membrane fraction. Lane 3 represents the flow-through fraction of the purification step. Lane 4 represents pure *L*-AlaDH after elution with 300 mM imidazole. The different protein fractions were analyzed by 12% SDS-PAGE and stained with Coomassie Blue. The purified enzyme resulted in a band corresponding to 44 kDa. (**Right**) Gel filtration chromatogram of the pure enzyme *L*-AlaDH. The gel filtration was performed by flow protein liquid chromatography (FPLC) using a Superdex TM 200, 10/300 GL. Reference markers (dotted line): 440 kDa, ferritin; 158 kDa, aldolase; 75 kDa, conalbumin and 43 kDa, ovalbumin. The purified enzyme obtained (black line) eluted as a major peak around 264 kDa corresponding to the total molecular weight of *L*-AlaDH indicating that the multimer is formed by 6 subunits (44 KDa/subunit).

As just mentioned, *L*-AlaDH from *Bacillus subtilis* presented a broad substrates scope for the reductive amination towards different α-keto

acids. On the contrary, such substrate versatility was not observed in the oxidative deamination of *L*-amino acids (**Table 5.1**). The enzyme did not oxidize glycine and phenylalanine and poorly oxidized serine and norvaline. These findings are in accordance with those previously reported for the recombinant and native enzymes purified from *E. coli* and *B. subtilis*, respectively.[14,28]

Table 5.1. Specific activity (SA) values of *L*-Alanine Dehydrogenase for amination and deamination reactions under non-radioactive conditions.

Amino acid	SA$_{deamination}$ (μmol x min^{-1} x mg^{-1})	SA$_{amination}$ (μmol x min^{-1} x mg^{-1})
Alanine	5.4±0.1 (*L*)	106±5
Glycine	N.D.	34.3±1.6
Serine[b]	0.039±0.001 (*L*) 0.003±0.001 (*D*)	22.5±3.1
Norvaline	0.002±0.001 (*L*)	18.6±1.2
Phenylalanine	N.D.	21.4±2.1

pH = 8; N.D. = non-detected

The effect of the pH on the reductive amination activity of *L*-AlaDH towards different α-keto acids was subsequently investigated (**Figure 5.3**). Optimal specific enzyme activity values for the biosynthesis of all tested amino acids, except *L*-serine, were observed at pH 8. For *L*-serine, optimal values were achieved at pH 9. Noteworthy, the specific enzyme activity of *L*-AlaDH towards 3-hydroxypyruvic acid at pH 9 was only 1.24 times lower than the activity towards pyruvic acid at pH 8. The activity-pH

profile of *L*-AlaDH for the reductive amination of pyruvic acid was wider than for other amino acid dehydrogenases.[32]
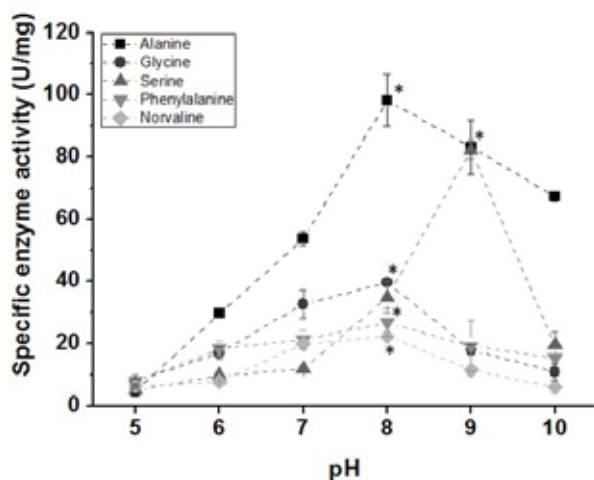

Figure 5.3. Activity-pH profile of *L*-AlaDH for the biosynthesis of *L*-alanine, glycine, *L*-serine, *L*-phenylalaline and *L*-norvaline. The reactions were carried out in the presence of 0.5 mM NADH, 450 mM ammonium chloride and 10 mM of the corresponding α-keto acid in 300 mM buffer solution at 25°C. Acetate buffer was used for pH 5-6; sodium phosphate buffer for pH 7-8 and sodium bicarbonate buffer for pH 9-10. Enzyme activity measurements were carried out for 2 minutes and blank experiments (without *L*-AlaDH) were performed to discard any stability issues of NADH that may lead to underestimation of the enzyme activity. Data are expressed as the mean ± standard deviation (n=3); (*) means the optimal pH value for the synthesis of the corresponding amino acid.
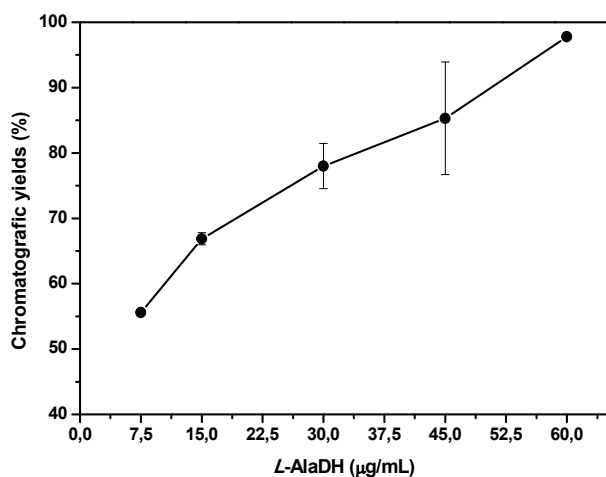
Synthesis of *L*-[¹³N]amino acids

A complete translation of the reaction parameters to radioactivity conditions is often not straightforward. If the carrier-free radioactive

precursor is used (in our case [^{13}N]NH$_3$), the concentration of this species is extremely low (around 15 µM in typical experiments conducted in our set up). Hence, the kinetics of the reaction might be significantly altered and careful refinement of the experimental conditions is usually required. In this work, we first attempted the synthesis of L-[^{13}N]alanine. With this purpose, 75 mM of pyruvic acid was incubated with cyclotron-produced [^{13}N]NH$_3$ (aqueous solution, 20-25 MBq, 100 µL) and L-AlaDH in the presence of NADH as the cofactor (0.5 mM) in a buffered solution at pH 8.0±0.1. The reactions were carried out in tubes with 50 KDa cut-off membranes to easily separate the enzymes from the final products by fast centrifugation. Chromatographic yields were monitored over time (**Figure 5.4**, solid line) and values were then corrected by radioactive decay at different reaction times (**Figure 5.4**, dotted line).
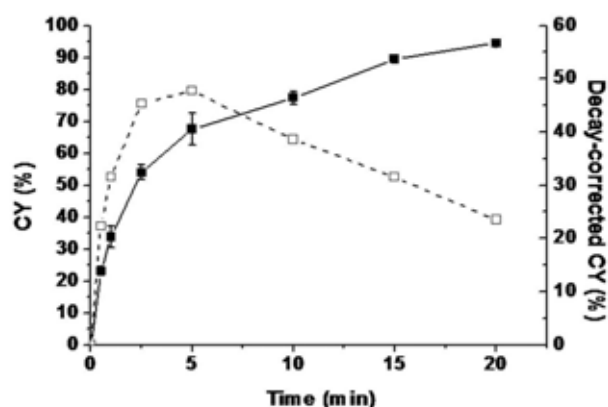
Figure 5.4. Chromatographic yields (solid line) and chromatographic yields corrected by taking into consideration the radioactive decay of the radionuclide (dotted line) at different reaction times obtained for the production of L-[^{13}N]alanine. The reactions were carried out in the presence of 20-25 MBq of [^{13}N]NH$_4$OH, 15 ug/mL of L-AlaDH, 0.5 mM of NADH, and 75 mM of pyruvic acid in 300 mM sodium phosphate buffer solution pH 8 at 25ºC.

Despite the low concentration of $[^{13}N]NH_3$, chromatographic yields of 68±5% were obtained after 5 minutes reaction; this value increased to 95±1% when the reaction was carried out for 20 min. Taking into account the short half-life of ^{13}N, incubation times of 10, 15 and 20 minutes proved to be less desirable than the 5 min period, because the gain in yield was negligible compared to the decay of nitrogen-13 (**Figure 5.4**, dotted line). Noteworthy, when the reaction time was set to 20 min, the amount of radiochemical impurities (mainly unreacted $[^{13}N]NH_3$) was <5%, enabling putative *in vivo* studies without the need of a purification step to remove unreacted $[^{13}N]NH_3$.

Figure 5.5. Effect of the amount of enzyme in the radiochemical synthesis of *L*-$[^{13}N]$alanine. The reactions were performed using a range of concentrations of L-AlaDH between (7.5-60 µg/mL) in the presence of 45-50 MBq of $[^{13}N]NH_3$, 0.5mM NADH, 75 mM pyruvic acid in 300 mM sodium phosphate buffer pH 8 at 25ºC. In all cases, the reaction time was 5 minutes. Results are expressed as a mean ± standard deviation, n≥3. Chromatographic yields were calculated from chromatographic profiles.

In order to gain further knowledge on the reaction kinetics, the radiochemical synthesis of L-[^{13}N]alanine was performed at different enzyme concentrations (**Figure 5.5**). As expected, fixing the optimal reaction time of 5 min, higher enzyme concentrations led to higher yields. Values of 68±5%, 78±4%, 85±9% and 98±1% were achieved when concentrations of enzyme of 15, 30, 45 and 60 µg/mL were used, respectively.
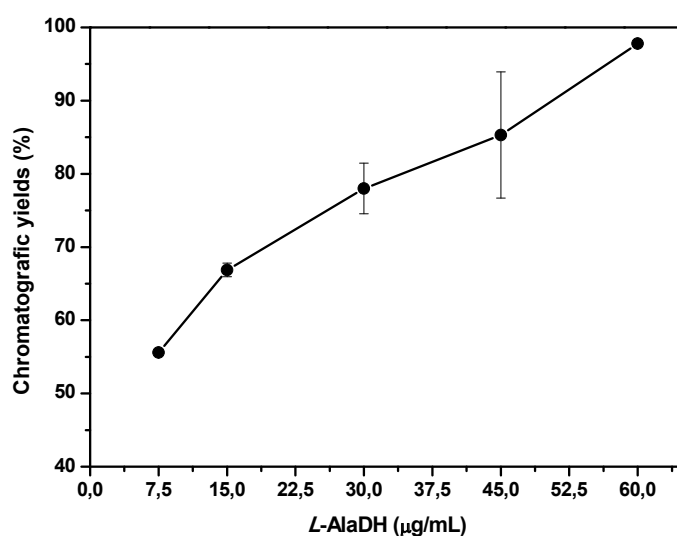
Figure 5.6. Effect of the amount of enzyme in the radiochemical synthesis of L-[^{13}N]alanine. The reactions were performed using a range of concentrations of L-AlaDH between (7.5-60 µg/mL) in the presence of 45-50 MBq of [^{13}N]NH$_3$, 0.5mM NADH, 75 mM pyruvic acid in 300 mM sodium phosphate buffer pH 8 at 25ºC. In all cases, the reaction time was 5 minutes. Results are expressed as a mean ± standard deviation, n≥3. Chromatographic yields were calculated from chromatographic profiles.

One of the major goals of the current work was to develop a versatile synthetic process, suitable for the efficient production of different amino acids. Additionally to L-[^{13}N]alanine, the preparation of [^{13}N]glycine and L-[^{13}N]serine was a priority for future use in animal studies. Hence, and in order to investigate the versatility of our approach, the synthesis of other two amino acids L-[^{13}N]phenylalaline and L-[^{13}N]norvaline were assayed using the same experimental set up as for L-[^{13}N]alanine. In all cases, the reactions were carried out for 5 minutes (optimal reaction time, **Figure 5.4**), using 60-300 µg/mL of L-AlaDH and under saturating concentration of the corresponding α-keto acid at the optimal pH values. Reactions of 20min were also investigated for the synthesis of [^{13}N]glycine and L-[^{13}N]serine. **Table 5.2** summarizes all the chromatographic yields obtained from the chromatographic profiles of the radiosynthesis of the above-mentioned amino acids.

Table 5.2. Chromatographic yields (CY) for the synthesis of different ^{13}N-labeled amino acids.

Amino acid	pH	CY (%)
Alanine	8	98±1[a]
Glycine	8	49±3[a] / 98±1[b]
Serine	8	7[a]
	9	42±5[a] / 99±1[c]
Norvaline	8	N.D. [a]
Phenylalanine	8	N.D. [a]

[a] 60 µg/mL of protein; [b] 180 µg/mL of protein; [c] 300 µg/mL of protein; N.D. = non-detected

146

Chromatographic yields of 49±3% and 42±5% were obtained for [^{13}N]glycine and *L*-[^{13}N]serine at short reaction times (5 min), respectively. These values increased up to >95% when the enzyme concentration was raised up to 180 and 300 µg/mL for the synthesis of [^{13}N]glycine and *L*-[^{13}N]serine, respectively (**Table 5.2**). The radiochemical synthesis of glycine and serine required higher enzyme concentrations because the specific enzyme activity of *L*-AlaDH was significantly lower towards glycolic acid and 3-hydroxypyruvic acid than towards pyruvic acid (**Table 5.1**). These findings are in accordance with our experiments under non-radioactive conditions, and confirm that *L*-AlaDH from *Bacillus subtilis* can catalyze the reductive amination of glycolic acid and 3-hydroxypyruvic acid, although reaction rates were lower than those observed for pyruvic acid. Interestingly, the synthesis of *L*-[^{13}N]serine at pH 8 resulted in chromatographic yields of 7% (**Table 5.2**). The results corroborate that the synthesis of *L*-serine is both kinetically and thermodynamically favored under alkaline conditions, as observed under non-radioactive conditions.

Unexpected results were obtained for the preparation of *L*-[^{13}N]phenylalaline and *L*-[^{13}N]norvaline. Although the enzyme was active towards the corresponding α-keto acids under non-radioactive conditions, no conversion was observed under radioactive conditions, regardless the reaction time. The absence of formation of *L*-[^{13}N]phenylalaline and *L*-[^{13}N]norvaline and the relatively low reaction rates obtained for [^{13}N]glycine and *L*-[^{13}N]serine could be initially attributed to an equilibrium between amination and deamination reactions. Nevertheless, the low specific activity of this enzyme for the deamination reactions using the different aminoacids as substrates discarded this hypothesis and

confirmed that the reductive amination is thermodynamically favoured at pH 8, as previously reported (**Table 5.1**).[31]

In an attempt to completely understand these low reaction rates, further investigation of the enzyme kinetics was performed. Steady-state kinetic parameters for ammonia were determined for the reductive amination of the different α-keto acids under non-radioactive conditions (see **Table 5.3**).

Table 5.3. Kinetic parameters by Michaelis-Menten model for ammonia, for the different amino acids.

Amino acid[a]	V_{max} (U/mg)	K_m (mM)
Alanine	100.46±4.30	47.0±11.4[a]
Glycine	51.96±6.05	527±149 [a]
Serine	74.63±1.26	2810±613[a] 150±21[b]
Norvaline	114.29±9.86	2231±544
Phenylalanine	ND	ND

[a] pH 8; [b] pH 9; N.D. = non-detected

All V_{max} values fell in the range 50-120 U/mg; however, K_m values for ammonia varied significantly from one amino acid to the next. K_m values for the synthesis of *L*-alanine and glycine at pH 8 were 47.0±11.4 and 527±149, respectively, while the K_m value for *L*-serine at pH 9 was 150±21 mM. However, the $K_{m[ammonia]}$ value for the synthesis of *L*-norvaline was 2231±544 mM, while the same parameter could not be determined for the synthesis of *L*-phenylalanine because the steady-state was never reached, regardless the concentration of ammonia. These values suggest that the

148

activity of the *L*-AlaDH is very sensitive to the concentration of ammonia, and such sensitivity strongly depends on the nature of the α-keto acid.[33] The $K_{m[ammonia]}$ values explain that high radiochemical yields are difficult to achieve with low enzyme concentrations at short reaction times both for [^{13}N]glycine and *L*-[^{13}N]serine. In the case of *L*-norvaline and *L*-phenylalanine, high concentration of ammonia is required for the reaction to occur at reasonable reaction rates; consequently, no formation of the amino acid can be observed under radioactive (no-carrier added) conditions, due to the low concentration of [^{13}N]NH$_3$ in the reaction media, even when a large excess of enzyme was used in the reaction mixture.

A similar effect was observed for the synthesis of *L*-serine at pH 8, which resulted in a $K_{m[ammonia]}$ as high as the one found for *L*-Norvaline, supporting the fact that, unlike *L*-[^{13}N]alanine, *L*-[^{13}N]serine was poorly synthesized at pH 8. The different $K_{m[ammonia]}$ values of *L*-AlaDH using different α-keto acids as amine acceptors suggest that the affinity of *L*-AlaDH for ammonia depends on the positioning of the α-keto acid into the active site. This fact is crucial to the success of the radiochemical synthesis, where extremely low concentrations of ammonia are used. In the light of these results, we point out that those enzymes or those substrates that facilitate the binding of the labeling agent to the active site (low K_m values), will lead to the best results in radiochemistry.

In sum, we have herein described a one-pot methodology that is clearly superior to previously published enzymatic methods,[34] and enables the preparation of *L*-[^{13}N]alanine, [^{13}N]glycine and *L*-[^{13}N]serine with chromatographic yields >95% in short reaction times. Specific activity values were in the range 15-35 GBq/μmol.

Synthesis of *L*-[^{13}N]alanine with *in situ* NADH regeneration

With the aim of simplifying the purification process, we envisioned the possibility to use lower concentrations of the cofactor by introducing a second enzyme in the reaction media capable to *in situ* regenerate NADH. The selected enzyme was formate dehydrogenase (FDH) from *Candida boidinii*, which is known to catalyze the oxidation of formate to carbon dioxide, by donating the electrons to a second substrate, such as NAD^+, regenerating thus NADH (see **Figure 5.1b**).
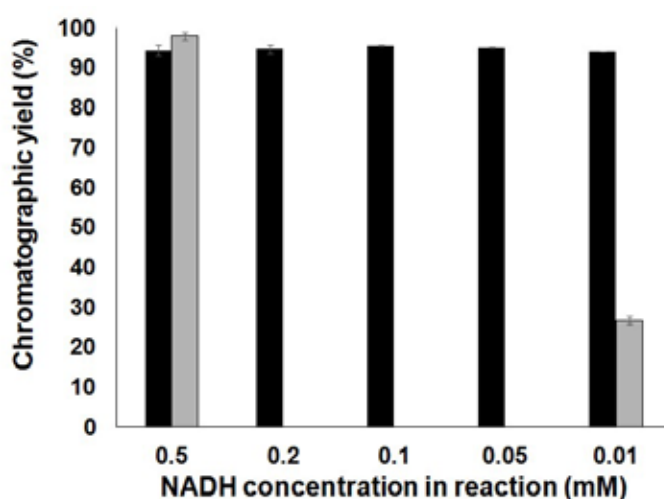
Figure 5.7. Chromatographic yields for the production of *L*-[^{13}N]alanine at different concentrations of NADH (black bars). Grey bars correspond to values under identical experimental conditions in the absence of FDH. Values are expressed as the mean ± standard deviation (n=3). The reactions were carried out in the presence of 20-25 MBq of [^{13}N]NH$_3$, 60 μg/mL of *L*-AlaDH, 0.01 to 0.5mM of NADH, and 75 mM of pyruvic acid in 300 mM sodium phosphate buffer at 25ºC and pH 8.

The one-pot, bi-enzymatic reaction offered exceptional results. The concentration of NADH in the starting solution could be decreased by 50-fold without a significant impact on chromatographic yields (**Figure 5.6**). The simultaneous addition of *L*-AlaDH and FDH led to the formation of *L*-[^{13}N]alanine with chromatographic yields of 95±2% by using NADH concentrations as low as 10 μM. These values are three times higher than those observed without FDH under identical experimental conditions. The FDH is fundamental to replenish the pool of NADH by consuming formate as sacrificing substrate; in this manner, the reduced form remains available for the *L*-AlaDH to catalyze consecutive cycles of the pyruvate reductive amination. These results substantially improve the synthetic scheme described by Baumgartner *et al.*[34] With our configuration, similar yields can be obtained but the concentration of cofactor is 100-fold lower.

In vivo experiments

Prostate cancer is the fourth cause of death by cancer worldwide, the second in the male population according to data published by the World Health Organization (WHO).[35,36] Notably, prostate cancer incidence is dramatically increasing in western societies in the past decades, suggesting that this type of tumor is intrinsically sensitive to lifestyle changes.[37] Despite the good response to standard therapies, a high number of patients exhibit recurrence and develop metastatic disease after the failure of subsequent therapeutic regimens. Hence, the molecular aspects related to disease progression and therapy response remain unclear. Phosphatase and tensin homolog (Pten) is one of the most commonly deleted/mutated tumor suppressor genes in human prostate cancer.[38,39] As a lipid phosphatase and a negative regulator of the PI3K/AKT/mTOR pathway, Pten controls

several cellular processes, including survival, growth, proliferation, metabolism, migration, and cellular architecture.[40] On the other hand, cancer cells have altered metabolism and have well-known metabolic abnormalities. Cancer cells need a continuous supply of nutrients that maintain abnormal growth and rapid division during cancer progression and depend on a high rate of aerobic glycolysis for continued growth and survival. Recent advances in cancer biology and cellular immunity reveal that not only glucose but also amino acids are essential to support the high metabolic demands of the tumor.[41,42] Because amino acids are the most highly consumed nutrients by cancer cells and biosynthetic pathways, they are always in demand for different cancer subtypes.[43,44] These processes of differentiation, proliferation and metabolism of cancer cells can be understood by using PET imaging technique and metabolic radiotracers, specifically radiolabeled glucose and amino acids.[45-48] The information obtained about metabolic alterations may aid the development of new therapies and tools for the early detection of cancer lesions.

In this study, and taking advantage of a collaboration with Prof. Carracedo, we decided to explore the *in vivo* behavior of three enzymatically labeled amino acids (*L*-[^{13}N]alanine, *L*-[^{13}N]serine, [^{13}N]glycine) in a mouse model of prostate cancer, created by depletion of the Pten which resembles the behavior of human prostate cancer. Before that, we explored the pharmacokinetics (PK) properties (mainly biodistribution) in healthy animals. [^{18}F]FDG and [^{11}C]Choline, typically used in the clinical setting for the detection of prostate cancer, were also used in the study with diseased animals for comparison.

Starting from 225 ± 25 MBq of cyclotron produced [^{13}N]NH$_4$OH (Volume of 100μL), 85 ± 6 MBq of pure *L*-[^{13}N]alanine, [^{13}N]glycine and *L*-

[^{13}N]serine could be obtained using the enzymatic approach previously described. The labeled amino acids were obtained with >98% purity, with decay-corrected radiochemical yields close to 70% in overall production times of 10 min. Specific activity values ranging 15-35 GBq/μmol were achieved.

PET studies were conducted also with [^{18}F]FDG, a glucose analogue in which the hydroxyl group at the 2-position is substituted with an ^{18}F atom; and [^{11}C]choline, an ^{11}C-labeled amino acid methyl typically used in the clinical setting for the detection of prostate cancer.[49] These tracers are widely used in the clinical diagnostic field for the early diagnose of prostate tumors, as well as for the evaluation of the response to treatment.[50-52] The basis behind accumulation of [^{18}F]FDG in tumor tissues is well known (**Figure 5.7**). [^{18}F]FDG is taken up and phosphorylated by cells through the same pathways as glucose, and finally trapped within the cells since the fluorinated and phosphorylated glucose cannot be metabolized in the glycolysis. As a result, [^{18}F]FDG concentration increases proportionally with the utilization rate of glucose and consequently with the cell growth, and therefore it can be used as an indirect proliferation marker. On the other hand, [^{11}C]choline incorporates into tumor cells through an active, carrier-mediated transport mechanism for choline and then is phosphorylated intracellularly by choline kinase, an enzyme frequently upregulated in human tumors, yielding phosphoryl [^{11}C]choline (**Figure 5.7**).[53] In turn, this phosphoryl [^{11}C]choline is integrated into phospholipids in the cell membrane as part of phosphatidyl[^{11}C]choline. As the proliferation of cancer cells is much higher than normal cells, tumor cells exhibit an increased rate of [^{11}C]choline uptake and incorporation, allowing tumor imaging with PET.

153
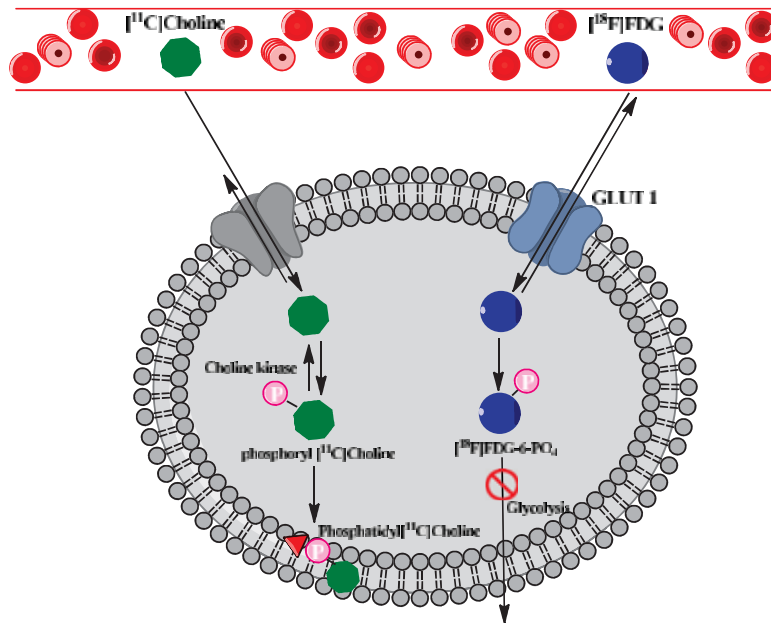
Figure 5.8. Intracellular metabolism of [11C]choline and [18F]FDG. Both are taken up by cells by means of membrane transporters. Once into the cell, they are phosphorylated to phosphoryl[11C]choline and [18F]glucose-6-phosphate, respectively. Then, phosphoryl[11C]choline is integrated into phospholipids in the cell membrane as part of phosphatidyl[11C]choline; [18F]glucose-6-phosphate does not undergo further metabolism and is trapped in the cell.

In vivo biodistribution studies in wild-type mice

Biodistribution of *L*-[13N]alanine, [13N]glycine and *L*-[13N]serine was first investigated in healthy animals. After image acquisition, volumes of interest (VOIs) were manually defined in the main organs on CT images and translated to the PET images for quantification, which resulted in time-activity curves (TACs) as represented by *L*-[13N]alanine in **Figure 5.8**. In this case, only those organs clearly visualized on the CT images (lung, heart, kidney, liver, brain and bladder) were delineated. Very similar

154

biodistribution patterns were obtained for all the labeled amino acids. The presence of radioactivity was detected in the heart at short times after administration, confirming the presence of radioactivity in the blood. The values rapidly decreased from ~30 %ID/cm^3 immediately after injection to approximately 2%ID/cm^3, value that was maintained for a long period of time. The presence of radioactivity in heart suggests the long residence time of the labeled species in the blood-pool. At longer time points, a progressive accumulation of radioactivity in the liver was observed, consistent with the anabolic function of this organ, with values below 5% ID/cm^3 for the case of L-[^{13}N]alanine. The highest accumulation of radioactivity was found in the abdominal region, especially in the intestine, as already reported in previous biodistribution studies for other amino acids.[45] Low accumulation of radioactivity was found in the brain, which may facilitate the potential localization of tumors in this organ. Normally, only the aromatic amino acids are presumed to influence brain function. The aromatic amino acids (e.g. tryptophan, tyrosine, phenylalanine) are the biosynthetic precursors for the neurotransmitters serotonin, dopamine, and norepinephrine. However, small neutral amino acids like alanine and glycine appear to be actively pumped out of the brain.[54]

Elimination via urine was negligible in the time window of the study for [^{13}N]alanine, with average accumulation around 1.5 ID%/cm^3 (**Figure 5.8 and 5.9**). A slow progressive elimination by urine was found to [^{13}N]glycine. However, for L-[^{13}N]serine, elimination via urine was preferential showing a high uptake in the bladder. This fact may limit application of this tracer to investigate the uptake in the prostate or prostate cancer.
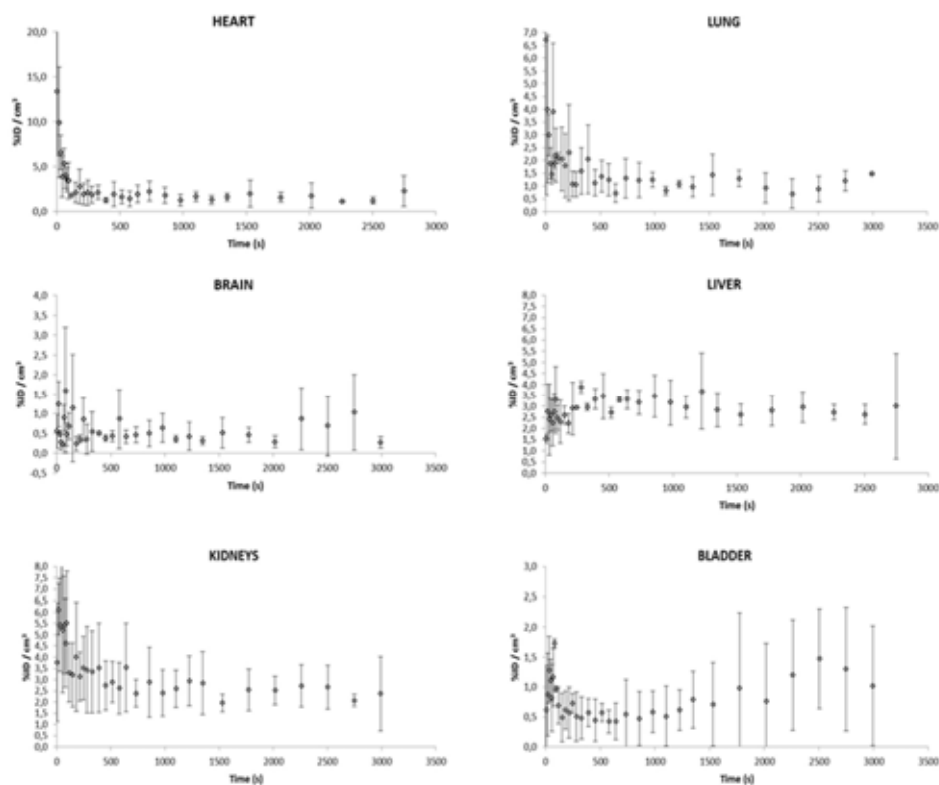
Figure 5.9. Accumulation of [^{13}N]alanine into the different organs after intravenous administration. Time-activity-curves are expressed as the percentage of the injected dose (%ID) per cm^3 of tissue. [^{13}N]alanine biodistribution in organs indicated above each panel. The Y axis scale is different in every graph.

In vivo studies: Prostate-specific Pten deletion cancer model

It is very well known that the amino acid transport is generally increased in malignant tumor cells.[43] This enhanced transport may be associated with specific cell surface changes in cancer cells.[44,55] Generally, the process of malignant transformation requires that cells acquire and use nutrients (glucose and amino acids) efficiently for energy, protein synthesis, and cell division. In this context, the amino acids transport is likely enhanced

in tumor cells to supply the upregulated amino acid metabolism and protein biosynthesis.
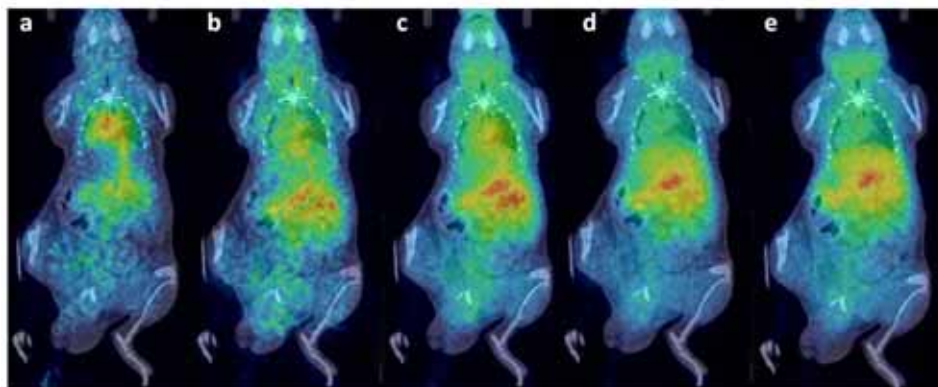
Figure 5.10. Representative PET-CT images obtained after intravenous administration of L-[^{13}N]alanine in mice. Coronal projections of PET images have been co-registered with representative CT slices for co-localization of the radioactive signal. Images correspond to data averaged in the following time frames: 0-30 s (**a**); 31-70 s (**b**); 71-230 s (**c**); 231-740 s (**d**); and 741-3020 s (**e**).

The three amino acids (L-[^{13}N]alanine, [^{13}N]glycine and L-[^{13}N]serine) labeled with nitrogen-13 by the action of L-AlaDH were tested in a prostate cancer mouse model, as potential imaging PET agents. Likewise [^{11}C]choline and [^{18}F]FDG, typically used in the clinical setting for the detection of prostate cancer, were also used in the study with comparison purposes.

Upon intravenous administration, accumulation of radioactivity in the tumor could be observed for L-[^{13}N]alanine and [^{13}N]glycine (see **Figure 5.10**). Visualization of the prostate after administration of L-[^{13}N]serine

was not possible due to the abovementioned accumulation of radioactivity in the bladder.

Precise quantification of the amount of radioactivity in the prostate was extremely challenging because the prostate could not be clearly visualized on the CT images. Hence, the images were only evaluated from a qualitative point of view. Visual inspection of PET images acquired after administration of L-[^{13}N]alanine and [^{13}N]glycine suggests a progressive accumulation of radioactivity in the prostate over time, regardless the presence of the tumour. However, such accumulation seems to be more significant in animals with tumour. Despite these promising preliminary results, further investigation is required in the future to assess the potential of the ^{13}N-labeled amino acids as metabolic markers in this tumour type.

The involvement of these two amino acids in the metabolism and proliferation of cancer cells is already known and studied by several investigators. Alanine has been already identified as an important non-invasive biomarker for prostate cancer detection and characterization in magnetic resonance imaging and ^{1}H high-resolution magic angle spinning (HR-MAS) spectroscopy.[56,57] Likewise, glycine metabolism in cancer cells has been associated with cancer cell proliferation. It has been recently shown that glycine uptake and catabolism can promote tumorigenesis and malignancy, suggesting that glycine metabolism could in principle be a target for the design of innovative therapeutic and diagnostic strategies.[26,58]
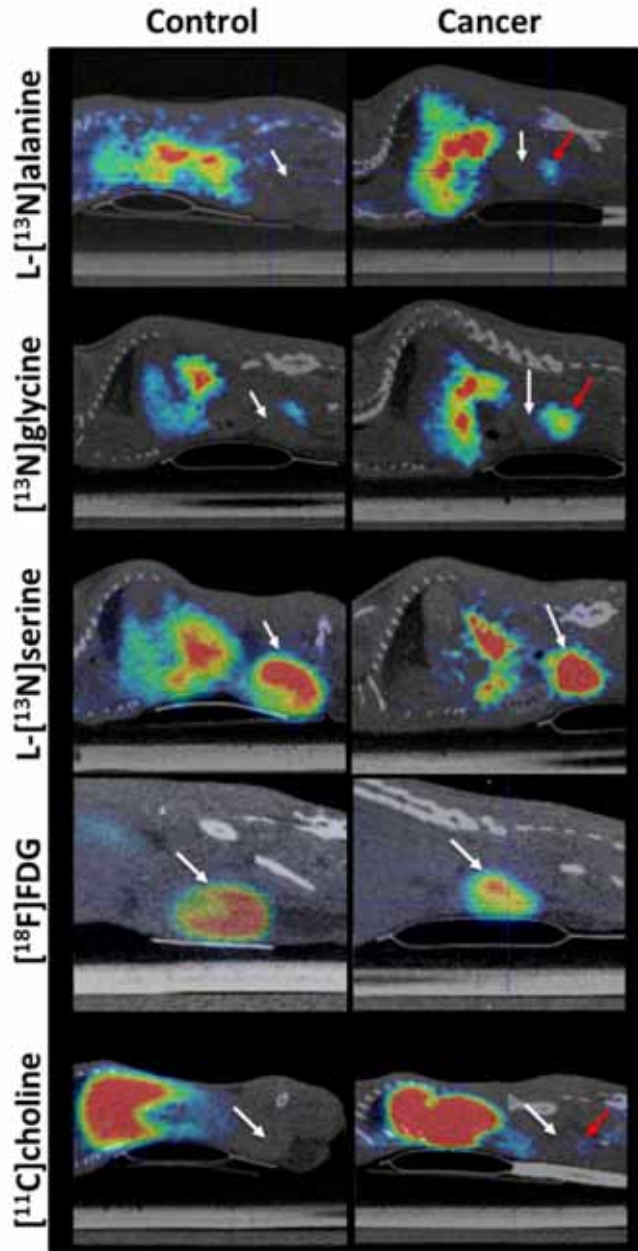
Figure 5.11. Sagittal PET projections of control and cancer animals resulting from averaged images (frames 1-33) obtained after administration of [^{13}N]-labeled amino acids, [^{18}F]FDG and [^{11}C]choline. The position of the bladder and the tumour are indicated with white and red arrows, respectively. Co-registration with CT images of the same animal is shown for localization of the radioactivity.

159

Regrettably, high elimination via urine is consistently found for L-[^{13}N]serine, hampering the visualization of the prostate for the intense uptake of the labeled amino acid in the region. This is a non-essential amino acid that is biosynthetically linked to glycine, and both together provide the essential precursors for the synthesis of both folate and methionine. These biosynthetic routes are responsible for the synthesis of proteins, nucleic acids, and lipids, which are essential biological processes for the uncontrolled growth of cancer cells.[26,59-61] Unfortunately, it was not possible to make use of *L*-[^{13}N]serine to assess the metabolism of serine in cancer prostate of mice. However, low uptake of *L*-[^{13}N]serine observed in the brain, neck, chest, pelvis, and extremities may open new opportunities to explore tumor localization in those areas. Many cancer cells are highly dependent on serine[62] which can provide novel translational opportunities for imaging, drug development, dietary intervention, and biomarker identification of human cancers.

Standard biodistribution of [^{11}C]choline was observed: relatively high accumulation in the pancreas, liver and kidneys, and variable uptake in the bowel, with insignificant urinary excretion (**Figure 5.10**). Radiolabeled choline PET has been found to be useful in imaging prostate cancer.[49,51,52,63,64] The biological basis of the radiolabeled choline uptake in tumors is the malignancy-induced upregulation of choline kinase, which leads to the incorporation and trapping of choline as phosphatidylcholine in the tumor cell membranes (**Figure 5.10**). Unpredictably, tumor uptake of [^{11}C]choline in our prostate cancer model was almost inexistent. Hence, the low uptake of [^{11}C]choline can be hypothetically explained by the hypoxia stage of the cancer cells in our animal model. According to Hara *et al.*, hypoxic cells significantly incorporate less [^{11}C]Choline, reflecting diverse biochemical responses to hypoxia.[65]

For [^{18}F]FDG, the typical biodistribution pattern for this tracer was observed in our studies: high accumulation was detected in the kidneys and the bladder due to elimination mainly via urine, while significant uptake was also observed in the heart and the brain, organs which are known to consume a significant amount of glucose (**Figure 5.10**). Due to its high elimination via urine, [^{18}F]FDG was mainly accumulated in the bladder, hampering thus visualizing proper visualization of the prostate and eventually the tumor, similarly to what we observed with *L*-[^{13}N]serine.

CONCLUSIONS

In conclusion, we have achieved a fast, efficient, and one-pot synthesis of *L*-[^{13}N]alanine, [^{13}N]glycine, and *L*-[^{13}N]serine catalyzed by *L*-AlaDH and using NADH as redox cofactor and FDH as recycling enzymatic partner. The synthesis of *L*-[^{13}N]alanine was significantly more efficient than the synthesis of [^{13}N]glycine and *L*-[^{13}N]serine. However, the synthesis of [^{13}N]glycine and *L*-[^{13}N]serine was successfully optimized by increasing the biocatalyst load in the reaction mixture. Unfortunately, the synthesis of artificial amino acids such as *L*-[^{13}N]norvaline and *L*-[^{13}N]phenylalanine was not achieved under no-carrier-added conditions, due to the high K_m values for ammonia.

The synthesis of *L*-[^{13}N]alanine was optimized by adding FDH to the reaction media in order to in situ regenerate NADH using formate as scarifying substrates for hydride transfer. This bi-enzyme system enabled the 50-fold reduction of NADH concentration in the reaction mixture without compromising radiochemical yields.

The utilization of the enzyme *L*-AlaDH shows an innovative synthetic strategy to manufacture ready-to-inject ^{13}N-labeled amino acids (*L*-[^{13}N]alanine, [^{13}N]glycine, and *L*-[^{13}N]serine) in sufficient amount and purity to approach *in vivo* studies. Upon intravenous administration, *L*-[^{13}N]alanine shows an interesting selective accumulation in the prostate which seems to increase in the presence of tumors. On the other hand, [^{13}N]glycine shows uptake in the healthy and cancer prostate. Unfortunately, *L*-[^{13}N]serine is eliminated via urine hampering the visualization of the tumor progression, similarly to what we observed with [^{18}F]FDG.

REFERENCES

(1) Gelbard, A. S. Biosynthetic methods for incorporating positron-emitting radionuclides into compounds of biomedical interest. *Journal of Labelled Compounds and Radiopharmaceuticals* **1981**, *18*, 933-945.

(2) N. Lembares; R. Dinwoodie; I. Gloria; Harper, P.; Lathrop, K. A rapid enzymatic synthesis of 10-min 13N-glutamate and Its pancreatic localization. *J. Nucl. Med.* **1972**, 786-786.

(3) Straatmann, M. G.; Welch, M. J. Enzymatic Synthesis of Nitrogen-13 Labeled Amino Acids. *Radiat. Res.* **1973**, *56*, 48-56.

(4) M.B. Cohen; L. Spolter; N.S. McDonald; Cassen, B. Enzymatic synthesis of 13N L-glutamine. *J. Nucl. Med.*, 422.

(5) Cooper, A. J.; Gelbard, A. S. The use of immobilized glutamate dehydrogenase to synthesize 13N-labeled L-amino acids. *Anal. Biochem.* **1981**, *111*, 42-48.

(6) Barrio, J. R.; Baumgartner, F. J.; Henze, E.; Stauber, M. S.; Egbert, J. E.; MacDonald, N. S.; Schelbert, H. R.; Phelps, M. E.; Liu, F.-T. Synthesis and Myocardial Kinetics of N-13 and C-11 Labeled Branched-Chain l-Amino Acids. *J. Nucl. Med.* **1983**, *24*, 937-944.

(7) Galkin, A.; Kulakova, L.; Yoshimura, T.; Soda, K.; Esaki, N. Synthesis of optically active amino acids from alpha-keto acids with Escherichia coli

cells expressing heterologous genes. *Applied and Environmental Microbiology* **1997**, *63*, 4651-4656.

(8)   Lu, J.; Zhang, Y.; Sun, D.; Jiang, W.; Wang, S.; Fang, B. The Development of Leucine Dehydrogenase and Formate Dehydrogenase Bifunctional Enzyme Cascade Improves the Biosynthsis of L-tert-Leucine. *Applied Biochemistry and Biotechnology* **2016**, *180*, 1180-1195.

(9)   Lerchner, A.; Jarasch, A.; Skerra, A. Engineering of alanine dehydrogenase from Bacillus subtilis for novel cofactor specificity. *Biotechnology and Applied Biochemistry* **2016**, *63*, 616-624.

(10)   Mutti, F. G.; Fuchs, C. S.; Pressnitz, D.; Sattler, J. H.; Kroutil, W. Stereoselectivity of Four (R)-Selective Transaminases for the Asymmetric Amination of Ketones. *Advanced Synthesis & Catalysis* **2011**, *353*, 3227-3233.

(11)   Baker, P. J.; Sawa, Y.; Shibata, H.; Sedelnikova, S. E.; Rice, D. W. Analysis of the structure and substrate binding of Phormidium lapideum alanine dehydrogenase. *Nature structural biology* **1998**, *5*, 561-567.

(12)   Abrahamson, M. J.; Wong, J. W.; Bommarius, A. S. The Evolution of an Amine Dehydrogenase Biocatalyst for the Asymmetric Production of Chiral Amines. *Advanced Synthesis & Catalysis* **2013**, *355*, 1780-1786.

(13)   Grimshaw, C. E.; Cleland, W. W. Kinetic mechanism of Bacillus subtilis L-alanine dehydrogenase. *Biochemistry* **1981**, *20*, 5650-5655.

(14)   Ye, W.; Huo, G.; Chen, J.; Liu, F.; Yin, J.; Yang, L.; Ma, X. Heterologous expression of the Bacillus subtilis (natto) alanine dehydrogenase in Escherichia coli and Lactococcus lactis. *Microbiol. Res.* **2010**, *165*, 268-275.

(15)   Siranosian, K. J.; Ireton, K.; Grossman, A. D. Alanine dehydrogenase (ald) is required for normal sporulation in Bacillus subtilis. *J. Bacteriol.* **1993**, *175*, 6789-6796.

(16)   Freese, E.; Park, S. W.; Cashel, M. The developmental significance of alanine dehydrogenase in bacillus subtilis. *Proc. Natl. Acad. Sci. U. S. A.* **1964**, *51*, 1164-1172.

(17)   da Silva, E. S.; Gomez-Vallejo, V.; Llop, J.; Lopez-Gallego, F. Efficient nitrogen-13 radiochemistry catalyzed by a highly stable immobilized biocatalyst. *Catalysis Science & Technology* **2015**.

(18)   Chenault, H. K.; Simon, E. S.; Whitesides, G. M. Cofactor regeneration for enzyme-catalysed synthesis. *Biotechnology & genetic engineering reviews* **1988**, *6*, 221-270.

(19)   Weckbecker, A.; Groger, H.; Hummel, W. Regeneration of nicotinamide coenzymes: principles and applications for the synthesis of chiral

compounds. *Advances in biochemical engineering/biotechnology* **2010**, *120*, 195-242.

(20) Barredo, J. L.: *Microbial Enzymes and Biotransformations*; Humana Press, 2005.

(21) Pongtharangkul, T.; Chuekitkumchorn, P.; Suwanampa, N.; Payongsri, P.; Honda, K.; Panbangred, W. Kinetic properties and stability of glucose dehydrogenase from Bacillus amyloliquefaciens SB5 and its potential for cofactor regeneration. *AMB Express* **2015**, *5*, 68.

(22) Woodyer, R.; Zhao, H.; van der Donk, W. A. Mechanistic investigation of a highly active phosphite dehydrogenase mutant and its application for NADPH regeneration. *The FEBS journal* **2005**, *272*, 3816-3827.

(23) Johannes, T. W.; Woodyer, R. D.; Zhao, H. Efficient regeneration of NADPH using an engineered phosphite dehydrogenase. *Biotechnol Bioeng* **2007**, *96*, 18-26.

(24) Schirwitz, K.; Schmidt, A.; Lamzin, V. S. High-resolution structures of formate dehydrogenase from Candida boidinii. *Protein Science : A Publication of the Protein Society* **2007**, *16*, 1146-1156.

(25) Bradford, M. M. A rapid and sensitive method for the quantitation of microgram quantities of protein utilizing the principle of protein-dye binding. *Analytical Biochemistry* **1976**, *72*, 248-254.

(26) Amelio, I.; Cutruzzola, F.; Antonov, A.; Agostini, M.; Melino, G. Serine and glycine metabolism in cancer. *Trends Biochem Sci* **2014**, *39*, 191-198.

(27) Albers, M. J.; Bok, R.; Chen, A. P.; Cunningham, C. H.; Zierhut, M. L.; Zhang, V. Y.; Kohler, S. J.; Tropp, J.; Hurd, R. E.; Yen, Y.-F.; Nelson, S. J.; Vigneron, D. B.; Kurhanewicz, J. Hyperpolarized 13C Lactate, Pyruvate, and Alanine: Noninvasive Biomarkers for Prostate Cancer Detection and Grading. *Cancer Res.* **2008**, *68*, 8607-8615.

(28) Yoshida, A.; Freese, E. Enzymatic properties of Alanine dehydrogenase of Bacillus subtilis. *Biochimica et biophysica acta* **1965**, *96*, 248-262.

(29) Baker, P. J.; Sawa, Y.; Shibata, H.; Sedelnikova, S. E.; Rice, D. W. Analysis of the structure and substrate binding of Phormidium lapideum alanine dehydrogenase. *Nat. Struct. Mol. Biol.* **1998**, *5*, 561-567.

(30) Fernandes, P.; Aldeborgh, H.; Carlucci, L.; Walsh, L.; Wasserman, J.; Zhou, E.; Lefurgy, S. T.; Mundorff, E. C. Alteration of substrate specificity of alanine dehydrogenase. *Protein Eng. Des. Sel.* **2015**, *28*, 29-35.

(31) Ohashima, T.; Soda, K. Purification and properties of alanine dehydrogenase from Bacillus sphaericus. *Eur. J. Biochem.* **1979**, *100*, 29-30.

(32)   Brunhuber, N. M.; Blanchard, J. S. The biochemistry and enzymology of amino acid dehydrogenases. *Crit. Rev. Biochem. Mol. Biol.* **1994**, *29*, 415-467.

(33)   Ohshima, T.; Soda, K.: Biochemistry and biotechnology of amino acid dehydrogenases. In *Bioprocesses and Applied Enzymology*; Springer Berlin Heidelberg: Berlin, Heidelberg, 1990; pp 187-209.

(34)   Baumgartner, F. J.; Barrio, J. R.; Henze, E.; Schelbert, H. R.; MacDonald, N. S.; Phelps, M. E.; Kuhl, D. E. 13N-labeled L-amino acids for in vivo assessment of local myocardial metabolism. *Journal of medicinal chemistry* **1981**, *24*, 764-766.

(35)   Cancer Research Uk. Worldwide cancer incidence statistics. http://www.cancerresearchuk.org/health-professional/cancer-statistics/worldwide-cancer/incidence.

(36)   Ferlay, J.; Soerjomataram, I.; Dikshit, R.; Eser, S.; Mathers, C.; Rebelo, M.; Parkin, D. M.; Forman, D.; Bray, F. Cancer incidence and mortality worldwide: Sources, methods and major patterns in GLOBOCAN 2012. *International Journal of Cancer* **2015**, *136*, E359-E386.

(37)   Moul, J. W.: Chapter 1 - Population Screening for Prostate Cancer and Early Detection A2 - Mydlo, Jack H. In *Prostate Cancer (Second Edition)*; Godec, C. J., Ed.; Academic Press: San Diego, 2016; pp 3-12.

(38)   Ugalde-Olano, A.; Egia, A.; Fernández-Ruiz, S.; Loizaga-Iriarte, A.; Zuñiga-García, P.; Garcia, S.; Royo, F.; Lacasa-Viscasillas, I.; Castro, E.; Cortazar, A. R.; Zabala-Letona, A.; Martín-Martín, N.; Arruabarrena-Aristorena, A.; Torrano-Moya, V.; Valcárcel-Jiménez, L.; Sánchez-Mosquera, P.; Caro-Maldonado, A.; González-Tampan, J.; Cachi-Fuentes, G.; Bilbao, E.; Montero, R.; Fernández, S.; Arrieta, E.; Zorroza, K.; Castillo-Martín, M.; Serra, V.; Salazar, E.; Macías-Cámara, N.; Tabernero, J.; Baselga, J.; Cordón-Cardo, C.; Aransay, A. M.; Villar, A. D.; Iovanna, J. L.; Falcón-Pérez, J. M.; Unda, M.; Bilbao, R.; Carracedo, A. Methodological aspects of the molecular and histological study of prostate cancer: Focus on PTEN. *Methods* **2015**, *77–78*, 25-30.

(39)   Nardella, C.; Carracedo, A.; Salmena, L.; Pandolfi, P. P. Faithfull modeling of PTEN loss driven diseases in the mouse. *Current topics in microbiology and immunology* **2010**, *347*, 135-168.

(40)   Jiang, B. H.; Liu, L. Z. PI3K/PTEN signaling in angiogenesis and tumorigenesis. *Advances in cancer research* **2009**, *102*, 19-65.

(41)   Ananieva, E. Targeting amino acid metabolism in cancer growth and anti-tumor immune response. *World Journal of Biological Chemistry* **2015**, *6*, 281-289.

(42)   Bhutia, Y. D.; Babu, E.; Ramachandran, S.; Ganapathy, V. Amino Acid transporters in cancer and their relevance to "glutamine addiction": novel

targets for the design of a new class of anticancer drugs. *Cancer research* **2015**, *75*, 1782-1788.

(43) Busch, H.; Davis, J. R.; Honig, G. R.; Anderson, D. C.; Nair, P. V.; Nyhan, W. L. The Uptake of a Variety of Amino Acids into Nuclear Proteins of Tumors and Other Tissues. *Cancer research* **1959**, *19*, 1030-1039.

(44) Isselbacher, K. J. Increased Uptake of Amino Acids and 2-Deoxy-D-Glucose by Virus-Transformed Cells in Culture. *Proceedings of the National Academy of Sciences* **1972**, *69*, 585-589.

(45) Jager, P. L.; Vaalburg, W.; Pruim, J.; de Vries, E. G.; Langen, K. J.; Piers, D. A. Radiolabeled amino acids: basic aspects and clinical applications in oncology. *Journal of nuclear medicine : official publication, Society of Nuclear Medicine* **2001**, *42*, 432-445.

(46) Crippa, F.; Alessi, A.; Serafini, G. L. PET with radiolabeled aminoacid. *The quarterly journal of nuclear medicine and molecular imaging : official publication of the Italian Association of Nuclear Medicine (AIMN) [and] the International Association of Radiopharmacology (IAR), [and] Section of the So* **2012**, *56*, 151-162.

(47) Hosios, A. M.; Hecht, V. C.; Danai, L. V.; Johnson, M. O.; Rathmell, J. C.; Steinhauser, M. L.; Manalis, S. R.; Vander Heiden, M. G. Amino Acids Rather than Glucose Account for the Majority of Cell Mass in Proliferating Mammalian Cells. *Developmental cell* **2016**, *36*, 540-549.

(48) Haberkorn, U.; Markert, A.; Mier, W.; Askoxylakis, V.; Altmann, A. Molecular imaging of tumor metabolism and apoptosis. *Oncogene* **2011**, *30*, 4141-4151.

(49) Jadvar, H. Prostate Cancer: PET with 18F-FDG, 18F- or 11C-Acetate, and 18F- or 11C-Choline. *Journal of Nuclear Medicine* **2011**, *52*, 81-89.

(50) Picchio, M.; Messa, C.; Landoni, C.; Gianolli, L.; Sironi, S.; Brioschi, M.; Matarrese, M.; Matei, D. V.; De Cobelli, F.; Del Maschio, A.; Rocco, F.; Rigatti, P.; Fazio, F. Value of [11C]choline-positron emission tomography for re-staging prostate cancer: a comparison with [18F]fluorodeoxyglucose-positron emission tomography. *The Journal of urology* **2003**, *169*, 1337-1340.

(51) Reske, S. N.; Blumstein, N. M.; Neumaier, B.; Gottfried, H. W.; Finsterbusch, F.; Kocot, D.; Moller, P.; Glatting, G.; Perner, S. Imaging prostate cancer with 11C-choline PET/CT. *Journal of nuclear medicine : official publication, Society of Nuclear Medicine* **2006**, *47*, 1249-1254.

(52) Murphy, R. C.; Kawashima, A.; Peller, P. J. The Utility of 11C-Choline PET/CT for Imaging Prostate Cancer: A Pictorial Guide. *American Journal of Roentgenology* **2011**, *196*, 1390-1398.

(53) Lockman, P. R.; Allen, D. D. The transport of choline. *Drug development and industrial pharmacy* **2002**, *28*, 749-771.

(54) Laterra J; Keep R; Betz LA; al., e.: Blood—Brain Barrier. In *Basic Neurochemistry: Molecular, Cellular and Medical Aspects.*; 6th ed.; Siegel GJ, A. B., Albers RW, et al., editors., Ed.: Philadelphia: Lippincott-Raven, 1999.

(55) Haase, C.; Bergmann, R.; Fuechtner, F.; Hoepping, A.; Pietzsch, J. L-Type Amino Acid Transporters LAT1 and LAT4 in Cancer: Uptake of 3-O-Methyl-6- 18F-Fluoro-l-Dopa in Human Adenocarcinoma and Squamous Cell Carcinoma In Vitro and In Vivo. *Journal of Nuclear Medicine* **2007**, *48*, 2063-2071.

(56) Tessem, M.-B.; Swanson, M. G.; Keshari, K. R.; Albers, M. J.; Joun, D.; Tabatabai, Z. L.; Simko, J. P.; Shinohara, K.; Nelson, S. J.; Vigneron, D. B.; Gribbestad, I. S.; Kurhanewicz, J. Evaluation of Lactate and Alanine as Metabolic Biomarkers of Prostate Cancer Using (1)H HR-MAS Spectroscopy of Biopsy Tissues. *Magnetic resonance in medicine : official journal of the Society of Magnetic Resonance in Medicine / Society of Magnetic Resonance in Medicine* **2008**, *60*, 510-516.

(57) Albers, M. J.; Bok, R.; Chen, A. P.; Cunningham, C. H.; Zierhut, M. L.; Zhang, V. Y.; Kohler, S. J.; Tropp, J.; Hurd, R. E.; Yen, Y. F.; Nelson, S. J.; Vigneron, D. B.; Kurhanewicz, J. Hyperpolarized 13C lactate, pyruvate, and alanine: noninvasive biomarkers for prostate cancer detection and grading. *Cancer research* **2008**, *68*, 8607-8615.

(58) Jain, M.; Nilsson, R.; Sharma, S.; Madhusudhan, N.; Kitami, T.; Souza, A. L.; Kafri, R.; Kirschner, M. W.; Clish, C. B.; Mootha, V. K. Metabolite profiling identifies a key role for glycine in rapid cancer cell proliferation. *Science (New York, N.Y.)* **2012**, *336*, 1040-1044.

(59) Yang, M.; Vousden, K. H. Serine and one-carbon metabolism in cancer. *Nat Rev Cancer* **2016**, *16*, 650-662.

(60) Mattaini, K. R.; Sullivan, M. R.; Vander Heiden, M. G. The importance of serine metabolism in cancer. *The Journal of Cell Biology* **2016**, *214*, 249-257.

(61) Tsun, Z. Y.; Possemato, R. Amino acid management in cancer. *Seminars in cell & developmental biology* **2015**, *43*, 22-32.

(62) Frezza, C. Cancer metabolism: Addicted to serine. *Nat Chem Biol* **2016**, *12*, 389-390.

(63) Krause, B. J.; Souvatzoglou, M.; Treiber, U. Imaging of prostate cancer with PET/CT and radioactively labeled choline derivates. *Urologic oncology* **2013**, *31*, 427-435.

(64) Vali, R.; Loidl, W.; Pirich, C.; Langesteger, W.; Beheshti, M. Imaging of prostate cancer with PET/CT using (18)F-Fluorocholine. *American Journal of Nuclear Medicine and Molecular Imaging* **2015**, *5*, 96-108.

(65) Hara, T.; Bansal, A.; DeGrado, T. R. Effect of hypoxia on the uptake of [methyl-3H]choline, [1-14C] acetate and [18F]FDG in cultured prostate cancer cells. *Nucl Med Biol* **2006**, *33*, 977-984.

Chapter 6

Design and full characterization of *L*-Alanine immobilized on solid and porous materials
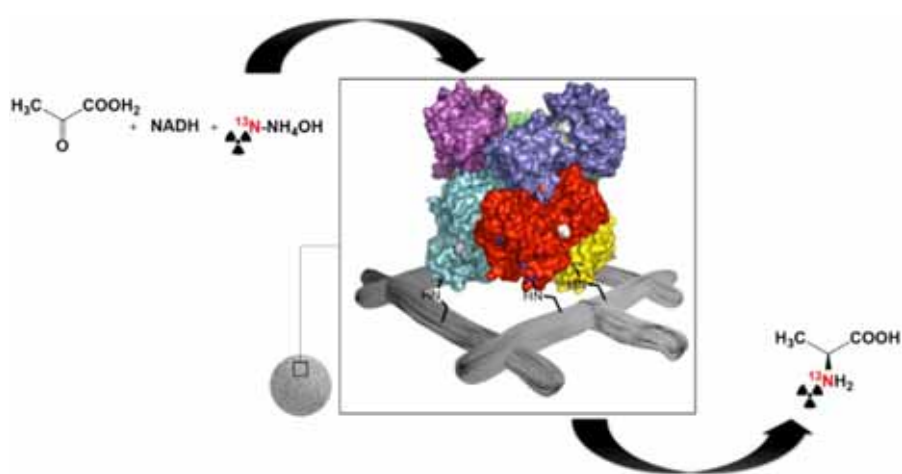
L-Alanine dehydrogenase from *Bacillus subtillis* has been intensively exploited in biocatalysis but its immobilized form is rarely used. In the present work, the immobilization of *L*-Alanine dehydrogenase from *Bacillus subtillis* on agarose microbeads activated with glyoxyl groups (aliphatic aldehydes) and other two carriers is presented. These immobilized enzyme preparations were extensively characterized towards temperature, pH and kinetic parameters. Finally, we have applied the optimal heterogeneous biocatalyst in the synthesis of *L*-[^{13}N]alanine using pyruvate and [^{13}N]NH$_4$OH, as substrates. Herein, we have fabricated a highly stable and active heterogeneous biocatalyst for reductive aminations of α-ketoacids that has an enormous potential in biocatalysis.

INTRODUCTION

As already described in Chapter 5, *L*-alanine dehydrogenase from *Bacillus subtilis* (*L*-AlaDH) was used for the radiochemical synthesis of a variety of *L*-[^{13}N]amino acids with excellent radiochemical yields and purities.[1] Moreover, *L*-AlaDH from *Bacillus subtilis* has been also exploited as an auxiliary enzyme to replenish the amine donor (*L*-alanine) in transamination reactions catalyzed by ω-transaminases.[2] These examples show the usefulness of this enzyme in synthetic chemistry. However, the use of enzymes in synthetic applications is frequently limited by their solubility and their low stability under operational conditions.

These limitations underlying the vast majority of the native enzymes have been addressed at once by using immobilization techniques.[3] Any immobilization technique overcomes the solubility problem; nevertheless, the immobilization itself does not guarantee the enzyme stabilization and sometimes reduces the catalytic activity of the enzymes.[3,4] Enzyme immobilization is still considered an intuitive technique where the optimal immobilization protocol is often found using the trial-and-error approach. However, a deep understanding of the molecular structure of enzymes combined with spectroscopic tools enable appropriate characterization of the interactions between proteins and solid materials, as well as the evaluation of the effects that the immobilization causes on both protein structure and functionality.[5] Such characterization can guide the optimization of the immobilization protocols to fabricate the most efficient heterogeneous biocatalysts.

To the best of our knowledge, *L*-AlaDH has been only successfully immobilized on amine surfaces activated with glutaraldehyde[6] and on sepharose microbeads activated with cyanogen bromide[7]. In the first

171

system, the immobilized enzyme retained more than 90% of its initial activity for weeks under storage conditions at 4°C, while in the second case, the enzyme kept 70% of its initial activity after one month at 37°C.

In this chapter, *L*-Alanine dehydrogenase from *Bacillus subtillis* has been immobilized through different immobilization chemistries. Structural modeling of *L*-AlaDH supported by kinetic and fluorescence studies was also performed to understand how the immobilization reduces the enzyme activity but greatly increases the enzyme stability. Finally, to demonstrate the potential of this heterogeneous biocatalyst in the context of radiochemistry, the radiosynthesis of *L*-[^{13}N]alanine was carried out.

EXPERIMENTAL SECTION

Reagents. β-Nicotinamide adenine dinucleotide, reduced disodium salt hydrate (β-NADH; purity >97%), pyruvic acid (CH$_3$COCOOH, purity ≥98%), ammonium chloride (NH$_4$Cl, for molecular biology, purity ≥99.5%), sodium phosphate dibasic (Na$_2$HPO$_4$, for molecular biology, purity ≥98.5%), sodium phosphate monobasic (NaH$_2$PO$_4$, purity ≥99.0%), *L*-alanine (purity ≥98%), SYPRO® Orange Protein Gel Stain and cyanogen bromide-activated sepharose 4B (Ag-CB) were purchased from Sigma Chemical Co. (St. Louis, IL, USA) and used without further purification. TALON resin was purchased from Clontech (Saint-Germain-en-Laye, France). Bio-Rad Protein Assay Dye Reagent Concentrate was purchased from Bio-Rad Laboratories (Madrid, Spain). Agarose 4BCL microbeads (ABT, Madrid) activated with aldehyde groups were prepared as described elsewhere.[8] All other reagents were of analytical grade.

Structural modelling of *L*-Alanine Dehydrogenase from *Bacillus subtilis.* Three different monomeric structural models of *L*-AlaDH based on sequence homology were built using as templates the alanine dehydrogenases from *Thermus thermophilus*, *Mycobacterium tubercolosis*, and *Phormidium lapideum* available in protein data bank.[9] The most accurate model was obtained by using the *L*-AlaDH from *Phormidium lapideum* (PDB: 1SAY) despite having lower sequence identity (58.86 %) with *L*-AlaDH from *Bacillus subtilis* primary sequence than the *L*-AlaDH from *Thermus thermophilus* (62.84 %). Finally, the hexamer of our *L*-AlaDH was constructed by using the biological assembly of *Phormidium lapideum* as a template. Protein models were visualized and aligned with their template structure by using PyMol 0.99 developed by DeLano Scientific LLC (San Francisco, CA). The electrostatic potential and the local flexibility of the most accurate model were calculated by using the Bluues[10,11] and COREX/BEST[12] servers, respectively.
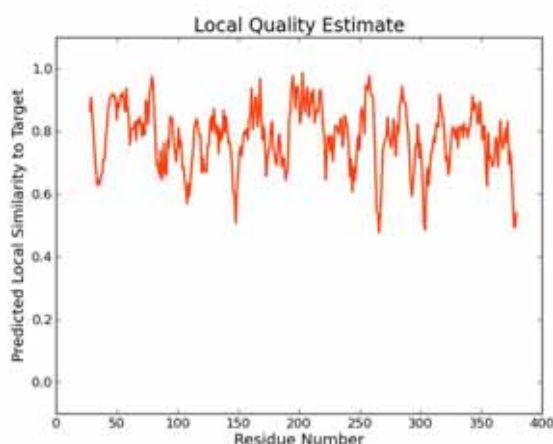
Figure 6.1. Plot showing predicted local similarity of *L*-AlaDH enzyme model by the homology-modeling server from Expasy (predicted local similarity versus residue number).

Protein and enzyme colorimetric assays. *Determination of the protein concentration.* The protein concentration of soluble *L*-AlaDH and FDH were measured as described in Chapter 4 for eNR. *Determination of enzyme activity.* The enzymatic activities of soluble and immobilized preparations were carried as described in Chapter 7.

Immobilization of *L*-Alanine Dehydrogenase from *Bacillus subtilis*. The immobilization of *L*-Alanine Dehydrogenase from *Bacillus subtilis* was performed on three different carriers: 1) porous 4BCL agarose microbeads activated with cyanogen bromide groups (Ag-CB); porous 4BCL agarose microbeads activated with aldehyde (glyoxyl) groups (Ag-G) and porous 6BCL agarose microbeads activated with cobalt-chelates. Ten milliliters of 16μg per mL *L*-AlaDH solution was added to 1 g of the carrier (Ag-CB, Ag-G and Ag-Co^{2+}). In the case of Ag-CB and Ag-Co^{2+}, the enzyme solution was prepared in 25 mM sodium phosphate buffer at pH 8. For Ag-G, the enzyme solution was prepared in 100 mM sodium carbonate buffer at pH 10. The mixtures were incubated under gentle stirring for 2h at 25°C. Periodically, samples of the supernatants and the enzyme-carrier suspensions were withdrawn and analyzed to evaluate the progress of the immobilization reaction. After completion of the immobilization, the samples with Ag-G were reduced with 1 mg x mL^{-1} NaBH$_4$ during 30 minutes at 4°C, whereas the samples with Ag-CB were incubated with 100 mM of hydroxylamine for 1 hour at 25°C. All the immobilized preparations were filtered, washed with distilled water and finally equilibrated with 25 mM phosphate buffer solution at pH 8.

Thermal Stability. Thermal stability was determined by incubating enzyme solutions or suspensions in 10 mM phosphate buffer at pH 8 and 60°C for 24 h in a thermo-shaker. Samples were taken at 0.5, 1, 2, 4, 6,

and 24 h of incubation, and their residual activity was measured as described above. The experimental data were fitted to first-kinetic equation ($A/A_o = e^{-k*t}$) using Origin 8.0. In this equation, A is the residual activity at different incubation times (t), A_o is the initial activity before incubations and k is the inactivation constant.

Activity-pH profile. The effect of pH on the activity of different enzyme preparations was determined by measuring the reductive amination of pyruvic acid in the presence of NADH at the different pH values (5-10) at 25°C. The expressed activity was measured as described before. Different 10 mM buffer solutions were used to set the right pH value; acetate buffer was used for pH 5 and 6; sodium phosphate buffer for pH 7 and 8 and sodium bicarbonate buffer for pH 9 and 10.

Fluorescence assays. Fluorescence Spectra were carried out with a Varioskan Flash fluorescence spectrophotometer (Thermo Scientific), using an excitation wavelength of 280 nm with excitation and emission bandwidths of 5 nm and recording fluorescence emission spectrum between 300 and 550 nm. All spectroscopic measurements were performed with a solution of 3μg x mL^{-1} of the enzyme (soluble or immobilized) in 10 mM sodium phosphate at pH 8 and 25°C.

Thermal-shift assay. This assay was performed using 3μg x mL^{-1} of the enzyme (soluble or immobilized) in 25 mM sodium phosphate buffer and 0.3% of SYPRO® Orange at pH 7. Then, this mixture was incubated in a StepOne-plus RT-PCR (Applied biosystems-ThermoFisher) by using a temperature ramp program from 25 to 95°C with a ramp rate of 0.5°C per minute.

Enzyme kinetic parameters. Michaelis constant value (K_m) and maximum rate (V_{max}) were determined by activity colorimetric assay at pH 8 and 25°C as previously described but using 0-1.8M ammonium chloride, 0-1mM NADH and 0-0.15M pyruvic acid. The experimental data were fitted to the Michaelis-Menten equation using Origin 8.0.

Production of the radiolabeling agent [^{13}N]NH$_3$. Nitrogen-13 (^{13}N) was produced in an IBA Cyclone 18/9 cyclotron via the ^{16}O(p,α)^{13}N nuclear reaction as described in chapter 5. Integrated currents around 0.2 μAh were used. The resulting solution was transferred to a 10mL vial and the activity was measured in a dose calibrator (Capintec CRC®-25 PET, New Jersey, USA).

Synthesis of *L*-[^{13}N]alanine. The radiosynthesis of *L*-[^{13}N]alanine was carried out by adding 100μL of a mixture containing 0.5mM NADH, 75mM pyruvic acid and 300mM sodium phosphate buffer solution at pH 8 (final concentrations in reaction) to a solution or suspension containing *L*-AlaDH (concentration in the range 15-45 μg/mL) and 100μL of [^{13}N]NH$_4$OH (35-45 MBq). Reactions were conducted in test-tubes with 50 KDa cut-off membranes in the case of the soluble enzymes and with micrometric filters in the case of immobilized. The corresponding mixture was incubated at 25°C under mild stirring for 2.5 to 20 min and subsequently filtered under centrifugation during one minute to remove the enzyme.

RESULTS AND DISCUSSION

Immobilization of *L*-AlaDH on porous agarose microbeads activated with different reactive groups

L-Alanine dehydrogenase from *Bacillus subtillis* was immobilized on porous 4BCL agarose microbeads activated with either cyanogen bromide groups (Ag-CB) or with aldehyde (glyoxyl) groups (Ag-G) and porous 6BCL agarose microbeads charged with a tetradentate chelator charged with cobalt (AG-Co^{2+}). At pH 8, the cyanogen bromide groups of Ag-CB react with the amine from the *N*-terminus of each subunit forming irreversible bonds,[13] and the cobalt chelates on the agarose surface of Ag-Co^{2+} preferentially interact with the imidazole rings of histidine tags located at the *N*-terminus of each subunit of *L*-AlaDH, creating reversible coordination bonds between the enzyme and the solid surface. On the other hand, the immobilization on Ag-G requires alkaline pH to enable the protein-carrier interactions. The aldehydes of the carrier form reversible imine groups with the primary amine groups of the enzyme (*N*-terminus and ε-NH_2 from the most exposed lysines) that are finally reduced to irreversible secondary amines by using a mild reducing agent such as sodium borohydride.[13]

As it can be seen at **Table 6.1**, 85-99% of the offered *L*-AlaDH was immobilized on the three carriers herein investigated, but the enzyme activity was reduced upon immobilization in all cases. Nevertheless, substantial differences were observed between the expressed activities of the enzymes immobilized on the different carriers; while the specific activity of *L*-AlaDH immobilized on Ag-CB was 67% of the soluble enzyme, *L*-AlaDH immobilized on Ag-Co^{2+} was 58% of the soluble

177

enzyme and *L*-AlaDH immobilized on Ag-G expressed 45% of the activity of the soluble one.

Table 6.1. Immobilization parameters of *L*-Alanine Dehydrogenase from *Bacillus Subtilis* immobilized onto agarose porous microbeads activated with different reactive groups.

CARRIER	Reactive group	Immobilization chemistry	Immobilized Activity Ai $(U/g)^a$	Immobilization yield ψ $(\%)^b$	Expressed Activity Ae $(U/g)^c/$ $(\%)^d$
Ag-CB	Cyanogen Bromide	Covalent bond through the primary amine group of the *N*-terminus	553±17	97±3	385±87 (67)
Ag-G	Glyoxyl	Multipoint covalent bond through the ε-NH2 of the lysines	566±79	85±12	295± 4 (45)
Ag-Co²⁺	Cobalt (Co²⁺)	Affinity binding through the His-tags	564±11	99±2	339±20 (58)

^{a}*Ai=The activity immobilized on 1 gram of carrier after the immobilization process. This activity was calculated as the difference between the offered activity and the activity in the supernatant after incubation with the carrier for 2h.* ^{b}*Immobilization yield (ψ) = (immobilized activity/offered activity) x 100.* ^{c}*The expressed activity (Ae) is defined as the measured activity of the immobilized enzyme after washing.* ^{d}*Relative expressed activity (Ae) = (expressed activity/immobilized activity) x 100.*

Similarly, previous works have demonstrated that the immobilization of two homolog *L*-AlaDHs from *Bacillus stearothermophilus*[6] and *Bacillus cereus*[7] on Ag-CB and aminated glass beads activated with glutaraldehyde, respectively, recovered 50-60% of the specific activity. Remarkably, in the present work, the *L*-AlaDH retained 50% of its initial activity upon the immobilization on Ag-G under alkaline conditions. Such high activity recovery after irreversible covalent attachment using Ag-G carrier has also been observed with the glutamate dehydrogenase from *Thermus thermophilus*.[14] The high stability of these two enzymes (*L*-alanine dehydrogenase and glutamate dehydrogenase) under alkaline conditions avoids their dramatic inactivation during the immobilization process at pH 10.[14,15] In contrast, lactate dehydrogenase from rabbit muscle loses 92%

of its initial activity upon immobilization on Ag-G without adding any enzyme stabilizers.[16]

Prediction of *L*-AlaDH orientation and attachment on the surface of different carriers

To better understand the molecular interaction between the *L*-AlaDH and the carrier, we built a structural model of the hexameric *L*-AlaDH. The model was built by using Swiss-Model Homology modelling server which utilizes structure-known proteins deposited in the protein data bank.[17,18] Moreover, we calculated the surface electrostatics[10,11] and the residue exposure of this model in order to know which are the most exposed lysines with the lowest pKa values (ε-NH$_2$) (**Table 6.2**).

Table 6.2. Surface exposure and apparent pK_a of the lysine residues found in *L*-AlaDH from *Bacillus subtilis*.

Position	Calculated pK_a	Total Surface area
32	11.686	188
35	12.244	166
87	11.19	226
97	12.925	3
99	12.226	50
111	10.727	234
132	11.027	123
134	11.892	7
174	10.922	347
176	11.112	173
179	12.564	124
193	12.308	109
208	10.814	155
239	11.089	261
268	12.502	214

Position	Calculated pK$_a$	Total Surface area
279	11.679	210
282	10.683	230
314	11.715	178
351	11.774	142
355	10.941	291

The values presented in this table were calculated by Bluues server using the pdb file generated in Swiss-Model server. pKa value corresponds to the ε-NH$_2$ of each lysine. Lysine residues with pKa lower than 11 are highlighted in red because they are predicted to be the most reactive ones under the immobilization conditions (pH 10) on Ag-G. These lysines are identified in the enzymatic model represented in **Figure 5.1**.

The hexamer contains 120 lysine residues (20 per subunit) distributed along its 3D surface; 5 lysine residues per subunit (K111, K174, K208, K282 and K355) present apparent pKa values lower than 11. This means that under the alkaline immobilization conditions, those 5 lysines and the *N*-terminus will be the only primary amino groups majorly unprotonated and thus ready to react with aldehyde groups on the Ag-G surface. Moreover, the *N*-terminus and the lysines K111, K174, K282 and K355 are fairly exposed to the solvent, which assures the geometrical congruence required for the immobilization reaction to take place.

After visualizing the 3D-model of *L*-AlaDH, it was suggested that *L*-AlaDH may be immobilized on Ag-G, Ag-CB and Ag-Co^{2+} through mainly one region, *Orientation 1*, that fairly displays 3 *N*-terminus and 6 out of 30 most reactive lysines (3 x K111 and 3 x K351). Ag-CB and Ag-Co^{2+} selectively attach the *N*-terminus, whereas Ag-G establishes bonds with the most reactive amine groups including *N*-terminus, K111 and K351. In addition, such region presents a suitable geometrical congruence (large flat surface) to attach at least 3 subunits to the solid surface (**Figure 6.2**).
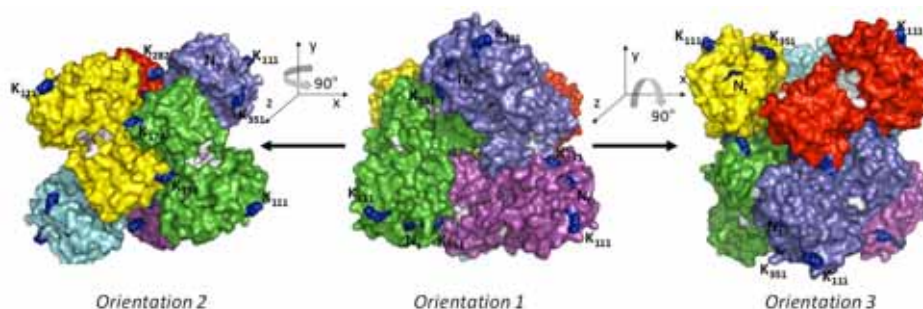
Figure 6.2. Different planes (orientations) of the *L*-AlaDH surface. The quaternary structure of *L*-AlaDH is formed by six subunits organized in three pairs of symmetrical faces giving rise to three different planar surfaces. None of the three faces displays more than three subunits with suitable geometrical and chemical congruence to react with the agarose surface. The 6 different subunits are colored in red, purple, violet, green, yellow and green, while all the active sites are colored in white. The *N*-terminus (*N*t) and the ε-NH$_2$ from the most exposed lysines with the lowest pKa values (calculated by Bluues server) are represented as blue spheres. The images were created with Pymol 0.99v.

Kinetics parameters of *L*-AlaDH immobilized on different carriers

The kinetics parameters of immobilized enzymes often differ significantly from those of the soluble enzymes. In our case, the immobilization of *L*-AlaDH on different carriers affected the kinetics parameters of the reductive amination of pyruvate in different manners (**Table 6.3**).

The catalytic efficiency towards NADH was significantly higher for the soluble enzyme than for the immobilized forms, mainly because the latter suffered a dramatic affinity loss for the redox cofactor (high K_m). The higher K_m values of the immobilized enzymes for NADH (up to 12.5-fold higher than the soluble enzyme) resulted in lower V_{max} values for all substrates. This effect was less dramatic when the enzyme was

immobilized on Ag-CB; in this case, the immobilized enzyme presented a 3.6 and 2.9-fold lower K_m for NADH than the enzyme immobilized on Ag-G and Ag-Co^{2+}, respectively. Noteworthy, *L*-AlaDH immobilized on Ag-G showed 8.5 and 3.4-fold lower K_m values for pyruvate and ammonia, respectively, than the soluble enzyme. Therefore, the aldehyde chemistry seems to enhance the affinity of the immobilized *L*-AlaDH for both ammonia and pyruvate which improves the catalytic efficiency 110 and 285%, respectively, with respect to the free enzyme.

Table 6.3. Kinetic characterization of free and immobilized *L*-AlaDH from *Bacillus Subtilis*.

|		Vmax	Km mM	Kcat s^{-1}	Kcat/Km s^{-1} x M^{-1}
NADH	AlaDH soluble	31.05±2.29	0.02±0.008	1.37E+02	6.83E+06
	AlaDH Ag-CB	22.00±1.52	0.07±0.017	9.68E+01	1.38E+06
	AlaDH Ag-Co^{2+}	17.79±2.69	0.20±0.08	7.82E+01	3.89E+05
	AlaDH Ag-G	17.92±2.5	0.25±0.12	7.88E+01	3.15E+05
NH₄Cl	AlaDH soluble	44.08±1.77	100.35±15.32	1.94E+02	1.93E+03
	AlaDH Ag-CB	39.45±2.52	120.86±28.02	1.73E+02	1.44E+03
	AlaDH Ag-Co^{2+}	14.90±0.62	29.91±6.80	6.55E+01	2.19E+03
	AlaDH Ag-G	14.02±1.20	29.16±6.53	6.24E+01	2.14E+03
Pyruvic acid	AlaDH soluble	55.39±2.20	0.17±0.04	2.44E+02	1.41E+06
	AlaDH CNBr	27.37±1.27	0.17±0.05	1.20E+02	7.10E+05
	AlaDH Ag-Co^{2+}	19.43±1.47	0.15±0.07	8.55E+01	5.84E+05
	AlaDH Glyoxyl	12.67±1.31	0.02±0.006	6.85E+01	4.03E+06

In all the cases, the immobilization of *L*-AlaDH driven by either the *N*-terminus, the His-tags or the primary amine groups with the lowest pK_a seems to orient the protein through a region where none of the active sites directly contact with the carrier surface (*Orientation 1*, see **Figure 6.2**).

Contrarily, the cofactor binding regions of at least three subunits seem to interact with the carrier surface, which may hamper the interaction of the immobilized enzyme with NADH. This fact may explain the high K_m values observed for NADH, which ultimately compromise the catalytic efficiency of the immobilized enzyme. Furthermore, the valence and the nature of the interaction between these protein regions and the carrier surface may differently distort tertiary and quaternary structures, thus explaining the changes in affinity observed for the other two substrates (ammonia and pyruvate).

Protein thermal stability of immobilized *L*-AlaDH preparations

The integrity of the protein structure under reaction conditions is fundamental to guarantee the protein stability during the operational process. *L*-AlaDH immobilized on different agarose-based microbeads was thermally inactivated at 60°C and compared with the soluble enzyme (**Figure 6.3** and **Table 6.4**).

Figure 6.3 shows that *L*-AlaDH immobilized on Ag-G, Ag-CB and Ag-Co^{2+} were 23.8, 3.3 and 1.2-fold more stable than the soluble enzyme, respectively. Moreover, at higher temperatures *L*-AlaDH immobilized on Ag-G presented 53% of its initial activity after 30 minutes incubation at 64°C, while the *L*-AlaDH immobilized on Ag-Co^{2+} and the soluble enzyme was almost completely inactivated (residual activity < 10%).
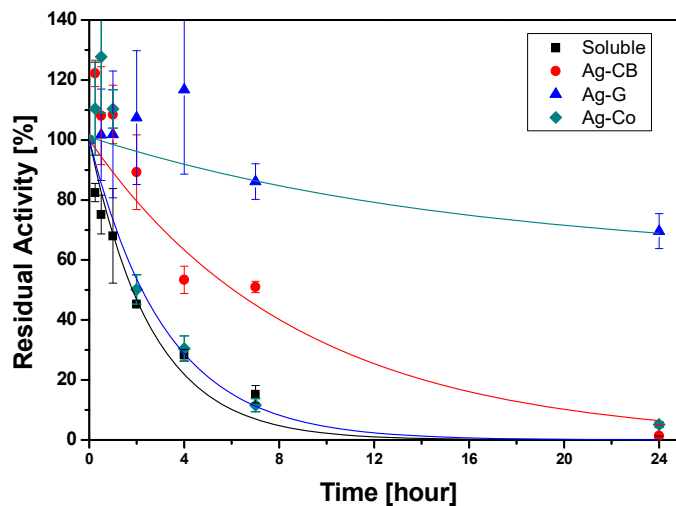
Figure 6.3. Thermal inactivation of soluble and immobilized *L*-AlaDH. The different enzymatic preparations were incubated at 60°C and pH 8: Soluble *L*-AlaDH (squares); *L*-AlaDH immobilized on Ag-CB (circles); *L*-AlaDH immobilized on Ag-Co^{2+} (diamonds); and *L*-AlaDH immobilized on Ag-G (triangles).

Table 6.4. Kinetics parameters of the thermal inactivation of different *L*-AlaDH preparations. The thermal inactivation was carried out at 60°C and pH 8 during 24h.

Carrier [a]	Inactivation constant (h^{-1})	Half-life time (h)[b]	Stabilization factor [c]
Soluble	0.38±0.04	1.82	-
Ag-CB	0.11±0.02	6.07	3.3
Ag-Co^{2+}	0.31±0.02	2.22	1.2
Ag-G	0.016±0.01	43.32	23.8

a) Experimental data from **Figure 5.2** *was fitted with a First-order kinetics equation considering total inactivation (A/A$_o$=e^{-k*t}). b) The half-life time was calculated introducing to the corresponding equation A/Ao=0.5. c) Stabilization factor means the half-life time of the corresponding immobilization preparation divided by the half-life time of the soluble enzyme.*

To evaluate the effect of the thermal inactivation on the protein structure of *L*-AlaDH immobilized on Ag-G, the intrinsic fluorescence of soluble and immobilized enzyme on Ag-G were measured before and after incubation at 60°C for 4 hours (**Figure 6.4A**).
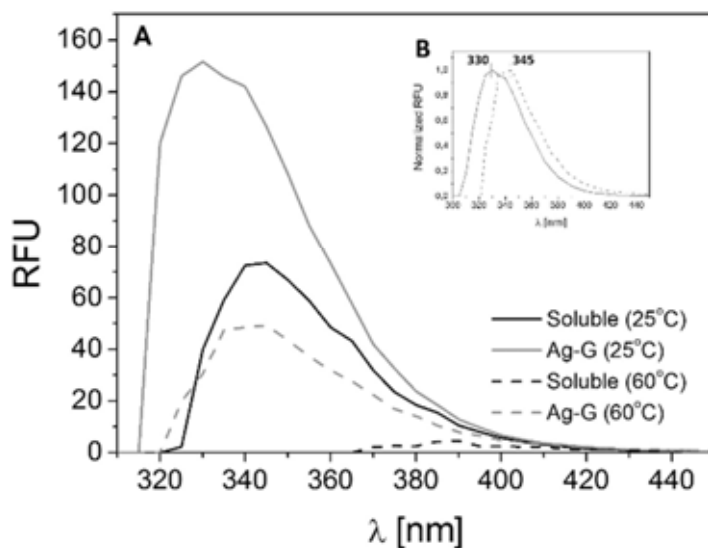
Figure 6.4. (**A**) Intrinsic fluorescence of soluble and immobilized *L*-AlaDH. The intrinsic fluorescence of tryptophan was measured for soluble (black lines) and immobilized (grey line) enzymes before (solid line) and after (dash line) sample heating at 60°C and pH 8 during 4 hours. (**B**) The inset figure shows the normalized fluorescence of immobilized *L*-AlaDH before and after the inactivation. All fluorescence values were normalized regarding the fluorescence at λ_{max} for each sample.

In one hand, the immobilization of *L*-AlaDH promoted a 20nm blue-shift of λ_{max} and 2-fold enhancement of the fluorescence intensity compared to

its soluble counterpart before thermal inactivation. These results suggest that *L*-AlaDH has suffered some conformational changes upon the immobilization that may explain the lower specific activity of the immobilized enzyme. The soluble enzyme presented 6% of its maximum fluorescence intensity and its λ_{max} was 45 nm red-shifted after thermal incubation, suggesting large structural changes driving the protein to unfolded states. On the other hand, the maximum fluorescence intensity of *L*-AlaDH immobilized on Ag-G was reduced to 32% and the λ_{max} red-shifted 15 nm after the thermal incubation (inset **Figure 6.4B**).
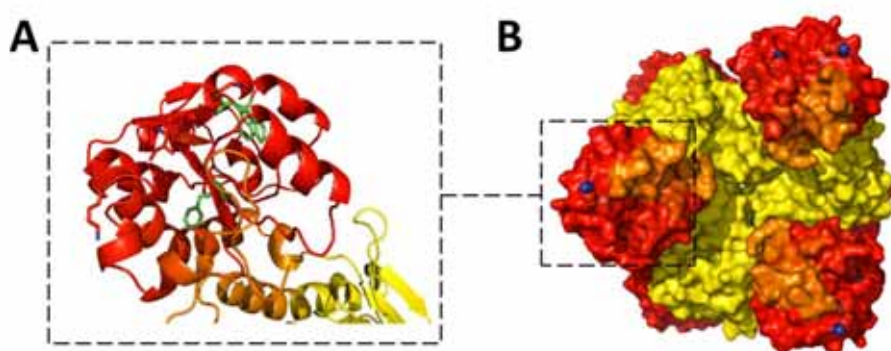

Figure 6.5. *In silico* representation of *L*-AlaDH local flexibility using a COREX/BEST server. (**A**) zoomed-in view of the interaction region of one subunit showing the highest density of low pKa amine groups. W and F residues are coloured in green; (**B**) rigid and flexible residues are coloured in red and yellow, respectively. Gradering between red and yellow (orange) represent moderately stable regions. The *N*-terminus (*N*t) and the ε-NH$_2$ from the most exposed lysines with the lowest pKa values (calculated by Bluues server) are represented as blue spheres. The images were created with Pymol 0.99v.

With the molecular model of *L*-AlaDH in hand, it was pointed that the fluorescence changes induced by thermal incubation may rely on some structural rearrangements that affect the protein environment of the unique tryptophan residue W90 (**Figure 6.4**). In the soluble enzyme, the loss of fluorescence intensity and the large red-shift of the λ_{max} suggest that W90 becomes dramatically exposed to the solvent. Contrarily, the immobilization of *L*-AlaDH on Ag-G seems to protect that region, alleviating the conformational changes in the vicinity of the W90 and resulting in a lower reduction in the fluorescence intensity and a smaller red-shift of the λ_{max}.

Finally, to rationalize why the immobilization on Ag-G through the proposed region increases the thermal stability of *L*-AlaDH, the residue stability constant of the *L*-AlaDH model was calculated by using COREX/BEST server.[12,19] **Figure 6.5B** shows that the interaction region for *Orientation 1* is composed of high, medium and low flexible local domains. Although, the most reactive groups (low pKa lysines and *N*-terminus) are located in the most rigid domains, additional bonds can involve lysines from other domains with medium and high flexibility which promote an artificial rigidification of that region. However, since the immobilization on Ag-CB is restricted to the interactions with the *N*-terminus of the enzyme (located at the rigid domains), further rigidification of the most flexible domains is more difficult. In fact, these results are supported by the SDS-PAGE analyses (**Figure 6.6**) that show how Ag-G irreversibly attaches the 6 subunits, while Ag-CB can only attach 2 out of the 6 subunits. SDS-PAGE studies showed that the 6 subunits of *L*-AlaDH were irreversibly attached to Ag-G likely due the flexibility of the agarose fibers that may enable a 3D interaction between

less accessible and reactive lysines and the aldehyde groups of the carrier surface (**Figure 6.6**).
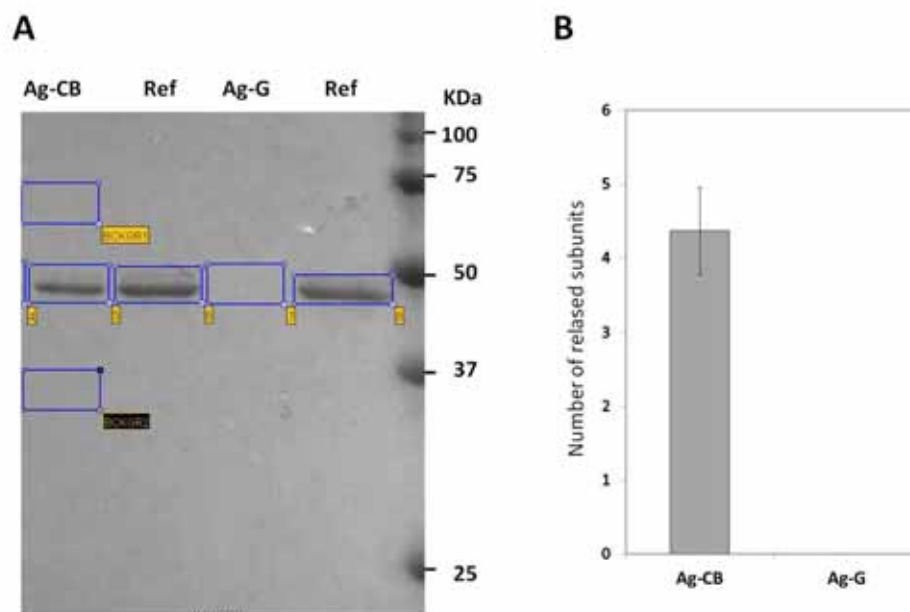
Figure 6.6. (A) SDS-PAGE (14%) of *L*-AlaDH immobilized on Ag-CB and Ag-G and their soluble references (Ref) for quantification. **(B)** Quantification of the number of subunits released under denaturing conditions (5 minutes at 99°C in presence of SDS-PAGE loading buffer). The quantification was carried out by image analysis quantifying the pixel intensity of the regions of interest shown in the gel picture. The raw data of each band was subtracted from the raw data of the background in order to only quantify the pixel intensity due to the protein stain. The reference was considered as the amount of protein corresponding to 6 subunits.

These results suggest that the most reactive amine groups can react with the carrier when the protein is in the bulk (inter-molecular reaction) driving the immobilization, but the less reactive lysines can only react with

the aldehydes when the protein surface has landed on the carrier surface (intra-molecular reaction). This fact was not observed when the enzyme was immobilized on Ag-CB, where only 2 out of 6 subunits were irreversibly attached to the surface according to electrophoresis results (**Figure 6.6**).

Therefore, despite both aldehyde and cyanogen bromide chemistries seem to orient the protein through the same region, the immobilization on Ag-G may stabilize the quaternary structure and rigidify the most flexible protein domains resulting in increased protein stability. In this scenario, it was suggested that the valence of the attachment is making the difference in terms of protein stability.

The higher thermal stability of the *L*-AlaDH immobilized on Ag-G compared to the soluble enzyme is also supported by thermodynamic denaturalization studies using a thermo-shift assay (**Figure 6.7**). The midpoint temperature where the protein suffers the hydrophobic exposure increased 1°C in the immobilized preparation, suggesting that the multivalent and irreversible immobilization on Ag-G stabilizes both tertiary and quaternary structures of *L*-AlaDH.

In previous studies, the stability of *L*-AlaDH from *Bacillus stearothermophilus* immobilized on aminated glass beads activated with glutaraldehyde and the stability of *L*-AlaDH from *Bacillus cereus* immobilized on Ag-CB have been investigated under moderate temperatures (37°C) and storage conditions.[6,7] Here, the stability of *L*-AlaDH immobilized on Ag-G was stressed under high temperatures, 60°C. Our positive results suggest that the valence of the attachment promoted by Ag-G is making the difference in terms of protein stability compared to the carriers activated with cyanogen bromide and with glutaraldehyde

groups. These results agree with different studies using fluorescence and force spectroscopy that demonstrate that aldehyde chemistry achieves higher protein stabilization than the cyanogen bromide chemistry, as the first promotes multivalent interactions through short spacer arms.[20,21]
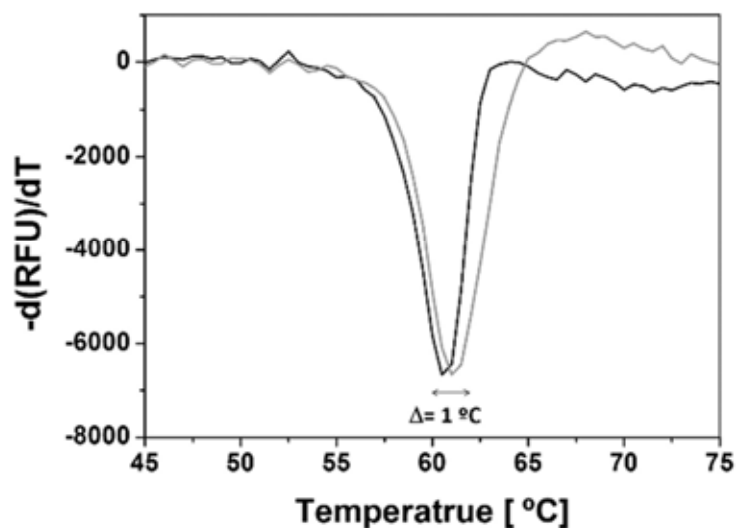
Figure 6.7. Thermal denaturation of soluble *L*-AlaDH (black line) and *L*-AlaDH immobilized on Ag-G. The negative first derivative of fluorescence regarding the temperature was determined by measuring the fluorescence of the different samples in a thermal shift assay using SYPRO Orange dye and a Real-Time PCR system. The *L*-AlaDH preparations were incubated in 10 mM sodium phosphate at pH 8 and submitted a gradient of temperatures.

The immobilization chemistry affects the activity-pH profile of *L*-AlaDH

The activities of soluble and immobilized enzyme preparations under different pH conditions were also measured. It has been reported that the immobilization can improve the pH tolerance of enzymes.[22] The soluble enzyme showed optimal reductive amination activity at pH values in the range 8-10 (**Figure 6.8**); such activity significantly decreased at pH lower than 7. The effect of the acidic pH was even more dramatic when *L*-AlaDH was immobilized on Ag-CB; this preparation showed optimal activity at pH 9, but its normalized activity considerably decreased at acidic pH values. Noteworthy, the immobilization of *L*-AlaDH on Ag-G yielded a highly robust enzyme that presents >75% of its optimal activity from pH 6 to 10, with a broader optimal pH range (8-10) than the soluble enzyme. These data demonstrate that the reductive amination is favoured at alkaline pH values likely because of the high stability of the enzyme at high pH values. Contrarily, under acidic conditions, the soluble enzyme undergoes a dramatic inactivation as reflected in its activity-pH profile. Such inactivation can be mitigated by immobilizing *L*-AlaDH on Ag-G. Overall, our results clearly show that the immobilization on Ag-G is able to protect *L*-AlaDH against acidic pH, broadening the pH spectrum where the enzyme can be utilized.
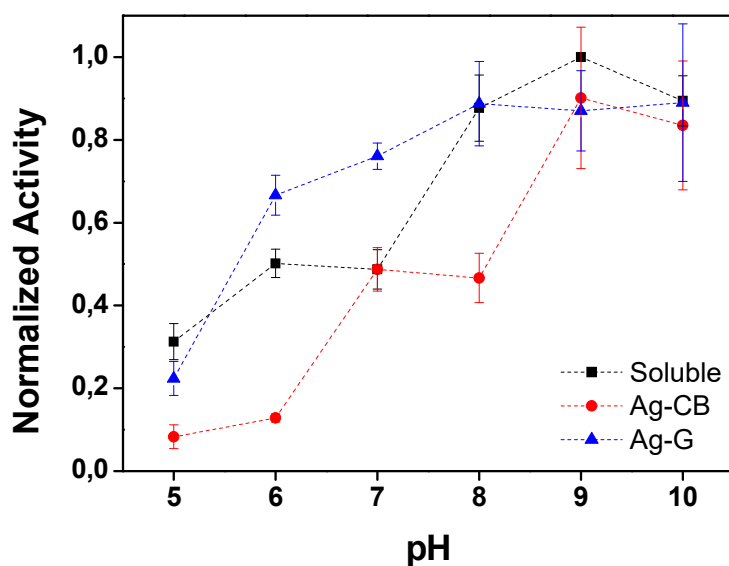
Figure 6.8. Effect of pH on *L*-AlaDH activity. The activity of soluble *L*-AlaDH in solution (squares) and immobilized *L*-AlaDH on Ag-CB (circles) and Ag-G (triangles) were assayed at different pH by using the appropriate buffers at 25°C. Acetate buffer was used for pH 5 and 6; sodium phosphate buffer for pH 7 and 8 and sodium bicarbonate buffer for pH 9 and 10.

Biotechnological application of highly stable *L*-AlaDH immobilized on Ag-G in radiochemistry

The immobilized *L*-AlaDH on Ag-G has shown an excellent thermal stability and acceptable activity for biotechnological purposes. Moreover, the 3-fold lower K_m value towards ammonia makes this heterogeneous biocatalyst highly interesting to be used in the asymmetric reduction of α-ketoacids to synthesize *L*-[^{13}N]amino acids using [^{13}N]NH$_4$OH as the radioactive precursor. In the radiochemical environment, the concentration of the radioactive precursor is rather limiting regarding the other

substrates, and hence biocatalysts with low K_m value for ammonia are promising for this application. As a proof of concept, we radiosynthesized *L*-[^{13}N]alanine with different biocatalyst loads in the presence of 75 mM pyruvic acid, 0.5 mM NADH and [^{13}N]NH$_4$OH (as a radioactive precursor) at pH 8. After 5 min, 45 μg of enzyme immobilized on Ag-G per mL of reaction achieved a 65% incorporation of the radionuclide; the yield could be increased up to 95% after 20 minutes of reaction.
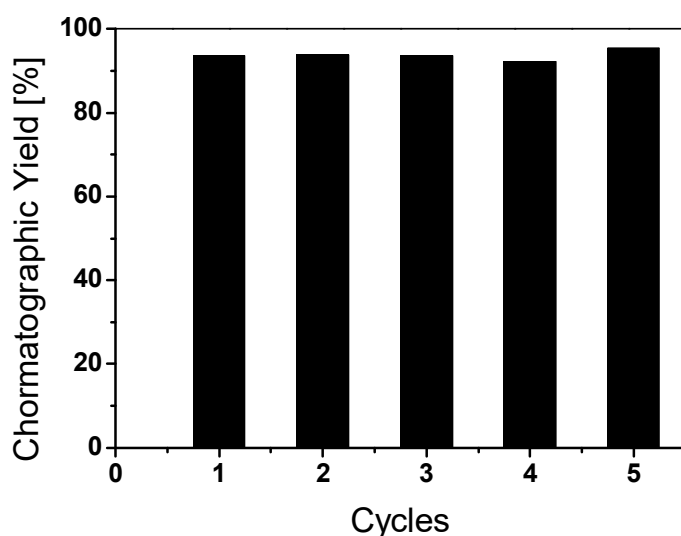
Figure 6.9. Reusing of *L*-AlaDH immobilized on Ag-G in the radiochemical synthesis of *L*-[^{13}N]-alanine. The reaction was carried out with 45 μg x mL-1 of immobilized biocatalyst at 25 °C and pH 8 during 20 minutes.

This immobilized enzyme showed unaltered efficiency in 5 consecutive operational batches (**Figure 6.9**). To the best of our knowledge, this is the first time that an immobilized *L*-alanine dehydrogenase is employed for

the one-pot/one-step reductive amination of pyruvate using $[^{13}N]NH_4OH$ as amine donor and producing L-$[^{13}N]$alanine. Another L-AlaDH from *Bacillus* species was used in its immobilized form for the selective deamination of L-$[^{11}C]$alanine to synthesize $[^{11}C]$-pyruvic acid[6] and for the two-step synthesis of L-$[^{15}N]$alanine from lactic acid[7]. Unlike L-AlaDH, a plethora of glutamate dehydrogenases from different sources have been immobilized on different carriers and applied to a variety of biotechnological applications.[23,24] In particular, glutamate dehydrogenase covalently immobilized on Ag-CB and on silica beads have also been utilized for the synthesis L-$[^{13}N]$amino acids. Depending on the systems and the amino acids produced, the radiochemical yield ranged between 35-70% in short times (<5minutes).[25] Our system achieves similar radiochemical yields after 5 minutes although performs worse than the soluble enzyme that can reach >95% of radiochemical yield in the same incubation time and with the same protein cocentration.[1]

CONCLUSION

Soluble L-alanine dehydrogenase from *Bacillus subtilis* has been intensively exploited in biocatalysis but rarely used as a heterogeneous biocatalyst. The immobilization of L-AlaDH on porous agarose microbeads activated with different reactive groups was performed. The immobilization of L-AlaDH on Ag-G greatly stabilizes the enzyme at the cost of activity reduction. Structural and conformational studies based on intrinsic fluorescence of both soluble and immobilized enzyme have demonstrated that protein inactivation is due to negative conformational changes induced by the temperature. The thermally-driven structural distortions are alleviated by the enzyme immobilization through a covalent

and multivalent attachment. Based on molecular modeling and physic-chemical calculations, the region that is more prone to react with Ag-G was identified. The physic-chemical properties and local flexibility of such identified region suggest an excellent chemical and geometrical congruence that may rigidify some of the most flexible domains of the protein, thus increasing its thermal stability. Finally, a proof of the utility and reusability of this robust heterogeneous biocatalyst for the radiosynthesis of L-[^{13}N]alanine was carried out showing excellent yields.

REFERENCES

(1)   da Silva, E. S.; Gómez-Vallejo, V.; Baz, Z.; Llop, J.; López-Gallego, F. Efficient Enzymatic Preparation of 13N-Labelled Amino Acids: Towards Multipurpose Synthetic Systems. *Chemistry – A European Journal* **2016**, *22*, 13619-13626.

(2)   Mutti, F. G.; Fuchs, C. S.; Pressnitz, D.; Sattler, J. H.; Kroutil, W. Stereoselectivity of Four (R)-Selective Transaminases for the Asymmetric Amination of Ketones. *Advanced Synthesis & Catalysis* **2011**, *353*, 3227-3233.

(3)   DiCosimo, R.; McAuliffe, J.; Poulose, A. J.; Bohlmann, G. Industrial use of immobilized enzymes. *Chemical Society Reviews* **2013**, *42*, 6437-6474.

(4)   Cantone, S.; Ferrario, V.; Corici, L.; Ebert, C.; Fattor, D.; Spizzo, P.; Gardossi, L. Efficient immobilisation of industrial biocatalysts: criteria and constraints for the selection of organic polymeric carriers and immobilisation methods. *Chemical Society Reviews* **2013**, *42*, 6262-6276.

(5)   Bolivar, J. M.; Eisl, I.; Nidetzky, B. Advanced characterization of immobilized enzymes as heterogeneous biocatalysts. *Catalysis Today* **2016**, *259, Part 1*, 66-80.

(6)   Ikemoto, M.; Sasaki, M.; Haradahira, T.; Okamoto, E.; Omura, H.; Furuya, Y.; Watanabe, Y.; Suzuki, K. A new synthesis of [3-11C]pyruvic acid using alanine racemase. *Applied Radiation and Isotopes* **1998**, *49*, 1557-1562.

(7)   Presecan, E.; Ivanof, A.; Mocanu, A.; Palibroda, N.; Bologa, M.; Gorun, V.; Oargă, M.; Bârzu, O. Preparation of 15N-labeled l-alanine by

immobilized l-alanine dehydrogenase: Differential incorporation of 15N in bacterial proteins. *Enzyme and Microbial Technology* **1987**, *9*, 663-667.

(8) Guisán, J. Aldehyde-agarose gels as activated supports for immobilization-stabilization of enzymes. *Enzyme and Microbial Technology* **1988**, *10*, 375-382.

(9) Berman, H. M.; Westbrook, J.; Feng, Z.; Gilliland, G.; Bhat, T. N.; Weissig, H.; Shindyalov, I. N.; Bourne, P. E. The Protein Data Bank. *Nucleic Acids Research* **2000**, *28*, 235-242.

(10) Walsh, I.; Minervini, G.; Corazza, A.; Esposito, G.; Tosatto, S. C.; Fogolari, F. Bluues server: electrostatic properties of wild-type and mutated protein structures. *Bioinformatics (Oxford, England)* **2012**, *28*, 2189-2190.

(11) Fogolari, F.; Corazza, A.; Yarra, V.; Jalaru, A.; Viglino, P.; Esposito, G. Bluues: a program for the analysis of the electrostatic properties of proteins based on generalized Born radii. *BMC bioinformatics* **2012**, *13 Suppl 4*, S18.

(12) Vertrees, J.; Barritt, P.; Whitten, S.; Hilser, V. J. COREX/BEST server: a web browser-based program that calculates regional stability variations within protein structures. *Bioinformatics (Oxford, England)* **2005**, *21*, 3318-3319.

(13) Mateo, C.; Abian, O.; Bernedo, M.; Cuenca, E.; Fuentes, M.; Fernandez-Lorente, G.; Palomo, J. M.; Grazu, V.; Pessela, B. C. C.; Giacomini, C.; Irazoqui, G.; Villarino, A.; Ovsejevi, K.; Batista-Viera, F.; Fernandez-Lafuente, R.; Guisán, J. M. Some special features of glyoxyl supports to immobilize proteins. *Enzyme and Microbial Technology* **2005**, *37*, 456-462.

(14) Bolivar, J. M.; Cava, F.; Mateo, C.; Rocha-Martin, J.; Guisan, J. M.; Berenguer, J.; Fernandez-Lafuente, R. Immobilization-stabilization of a new recombinant glutamate dehydrogenase from Thermus thermophilus. *Applied microbiology and biotechnology* **2008**, *80*, 49-58.

(15) Yoshida, A.; Freese, E. Enzymatic properties of Alanine dehydrogenase of Bacillus subtilis. *Biochimica et biophysica acta* **1965**, *96*, 248-262.

(16) Jackson, E.; López-Gallego, F.; Guisan, J. M.; Betancor, L. Enhanced stability of l-lactate dehydrogenase through immobilization engineering. *Process Biochemistry* **2016**, *51*, 1248-1255.

(17) Biasini, M.; Bienert, S.; Waterhouse, A.; Arnold, K.; Studer, G.; Schmidt, T.; Kiefer, F.; Gallo Cassarino, T.; Bertoni, M.; Bordoli, L.; Schwede, T. SWISS-MODEL: modelling protein tertiary and quaternary structure using evolutionary information. *Nucleic Acids Res* **2014**, *42*, W252-258.

(18) Arnold, K.; Bordoli, L.; Kopp, J.; Schwede, T. The SWISS-MODEL workspace: a web-based environment for protein structure homology modelling. *Bioinformatics (Oxford, England)* **2006**, *22*, 195-201.

(19) Pan, H.; Lee, J. C.; Hilser, V. J. Binding Sites in Escherichia coli Dihydrofolate Reductase Communicate by Modulating the Conformational Ensemble. *Proceedings of the National Academy of Sciences of the United States of America* **2000**, *97*, 12020-12025.

(20) Orrego, A. H.; García, C.; Mancheño, J. M.; Guisán, J. M.; Lillo, M. P.; López-Gallego, F. Two-Photon Fluorescence Anisotropy Imaging to Elucidate the Dynamics and the Stability of Immobilized Proteins. *The Journal of Physical Chemistry B* **2016**, *120*, 485-491.

(21) Gregurec, D.; Velasco-Lozano, S.; Moya, S. E.; Vazquez, L.; Lopez-Gallego, F. Force spectroscopy predicts thermal stability of immobilized proteins by measuring microbead mechanics. *Soft Matter* **2016**, *12*, 8718-8725.

(22) Bolivar, J. M.; Wilson, L.; Ferrarotti, S. A.; Fernandez-Lafuente, R.; Guisan, J. M.; Mateo, C. Stabilization of a Formate Dehydrogenase by Covalent Immobilization on Highly Activated Glyoxyl-Agarose Supports. *Biomacromolecules* **2006**, *7*, 669-673.

(23) Zhao, H.; van der Donk, W. A. Regeneration of cofactors for use in biocatalysis. *Current opinion in biotechnology* **2003**, *14*, 583-589.

(24) Doong, R.-a.; Shih, H.-m. Glutamate optical biosensor based on the immobilization of glutamate dehydrogenase in titanium dioxide sol–gel matrix. *Biosensors and Bioelectronics* **2006**, *22*, 185-191.

(25) Cohen, M. B.; Spolter, L.; Chang, C. C.; MacDonald, N. S.; Takahashi, J.; Bobinet, D. D. Immobilized enzymes in the production of radiopharmaceutically pure amino acids labeled with 13N. *Journal of Nuclear Medicine* **1974**, *15*, 1192-1195

Chapter 7

General conclusions

In this thesis, we have demonstrated that the application of biosynthetic methods enables the efficient and selective radiosynthesis of labeled compounds that would be hard to address by using chemical methods. The excellent results obtained herein rely on the capability of enzymes to catalyze a wide variety of chemical reactions and on their high regio-, chemo- and stereo-selectivity in the chemical processes. We have demonstrated that enzymes can be used either in their free form (in solution) or immobilized on a solid carrier. In the context of this PhD thesis, the enzymatic processes have been applied in the context of ^{13}N radiochemistry.

The main conclusions of the work conducted are:

1- The selective radiochemical reduction of $[^{13}N]NO_3^-$ to $[^{13}N]NO_2^-$ can be achieved by using a NADPH-dependent eukaryotic nitrate reductase. Under optimal conditions, such reduction could be achieved in >90% radiochemical yield.

2- By controlling the immobilization chemistry and physicochemical properties of the carrier, an optimal heterogeneous biocatalyst (Nitrate reductase immobilized in Ag-DEAE) with high potential in synthetic chemistry could be fabricated. The immobilized enzyme was 12-fold more stable than the soluble enzyme and could be re-used for the radiochemical reduction of $[^{13}N]NO_3^-$ up to 7 cycles without compromising the efficiency of the reduction.

3- The ^{13}N-labeled radiotracer $[^{13}N]GSNO$ could be synthesized in 95% chromatographic yield using the abovementioned immobilized enzyme, following a two-step chemo-enzymatic process and starting from cyclotron-produced $[^{13}N]NO_3^-$.

4- A fast, efficient, and one-pot enzymatic synthesis of L-[^{13}N]alanine, [^{13}N]glycine, and *L*-[^{13}N]serine was achieved using a NADH-dependent *L*-AlaDH in 5 min reaction. This strategy is not suitable for the preparation of *L*-[^{13}N]norvaline and *L*-[^{13}N]phenylalanine under no-carrier-added conditions, due to the high K$_m$ values for ammonia.

5- For the enzymatic synthesis of *L*-[^{13}N]alanine, the addition of FDH to the reaction media to regenerate NADH enabled a 50-fold decrease in the concentration of NADH without compromising radiochemical yields

6- Upon intravenous administration, *L*-[^{13}N]alanine, [^{13}N]glycine and *L*-[^{13}N]serine accumulate in the abdominal region. Contrary to *L*-[^{13}N]serine, *L*-[^{13}N]alanine and [^{13}N]glycine are not eliminated via urine and enable proper visualization of the accumulation of the tracer in the prostate. Visual inspection of the images suggests increased uptake of these amino acids in the prostate of animals with specific Pten deletion.

7- The immobilization of *L*-AlaDH from *Bacillus subtillis* on Ag-G greatly stabilizes (approx. 24-fold more than soluble enzyme) the enzyme at the cost of activity reduction.

8- Structural and conformational studies based on intrinsic fluorescence of both the soluble and immobilized forms of *L*-AlaDH have demonstrated that protein inactivation is due to negative conformational changes induced by the temperature.

9- The thermally-driven structural distortions are alleviated by the enzyme immobilization through a covalent and multivalent attachment on Ag-G.

10- This robust heterogeneous biocatalyst enables the radiosynthesis of [^{13}N]amino acids with excellent yields (>95%).

List of abbreviations

λ_{max}	Emission wavelength
2D	Two dimension
3D	Three dimension
AADH	Amino acid dehydrogenase
Ag-CB	Cyanogen bromide-activated agarose
Ag-Co^{2+}	Cobalt agarose
Ag-DEAE	Diethyl-aminoethyl agarose
Ag-DS	Dextran-sulphate agarose
Ag-G	Glyoxyl agarose
Ag-MANAE	Monoaminoethyl-*N*-aminoethyl agarose
Ag-PEI	Polyethyleneimine agarose
ATP	Adenosine triphosphate
BSA	Bovine serum albumin
CoA	Coenzyme A
CT	Computerized tomography
CY	Chromatographic yield
Cys	Cystine

eNR	Eukaryotic nitrate reductase
FAD$^+$	Flavin adenine dinucleotide
FDA	5'-fluoro-5'-deoxyadenosine
FDG	Fluorodeoxyglucose
FDH	Formate dehydrogenase
FDI	5'-fluoro-5'-deoxyinosine
FDR	5′-deoxy-5'-fluoro-D-ribose
FLPC	Fast protein liquid chromatography
GABA	Aminobutyric acid
Glu	Glutamate
GSH	Glutathione
GSNO	*S*-nitrosoglutathione
Hist	Histidine
HPLC	High performed liquid chromatography
HPLC-MS	High-performance liquid chromatography-mass spectrometry
HR-MAS	^{1}H high-resolution magic angle spinning
ID	Injected dose
IPTG	Isopropyl β-D-1-thiogalactopyranoside
K$_m$	Michaelis constant
KG	Ketoglutarate

L-AAO	*L*-amino acid oxidase
L-AlaDH	*L*-Alanine dehydrogenase
LB	Luria-Bertani media
L-DOPA	*L*-3,4-dihydroxyphenylalanine
L-FMAU	2′-Fluoro-5-methyl-β-*L*-arabinofuranosyluracyl
LOR	Lines of response
Lys	Lysine
MOCO	Molybdenum cofactor
MOF	Metal organic framework
MRI	Magnetic resonance imaging
NAD^+ / NADH	Nicotinamide adenine dinucleotide
NADPH	β-Nicotinamide adenine dinucleotide 2′-phosphate
N*t*	N-*terminus*
OD_{600nm}	Optical density of 600nm
PDB	Protein data bank
PET	Positron emission tomography
PK	Pharmacokinetics
Pten	Phosphatase and tensin homolog
RNA	Ribonucleic acid
RT-PCR	Reverse transcription polymerase chain reaction

SAM	*S*-adenosyl-*L*-methionine
SDS-PAGE	Sodium dodecyl sulphate-Polyacrylamide gel electrophoresis
SA	Specific activity
SPECT	Single-photon emission computed tomography
TFA	Trifluoroacetic acid
TOF	Time of flight
Trp	Tryptophan
UDP	Uridine diphosphate
UPLC	Ultra-Performance Liquid Chromatography
UV	Ultraviolet
V$_{max}$	Maximum initial velocity
WHO	World Health Organization

Acknowledgments

After more than 3 years in Donosti, now I am in the last stage of my thesis, and probably most difficult pages. So, *last but not least*, I would like to express my gratitude to all of you that directly or indirectly made this thesis a reality.

First and foremost, I would like to express my gratitude to Prof. Manuel Martín Lomas and Prof. Luis M. Liz Marzán, former and current scientific directors of CIC biomaGUNE, respectively, for giving me the opportunity to develop the experimental work of this PhD in the outstanding facilities of the centre.

As for you Dr. Jordi Llop and Dra. Vanessa Gomez-Vallejo, for giving me the opportunity to conduct this superb international PhD project. I am especially grateful to be given the chance to participate in high quality international congresses and meetings which opens my mind and sight to the world of Radiochemistry and Nuclear Medicine. Also to you, Jordi, as supervisor, I would like to thank you for the kindly suggestion of the subject of my thesis. Also, I thank you for your priceless support, observations, inspiration and valuable suggestions throughout the years of the thesis. Without your supervision, guidance, the achievement of this thesis would not have been possible. I thank you for providing me the opportunity to work with talented researchers.

Furthermore, I would like to thank Dr. Fernando Lopez, who has been my teacher and supervisor in scientific and technical work with enzymes, for accepting this challenging collaboration. Fernando, thank you for your perseverance, tolerance and daily supervision. I also thank you for your excellent and tireless guidance and encouragement during this almost 3

years of work together. All your exigent observations, comments and suggestions helped me to establish the overall direction of the research.

You always were there when I need and you always found time for me in your busy agenda.

I take this moment to shower my words of gratitude to all my past and present colleagues in the Radiochemistry & Nuclear Imaging Lab, Izaro, Ana, Carlos, Maria, Beatriz, Mikel Errasti, Mikel Gonzalez, Zuriñe, Aitor, Larraitz, Kiran, Jaya, Sameer, Unai, Xabi, Angel and Luis, it was a pleasure for me meeting you all here. Thank you all!

To Zuriñe, I thank you for your help in all bureaucratic steps of my all my PhD, since the beginning to the end.

Very warm and big thanks for the entire Fernando's and Valery's Lab colleagues, Susana (*Chili girl*), Anabel (*Transformer*), Laura, Ruta, Javi and Bea. Thank you for the warm welcome in your lab team! I am very grateful that I made this adventurous journey with your company. I am very thankful for all pleasant and FUNtastic days we had in the lab. Couldn't imagine a better place and better colleagues to work with.

To my office mates, Maria, Dorleta, Unai, Manu, Andrea, Ana, Juan and Silvia for all the fun moments, support and exchanged knowledge. Thank you for sharing your space, food, brainstorms and thoughts!

To RADIOMI family, thank you all for the amazing moments that we share over theses years during the meetings and schools!

A special thanks to Ainhoa and Ander for your support during animal studies and Bogdan for imaging. Also, thank you all for the amazing moments and conversations!

O mesmo posso dizer a ti mana, cunhado e sobrinhas quero-vos agradecer a vossa amizade e o vosso carinhoso e sempre disponível apoio nesta minha etapa.

A ti mano, futura cunhada e sobrinhos obrigado por toda a motivação e admiração.

A todos os meus amigos que me acompanharam nesta batalha, obrigado pelo apoio e amizade, especialmente a ti Tininha, Susana, Rute e Tânia.

Mila esker!
Thank you all!
Muito obrigado!
Muchas gracias!

Há coisas que nunca se poderão explicar por palavras…

José Saramago

Eunice Sofia da Silva Fernandes

E-mail: eunicesofiasilva@gmail.com

ACADEMICS

CIC biomaGUNE/University of the Basque Country, UPV-EHU
  PhD student in Synthetic and Industrial Chemistry; Marie-Curie Fellow within the Marie Skłodowska-Curie Innovative Training Network
  RADIOMI project research- Innovative Radiochemistry to Advance Molecular Imaging, FP7-PEOPLE-2012-ITN (www.radiomi.chem.ox.ac.uk)
  Supervisor: Jordi Llop Roig, PhD and Fernando Lopez-Gallego, PhD

San Sebastian, Spain, 2013-2017

University of Coimbra, Faculty of Pharmacy
  MSc in Industrial Pharmaceutical Chemistry (grade: 18/20)
  Supervisor: Prof. Carlos Cavaleiro, PhD
  Collaboration with Chimie et Biomasse Group - CNRS 6134 of University of Corsica Pascal Paoli

Coimbra, Portugal, 2011-2013

University of Coimbra, Faculty of Pharmacy
  Post-graduation in Industrial Pharmaceutical Chemistry (grade: 16/20)

Coimbra, Portugal, 2010-2011

Health Science Technology School
  BSc in Pharmacy (grade: 17/20)

Coimbra, Portugal 2006-2010

PROFESSIONAL SKILLS

- Pharmacy:
    - Laboratory (Techniques incl. analytical, for drug development and identification);
    - Industry (GLP, GMP, synthesis, fractioning, quality control, dispensing and packing of radiopharmaceuticals);
    - Hospital (<u>*General:*</u> Traditional distribution; Replacement for stock levels; Unit Dose; Pharmacotechnics, Visualization and support the preparation of cytostatics. <u>*Paediatric:*</u> Reception and storage of orders; Traditional Distribution; Replacement for stock levels; Unitary Doses; Clinic; Visualization and support in the preparation of cytostatics and support, and preparation of parenteral nutrition bags.
    - Community (Orders and receipt request; Checking stocks; Dispensing and counselling; Conducting galenic formulations (Handled); Conducting Blood sugar, Cholesterol, Triglycerides and Blood Pressure screenings; Prescription conference)

- Radiochemistry/Radiopharmacy: GLP/GMP synthesis, fractioning, quality control and dispensing of [^{18}F]FDG and others ^{18}F and ^{11}C radiopharmaceuticals; synthesis of radiotracers with PET isotopes; enzymatic catalysis in the preparation of PET radiotracers; Quality Control (Development of analytical methods and labelling of new molecules); Cyclotron operation.

- Chemistry: Chemical synthesis; Purification and structural analysis techniques (including but not exclusively, Analytical and Preparative HPLC, NMR, mass and UV Spectroscopy, Confocal microscopy and Cell observer); Design and development of new drugs: Scale of synthesis transposition.

- Biochemistry/biotechnology: Analytical techniques involved in natural, biotechnological compounds and enzymes (Transformation and Expression of proteins; Fluorescence spectroscopy, SDS-page; Protein Thermal Shift); Functionalization of solid materials for enzyme immobilisation.

- Physiotherapy: Thermotherapy (Paraffin, Parafango, Infrared); Electrotherapy (Ultrasound, Microwave, Electrophoresis); Mobilization and Massage.

- Software: Microsoft Office, ChemDraw, Origin8, Graphpad, Photoshop, Illustrator CC adobe, Systems Laboratory Techniques associated with the analysis GC, GC-MS, HPLC, NMR.

TEACHING EXPERIENCE

Health Science Technology School, Coimbra
  Invited Auxiliary Professor
  Lecturer of Pharmacognosy Practice

Coimbra, Portugal 2012-2013

PROFISSIONAL EXPERIENCE

Syncom BV.   **Groningen, The**
    Chemical and pharmaceutical industry   **Netherlands**
    Analytical Scientist   **Since Jan2017**

Farmácia Luz Marques, Lda.   **Penacova, Portugal**
    Community Pharmacy   **2010-2013**
    Pharmacy Technician

Drug Discovery group, Centre for Pharmaceutical Studies, Faculty of Pharmacy,   **Coimbra, Portugal**
University of Coimbra   **2011-2013**
    Research
    Student Researcher

Chimie et Biomasse Group - CNRS 6134 of University of Corsica Pascal Paoli   **Corsica, France**
    Research   **2012**
    Student Researcher

Hospital Pediátrico de Coimbra   **Coimbra, Portugal**
    Hospital Pharmacy   **Nov2009-Jan2010**
    Curricular training

Instituto de Ciências Nucleares Aplicadas à Saúde   **Coimbra, Portugal**
    Industry- Radiopharmacy Laboratory   **Sept2009-Nov2009**
    Curricular training

Laboratório Militar e Produtos Químicos Farmacêuticos, Sucursal de Coimbra   **Coimbra, Portugal**
    Community Pharmacy   **Feb2009-April2009**
    Curricular training

PUBLICATIONS

As first author:

Publication **Biocatalysis in Radiochemistry; Enzymatic Incorporation of PET radionuclides into molecules of biomedical interest.** Eunice S. da Silva, Vanessa Gómez-Vallejo, Fernando López-Gallego, Jordi Llop. *Submitted*

Poster Communication: **Efficient enzymatic synthesis of 13N-labelled amino acids and evaluation as diagnostic tools in a mouse model of prostate cancer.** Eunice S. da Silva, Vanessa Gómez-Vallejo, Zuriñe Baz, Amaia Zabala, Arkaitz Carracedo, Fernando López-Gallego and Jordi Llop. ISRS 2017. Dresden, Germany

Publication **Structural, kinetic and operational characterization of an immobilized L-aminoacid dehydrogenase**. Eunice S. da Silva, Vanessa Gómez-Vallejo, Jordi Llop, Fernando López-Gallego. Process Biochemistry, Available online 8 March 2017, *In press*

Poster Communication: **Efficient biosynthetic method for incorporating nitrogen-13 into aminoacids of biomedical interest in prostate cancer.** Eunice S. da Silva, Vanessa Gómez-Vallejo, Zuriñe Baz, Amaia Zabala, Arkaitz Carracedo, Fernando López-Gallego and Jordi Llop. International Symposium: Molecular Imging Agents in Medicine, UMCG, The Netherlands. February 2017

Publication: **Efficient Enzymatic Preparation of 13N-labelled amino acids: Towards Multi-Purpose Synthetic Systems.** Eunice S. da Silva, Vanessa Gómez-Vallejo, Jordi Llop and Fernando López-Gallego. Chemistry - A European Journal , 2016, vol.22, 38. 13619–13626

Publication: **Efficient nitrogen-13 radiochemistry catalyzed by a highly stable immobilized biocatalyst.** Eunice S. da Silva, Vanessa Gómez-Vallejo, Jordi Llop and Fernando López-Gallego. Catal. Sci. Technol., 2015,5, 2705-2713.

Oral Communication: **Efficient and sustainable synthesis of L-13N-Alanine catalyzed by heterogeneous biocatalyst.** International Molecular Imaging Workshop 2015. CIC biomaGUNE, San Sebastian-Donostia.

Oral Communication: **Application of biocatalysis in sustainable Nitrogen-13 chemistry.** 2nd Workshop UFI-QOSYC, Pharmacy Faculty, UPV, Vitória-Gasteiz, Spain;

Poster Communication: **Biocatalyzed synthesis of L-13N-Alanine by L-Alanine dehydrogenase from *bacillus subtilis*.** November 2015. bioMAPP15, CIC biomaGUNE, San Sebastian-Donostia

Poster Communication: **New advances in Nitrogen-13 chemistry: Preparation of 13N-labelled polysubstituted triazoles via Huisgen cycloaddition and biocatalyzed synthesis of L-13N-Alanine by L-Alanine dehydrogenase from** *bacillus subtilis.* November 2015. ISAB, CIC biomaGUNE, San Sebastian-Donostia

Poster Communication: **Efficient [13N]nitrate reduction catalyzed by** *Aspergillus niger* **nitrate reductase immobilized on positively charged carrier**. May 2015, University of Missouri, USA, ISRS2015

Oral Communication: **Combination of capillary GC, GC/MS and 13C-NMR for the analysis of the volatile extracts of** *E. dilatatum* **and** *E.pandanifolium.* CEF2012. Eunice Fernandes, Lígia Salgueiro, Carlos Cavaleiro. Coimbra, September 2012.

Poster Communication: **Composition and variability of the volatile oils of** *Eryngium campestre.* L. CEF2012. Eunice Fernandes, Lígia Salgueiro, Carlos Cavaleiro. Coimbra, September 2012.

Poster Communication: **Composition of the volatile oils of E**. *dilatatum Lam.* **and** *E. Pandanifolium.* Cham. & Schltdl**.** 43rd International Symposium on Essential Oils (ISEO2012), Lisbon, 5-8 September 2012, Abstract Book, p. 155

Poster Communication: **Composition of the volatile oil of** *Eryngium dilatatum* **Lam.** 3PYCHEM no Porto. Eunice Fernandes, Lígia Salgueiro, Carlos Cavaleiro. Porto, May 2012.

Publication: Current Radiopharmaceuticals. **Positron Emitting Tracers in Pre-Clinical Drug Development.** E. Fernandes, Z. Barbosa, G. Clemente, F. Alves and A. J. Abrunhosa, Volume 5, Number 2, April 2012. Pp.90-98

Poster: **PET and SPECT in Drug development and discovery of new drugs** CEF2010, Faculty of Pharmacy, Coimbra. E. Fernandes, Z. Barbosa, G. Clemente.

Poster: **Synthesis of 18F-FDG on Synthera® module** XII National Congress of Nuclear Medicine, Portuguese Society of Nuclear Medicine. E.Fernandes, R.Vitório, J. P Oterelo, G. S. Clemente, M. C. Rodrigues, C. Guerreiro, A. Abrunhosa, A. Rodrigues. Mealhada, 2009

Collaborations:
Poster Communication**: Automated synthesis box based on microfluidics for solid phase supported synthesis: application to** ^{18}**F and** ^{13}**N.** 17th European Symposium on Radiopharmacy and Radiopharmaceuticals-ESRR'14. Jorge Elizalde, Javier Berganzo, Jesús M. Ruano-López, Vanessa Gómez-Vallejo, Kiran B. Gona, Beatriz Rodríguez, Ana Lima, Eunice Sofia da Silva, Jordi Llop. Pamplona, April 2014.

AWARD

MARIE CURIE Fellowship. September 2013

Best Presentation Award Panel in "Drug Discovery", presented at the Conference CEF2012. September 2012

LANGUAGES
- Portuguese: Native.
- English: Pre-advanced level (oral and write communication).
- Spanish: Advanced level (oral and write communication).
- French: Low Intermediate level (oral and write communication).

ADDITIONAL INFORMATION

Courses & Certificates:
- RADIOMI School 4, CIC biomaGUNE, Donostia, Spain (2015)
- RADIOMI School 3, University of Turku, Turku, Finland (2015)
- RADIOMI School 2, VU University Medical Center, Amsterdam (2014)
- Positron Emission Tomography: Technology and Application Course by Division of Imaging Sciences and Biomedical Engineering, King's College London, London, UK.(2014)
- Training in Technology Transfer Project Management by ISIS Innovation, University of Oxford, Oxford, UK (2014)
- RADIOMI School 1, Department of Chemistry, University of Oxford, Oxford, UK (2014)
- Radioprotection and Security in radioactive facilities by CIC biomaGUNE, San Sebastian, Spain (2014)
- Photoshop Course. (2013)
- Injectable Administration Course by the Associação Portuguesa de Licenciados em Farmácia. (2012)
- European Basic Life Support Course by Portuguese Red Cross School. (2011)
- Magisterial Dermatology Formulation Course by Cofanor. (2011)
- Sifarma 2000 Patients Tracking Course by Post Graduation Scholl of Health and Management. (2011)
- European Course of First Aids by Portuguese Red Cross School. (2010)
- Inhalation Therapy Course by Cofanor. (2010)
- Initial Trainers Teaching Course by Conclusão - Estudos e Formação, Lda. (2010)

- Veterinary Pharmacy Course by Health Science Technology School, Coimbra. (2010)
- Homeopathy Course by Health Science Technology School, Porto. (2010)
- Professional Formation on Recovery Massages by Sindicato Nacional de Massagistas de Recuperação e Cinesioterapeutas. (2005-2006)

Other collaborations:
- Collaboration in Pharmacy Introduction signature (Pharmacy graduation) with the lecture: *"New job opportunities in Pharmacy"*, November 2014
- Member of the evaluation panel for the subject "Estágio II", on ESTeS de Coimbra. 2011-2013
- Organizing Committee of I Jornadas do Departamento de Farmácia da ESTeSC (Theme: "Community Pharmacy - Counselling and Health Care Provision"), position of secretary. 2009-2010
- Organising Committee of Semana das Ciências Aplicadas na Saúde 2009 (SCAS 2009).